TRANSPORT PROPERTIES OF LITHIUM AND SODIUM IONS IN GASES

A THESIS

Presented to

The Faculty of the Division of Graduate Studies

by

Garth Russell Akridge

In Partial Fulfillment

of the Requirements for the Degree

Doctor of Philosophy in the School of Physics

Georgia Institute of Technology

December, 1975

TRANSPORT PROPERTIES OF LITHIUM AND SODIUM IONS IN GASES

Approved:

Earl W. McDaniel, Chairman

I. R. Gatland

L. D. Wyly

Date approved by Chairman 12/14/75

This thesis is dedicated to

my parents, my wife Anita,

and my children Floyd and Sheryl.

ACKNOWLEDGMENTS

It is with pleasure that acknowledgment is made of the interest and assistance of those who have contributed to the work described in this thesis. The author wishes to acknowledge the guidance, encouragement, and teaching of his thesis advisor, Dr. Earl McDaniel, throughout this research. The comments of Dr. Ian Gatland and Dr. L. D. Wyly, who served on the thesis reading committee were highly valued.

The assistance of Dr. H. W. Ellis, and Dr. Bob Pai, who aided the author in obtaining the data presented here and with whom many fruitful discussions were held, is greatly appreciated. The contributions of those who preceded the author in this laboratory--Dr. Dan Albritton, Dr. Tom Miller, Dr. John Moseley, Dr. Bob Snuggs, Dr. George Thompson, Dr. John Schummers, Dr. Ed Graham IV, and Dr. Randy James--are acknowledged.

The research reported here was sponsored by the Office of Naval Research.

TABLE OF CONTENTS

TABLE OF CONTENTS (Continued)

LIST OF TABLES

LIST OF ILLUSTRATIONS

LIST OF ILLUSTRATIONS (Continued)

SUMMARY

The drift velocities, mobilities, and longitudinal diffusion coefficients of mass-identified Li^+ ions in He, Ne, and Ar, and of Na^+ ions in He, Ne, Ar, and CO_2 were measured as a function of E/N, where E is the electric field intensity, and N is the number density of the neutral gas. Deviations from purely Fickian diffusion were examined over a limited range of high E/N. All measurements were carried out at gas temperatures of approximately 300° K and at gas pressures ranging from 0.00246 Torr to 0.493 Torr.

The measurements were made using a drift tube of ultrahigh vacuum construction. The Li^+ and Na^+ ions were produced in the source by thermionic emission. Bursts of ions of known spatial extent and temporal duration were repetitively gated into the drift region by an electric shutter. In the drift region, the ions reached an equilibrium drift velocity. The ions diffused longitudinally and transversely as they drifted a known distance through the neutral gas. A sample of the ions was mass analyzed, detected, and sorted according to the time of flight. This information was used to build an arrival time histogram. From the average arrival time, the drift velocity, and hence the mobility, was calculated. The longitudinal diffusion coefficient was determined by fitting the theoretical curve to the measured arrival time histogram. The deviations from purely Fickian diffusion were determined by fitting a theoretical curve, which took into account both Fickian and non-Fickian diffusion, to the arrival time histogram.

The reduced mobilities for Li^+ ions and for Na^+ ions in He, Ne, and Ar exhibited the same general behavior. For each ion-gas combination, there was a range of low E/N in which the reduced mobility had a constant value, the zero field reduced mobility. The zero field reduced mobilities measured in cm^2/V-sec were as follows: Li^+ -He (23.06 $\pm$ 0.67), Li^+ -Ne (10.17 $\pm$ 0.27), Li^+ -Ar (4.63 $\pm$ 0.13), Na^+ -He (22.64 $\pm$ 0.61), Na^+ -Ne (8.27 $\pm$ 0.22), and Na^+ -Ar (3.09 $\pm$ 0.08). As E/N was increased, the reduced mobility first increased to a maximum, then decreased producing a familiar "hump." Clustering prevented an accurate determination of the zero field reduced mobility for Na^+ in CO_2. The reduced mobility for Na^+ in CO_2 at the lowest value of E/N used was (1.63 $\pm$ 0.04) cm^2/V-sec. at E/N = 51.8Td. For Na^+ in CO_2, the reduced mobility first decreased, then increased as E/N was increased.

The longitudinal diffusion coefficients for Li^+ ions in He, Ne, and Ar, and for Na^+ ions in He, Ne, Ar, and CO_2 exhibited the same general behavior, although the data for Na^+ in CO_2 showed slight differences from the other six ion-gas combinations. In each case, the longitudinal diffusion coefficient approached the value given by the Einstein relation at low E/N. Increasing E/N resulted in a rapidly increasing longitudinal diffusion coefficient. The experimental data were compared with four theories: The Wannier theory, the modified Wannier theory, the Viehland-Mason theory, and the improved Viehland-Mason theory. All four theories reduced to the same limit at low E/N. For intermediate E/N, the Viehland-Mason theory gave the best agreement with the experimental data. For the high E/N range, the improved Viehland-Mason theory gave the best

agreement with the experimental data.

The non-Fickian coefficients for Na^+ in Ar and for Li^+ in Ne were measured at high E/N and were found to increase with increasing E/N. Inclusion of non-Fickian effects, important only at high E/N, resulted in a slightly smaller longitudinal diffusion coefficient.

CHAPTER I

INTRODUCTION

This thesis examines the low energy interaction of positive ions with neutral gas atoms and molecules. The ion-gas combinations used were Na^+ in He, Ne, Ar, and CO_2, and Li^+ in He, Ne, and Ar. The interaction energies ranged from approximately thermal to a maximum of 10.1 eV in the case of Li^+ in He and a few eV less in the other combinations.

The Georgia Tech drift tube mass spectrometer was used to gather the experimental data on the ion-neutral interaction. The drift tube contained the neutral gas at low pressure to minimize ion-neutral reactions. Ions were pulsed into the gas by the ion source at the top of the drift region. A uniform electrostatic field set up in the drift region forced the ions through the neutral gas. As the ions traveled through the gas, they gained energy from the external field, but they lost energy when they collided with neutral gas molecules. After a few collisions, the ions reached an equilibrium drift velocity $\vec{v}_d$. For low electric field strengths the drift velocity varied directly with the electric field $\vec{E}$. The ratio of drift velocity $\vec{v}_d$ to the electric field, E, is defined as mobility K,

$$K = \frac{v_d}{E} \quad . \tag{1-1}$$

It can be shown that the drift velocity depends on both the electric field E and the gas number density N through the ratio E/N. A convenient unit for

expressing E/N is the "Townsend," or Td, where 1 Td is 10^{-17} V-cm^2.

Mobilities were measured at a variety of temperatures and pressures. Therefore, it was convenient to normalize the mobilities measured at pressure p (Torr) and temperature T(^{o}K) to a standard temperature of 0^{o}C (273.16^{o}K) and a standard pressure of 760 Torr. The mobility at the measured value of E/N and the standard temperature and pressure is defined as the reduced mobility K_0. The reduced mobility is related to the mobility by

$$K_0 = K\left(\frac{p}{760}\right)\left(\frac{273.16}{T}\right) . \qquad (1\text{-}2)$$

The reduced mobility is then the mobility which one would obtain if the gas number density were 2.687×10^{19} molecules/cm^3, the number density at standard temperature and pressure.

At low E/N, the reduced mobility was independent of E/N. The limiting value of reduced mobility at low E/N is defined as the zero field reduced mobility $K_0(0)$ or

$$K_0(0) = \lim_{E/N \to 0} K_0 . \qquad (1\text{-}3)$$

Gradients in the spatially non-uniform ion distribution give rise to diffusion. The diffusion current in a given direction is proportional to the ion density gradient in that direction. The constant of proportionality is defined as the diffusion coefficient. In general, the proportionality constant for diffusion parallel to the electric field is different from the proportionality constant perpendicular to the

electric field. The diffusion current density $\vec{j}_d$ is then given by Fick's law in tensor form

$$\vec{j}_d = -\overleftrightarrow{D} \cdot \vec{\nabla} n \, , \tag{1-4}$$

where the tensor $\overleftrightarrow{D}$ is

$$\overleftrightarrow{D} \quad \begin{pmatrix} D_T & 0 & 0 \\ 0 & D_T & 0 \\ 0 & 0 & D_L \end{pmatrix} . \tag{1-5}$$

For low enough E/N both the longitudinal diffusion coefficient, D_L, and the transverse diffusion coefficient, D_T, reduce to a common value D given by the Einstein relation

$$\frac{D}{K} = \frac{kT}{e} \, . \tag{1-6}$$

In the above equation k is Boltzmann's constant, T is the temperature, and e is the charge on the ion.

The total ion current density $\vec{j}$ is due both to the drift of the center of the ion swarm through the gas and to the diffusion of ions. The ion current due to drift of the center of the ion swarm is, from equation (1-1),

$$n\vec{v}_d = nK\vec{E} \, . \tag{1-7}$$

Combining this equation with equation (1-4) results in

$$\vec{j} = nK\vec{E} - \overleftrightarrow{D} \cdot \vec{\nabla} n. \tag{1-8}$$

Ions may react with the neutral gas molecules. If ion-neutral reactions occur, they are characterized by a reaction frequency α. This reaction frequency is defined as the rate per ion at which a given reaction occurs. The reaction frequency depends upon the number of molecules involved in the reaction. For a two-body reaction, the reaction frequency will be proportional to N, the gas number density. For a three-body reaction, the reaction frequency will be proportional to N^2, etc. The constant of proportionality between the reaction frequency α and the appropriate power of N is defined as the reaction rate coefficient k. The units of k will depend on the number of bodies involved in the reaction.

The motivation for the research reported here has both theoretical and practical aspects. First of all, experimental data on ionic transport properties are needed to test two recent theoretical advances. The Viehland-Mason theory makes available a formula for predicting diffusion coefficients at high E/N. An accurate diffusion theory would allow diffusion coefficients to be theoretically calculated. This development would eliminate the necessity of measuring diffusion coefficients in every case. Mobilities are relatively easy to measure, but longitudinal diffusion coefficients are relatively difficult to measure. The Viehland-Mason theory uses measured mobilities to calculate longitudinal diffusion coefficients. The measured diffusion coefficients reported in this thesis provided a large body of data, taken over a wide range of pressures and E/N, which allowed a definitive test of the Viehland-Mason theory. The second theoretical advancement was Catlow's ab initio quantal calculation of the Li^+ -He interaction potential covering a wide range of ion-atom separation distances.

The experimentally determined mobility of Li^+ in He reported here provided the experimental data to test this theory over the wide range of energies below those covered by ion beam experiments.

Drift velocities are needed in measurements on ion-molecule reactions. For example, in determining the association or dissociation rate from an arrival time spectrum, the drift velocities of the individual species must be known. Ion mobilities and diffusion coefficients are also needed to aid in a quantitative understanding of electrical discharges. Another practical area in which ionic transport data are needed is that of modeling of gas lasers. It is hoped that the efficiency and power output of gas lasers can be increased by incorporating measured transport data into a study of the ionic-molecular processes in the gas between pulses. Mobilities are also needed in the development of MHD power generators.

Review of Past Experimental Research

In the late 1930's Tyndall[1] made the first reliable measurements of the mobilities of ions in gases. The mobilities of most of the ion-gas combinations reported here have not been thoroughly examined since Tyndall measured them.

Tyndall's early drift tube consisted of an ion source gated by electrical pulses, a drift region surrounded by guard rings, and an electrometer to collect the ions that had drifted through the gas. The apparatus did not contain a mass spectrometer, so that direct ionic identification was not possible.

Tyndall's work was done at pressures of approximately 1 Torr and room temperature, but he normalized his mobility data to 760 Torr and $27^{o}C$. Since the standards for modern mobility work are 760 Torr and $0^{o}C$, the zero field

reduced mobilities reported by Tyndall were multiplied by the temperature correction factor 273.16/291.16 = 0.93818 before comparing them with the zero field reduced mobilities reported in this thesis. Tyndal made no measurements of diffusion coefficients or reaction rate coefficients.

In 1973 Keller and Beyer[2] measured both the association-rate coefficient and the dissociation-rate coefficient for Na^+ in CO_2. Their source of ions was a platinum gauze filament coated with β-eucriptite enriched in the mass 7 isotope of Li. Their drift distances could be varied up to a maximum of 44 cm. The analysis region consisted of a quadrupole mass spectrometer and a detector. Their experiments were carried out at a temperature of $310^{o}K$ and at E/N = 12 Td. For the reaction

$$Na^+ + CO_2 + CO_2 \rightleftarrows Na^+ \cdot CO_2 + CO_2$$

they found the association-rate coefficient to be $2 \times 10^{-29} cm^6/sec$, and the dissociation-rate coefficient to be $1 \times 10^{-14} cm^3/sec$. For the reaction

$$Na^+ \cdot CO_2 + CO_2 + CO_2 \rightleftarrows Na^+ \cdot 2CO_2 + CO_2$$

they found an association-rate coefficient of $5 \times 10^{-29} cm^6/sec$, and a dissociation-rate coefficient of $5 \times 10^{-13} cm^3/sec$.

Also in 1971, Johnsen, Brown, and Biondi[3] measured the zero field reduced mobility of Na^+ in He. The drift tube used for their measurements was constructed primarily to measure reaction rate coefficients. Their measured value for the zero field reduced mobility of Na^+ in He was $20.7 \pm 1\ cm^2/V\text{-}sec$.

In 1973 Keller, Beyer, and Colonna-Romano[4] measured the association-rate coefficient, the longitudinal diffusion coefficient, and the zero field reduced mobility for Li^+ in Ar. The measurements were carried out at a temperature of 319°K and at pressures from 0.5 Torr to 1.5 Torr. In their experiments E/N ranged from 9 Td to 24 Td. They found that the association-rate coefficient was $1.8 \times 10^{-31} cm^6/sec$ over the entire E/N range, and the dissociation-rate coefficient increased from $2.0 \times 10^{-13} cm^3/sec$ at an E/N of 9 Td to $3.2 \times 10^{-13} cm^3/sec$ at an E/N of 24 Td. The ratio of longitudinal diffusion coefficient to the Einstein diffusion coefficient increased from 1.1 at an E/N of 9 Td to 1.75 at an E/N of 24 Td. They found the zero field reduced mobility of Li^+ in Ar to be 4.57 ± 0.12 $cm^2/V\text{-}sec$.

Review of Past Theoretical Research

In 1905 Langevin[5] used Maxwell's momentum transfer method to produce the first detailed work on the mobility of ions in a gas. Langevin assumed that a neutral molecule of the gas behaved as a perfectly elastic sphere which became polarized in the presence of the ion. Langevin's use of a Boltzmann velocity distribution for the ions limited his results to low fields. Langevin found

$$K_0(0) = \frac{35.9}{(\mu\alpha)^{\frac{1}{2}}} , \tag{1-9}$$

where μ is the reduced mass in amu, α is the polarizability in Å^3, and $K_0(0)$ is the zero field reduced mobility in $cm^2/V\text{-}sec$.

In 1916-17 Chapman and Enskog[6] arrived at an expression for D_L. Their

results were valid for elastic collisions and for any central potential interaction, so they contained Langevin's result for the special case of the ion-induced dipole interaction. In the zero field limit Chapman and Enskog found

$$D_L = \frac{kT}{e} K = \frac{3}{16N}\left(\frac{2\pi kT}{\mu}\right)^{\frac{1}{2}} \frac{1}{\bar{\Omega}^{(1,1)}(T)} , \qquad (1\text{-}10)$$

where e is the charge on the ion, k is Boltzmann's constant, N is the neutral gas number density, μ is the reduced mass of the ion-neutral pair, and $\bar{\Omega}^{(1,1)}(T)$ is a collision integral defined by equation (3-31).

In 1953 Wannier[7] examined longitudinal diffusion for E/N above the zero field limit. Expressed in quantities convenient for this thesis, Wannier's result for the polarization model was

$$D_L = \frac{KkT}{e} + \frac{KM(M+3.72m)}{3e(M+1.908m)} v_d^2 \qquad (1\text{-}11)$$

In the above equation M is the mass of the neutral gas molecule, m is the mass of the ion, k is Boltzmann's constant, T is the gas temperature, and K is the mobility.

In 1953 Kihara[8] extended mobility theory beyond the zero field region to the medium field region where the reduced mobility was no longer independent of E/N, but where polarization was still the dominant interaction. The following is a summary of Kihara's analysis. Ions, forced through the neutral gas by an external electric field, were assumed to move with constant velocity. The gas distribution was taken to be Maxwellian, and the ion distribution was taken to be Maxwellian times a correction factor. The ion distribution correction factor was expanded

in Burnett functions and substituted into the Boltzmann transport equation. Multiplying this equation by an arbitrary Burnett function and integrating gave a series of moment equations. To solve the moment equations to first order, Kihara assumed polarization was the only interaction. Kihara's first order result for the mobility was identical to the Chapman and Enskog result, equation (1-10). To solve the moment equations to second order, Kihara assumed that other interactions were present, but that polarization was the dominant interaction. Kihara's second order result was

$$K = \frac{3e}{16N}\left(\frac{2\pi}{\mu kT}\right)^{\frac{1}{2}} \frac{1}{\bar{\Omega}^{(1,1)}(T)}\left[1 + \sum_{r=1}^{\infty} b_r' T^r (E/N)^{2r}\right]^{-1} \qquad (1\text{-}12)$$

where each b_r' depends on r, collision integrals, and ratios of masses, but does not depend directly on E. Thus, Kihara's result for the mobility for moderate fields was the Chapman and Enskog result multiplied by an expansion in powers of $(E/N)^2$. Kihara did not use his expansion technique to obtain an expression for D_L.

In 1974 Whealton and Mason[9] applied the Kihara method of solution to the Boltzmann equation with a diffusion term included. Like Kihara, they obtained mobility as a series in $(E/N)^2$ in the medium field region. However, whereas Kihara had not dealt with diffusion, Whealton and Mason derived an expression for D_L expressed as a series in powers of $(E/N)^2$. They found that in the medium field region D_L was related to the reduced mobility K_0 by the expression

$$D_L = D_L^W \left[1 + \frac{d \ln K_0}{d \ln (E/N)} \right] , \qquad (1\text{-}13)$$

where D_L^W was the Wannier diffusion coefficient given by equation (1-11).

Whealton and Mason also examined deviations from Fick's law of diffusion as expressed by equation (1-4). They considered the results of a diffusion current of the form

$$\vec{j}_d = - \overleftrightarrow{D} \cdot \vec{\nabla} n + \vec{\nabla} n \cdot \overleftrightarrow{Q} \cdot \vec{\nabla} n ,$$

where the tensor $\overleftrightarrow{Q}$ is a measure of the departure from Fickian diffusion. Using a polarization model, their result for the longitudinal component of the tensor Q was

$$Q_{zzz} = \frac{2kTmK^2 v_d}{e^2} (-2 + q_1 \mathcal{E}^2) , \qquad (1\text{-}14)$$

where $\mathcal{E}$ is proportional to E/N and q_1 depends on ratios of collision integrals.

In 1975 Viehland and Mason[10] expanded the earlier Whealton and Mason result by giving the ions an effective temperature due to both the random thermal energy and the energy associated with the drift through the neutral gas. This effective ion temperature produced better convergence of the series for mobility and diffusion coefficient. The effective ion temperature also gave an equivalence between ion energies due to high temperatures or due to large drift velocities. Using these results, mobilities and collision integrals for temperatures inaccessible to experiment can be found from experiments done at room temperature and

large drift velocities. Viehland and Mason found the same relation, equation (1-13), between D_L and K_0 that Whealtom and Mason had found earlier. However, their use of an effective ion temperature showed that equation (1-13) should hold for arbitrary E/N.

Goals of the Present Research

The goals of this research are as follows:

(1) To determine zero field reduced mobilities of Li^+ and Na^+ in He, Ne, and Ar.

(2) To measure the reduced mobilities of Li^+ in He, Ne, and Ar, and of Na^+ in He, Ne, Ar, and CO_2 over as wide a range of E/N as possible.

(3) To measure the longitudinal diffusion coefficients of Li^+ in He, Ne, and Ar and of Na^+ in He, Ne, Ar, and CO_2 over as wide a range of E/N as possible.

(4) To compare the measured reduced mobilities and longitudinal diffusion coefficients with the predictions of recently developed theory.

CHAPTER II

EXPERIMENTAL APPARATUS

The apparatus used for measuring the ion-gas transport properties was a drift tube mass spectrometer of ultra-high vacuum construction. Figure 1 shows a cut-away view of the apparatus and a block diagram of the ion production and detection systems. Only a brief description of the apparatus[11] as modified[12, 13, 14, 15] is presented here, because it has been described in detail elsewhere.[16]

Fig. 1 shows the apparatus consisting of the feed line system, the movable source, the drift region, the outer vacuum enclosure, the analysis region, and the supporting electronics equipment. The feed line contained the high pressure gas, and a liquid nitrogen trap to remove impurities from the gas. The ion source could be operated in either the electron-impact mode or the alkali mode, and could be raised or lowered to produce any desired drift distance up to approximately 44 cm. The drift region was surrounded by the drift field guard rings to produce the electric field exerted on the ions. The drift region also contained thermocouple leads, and the capacitance manometer leads to control the servo gas inlet valve in order to maintain a predetermined drift region pressure. The outer vacuum enclosure was differentially pumped by six-inch and four-inch diffusion pumps. The analysis region contained an RF quadrupole mass spectrometer and a channeltron multiplier and detector. The output of the channeltron was fed through a preamplifier to a 256-channel time of flight analyzer whose

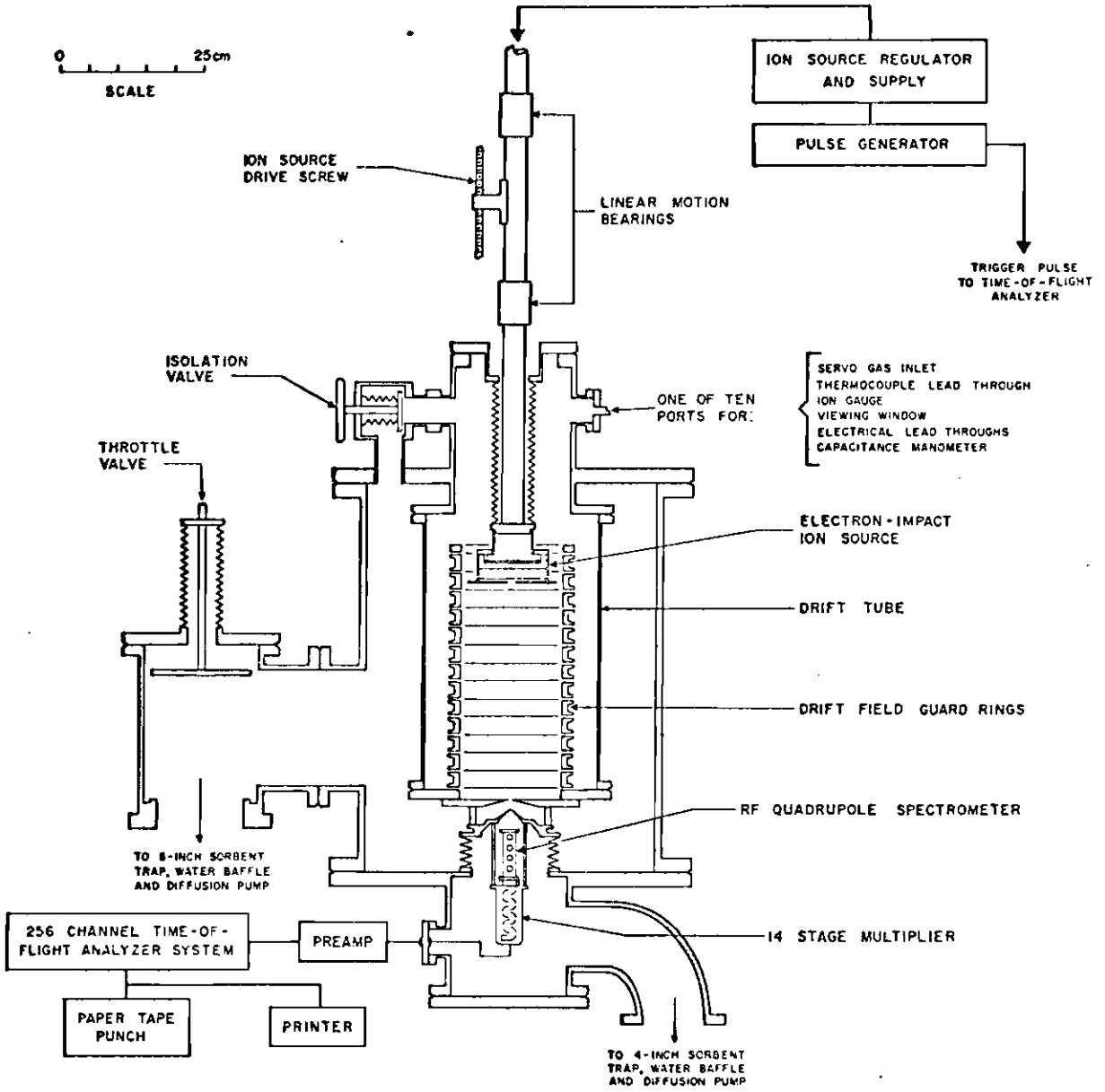

Figure 1. Sectioned View of the Drift Tube, the Outer Vacuum Enclosure, and the Analysis Region.

output was stored on paper tape.

System Preparation

The drift tube system was baked to expel gases absorbed by the interior metal surfaces after changing gases or after any repair that required the system to be opened to the atmosphere. The molecular sieve traps were baked at 450°C, and the rest of the system was baked at 250°C while under high vacuum. Almost 24 hours was required to reach final baking temperature throughout the entire system, because of the large mass of the system. The entire system was then baked for 24 hours. Cooling to ambient temperature required three days. At this time a base pressure of approximately 2×10^{-9} Torr was obtained.

System Operation

Gas

The CO_2, Ar, He, or Ne gas in which the Na^+ and Li^+ ions were studied was originally stored in commercially available high pressure tanks. The gas was admitted into the feedline by first admitting a small quantity at high pressure into a short section of the feedline. The high pressure gas bottle was closed, and the small quantity of high pressure gas was allowed to expand through a leak valve to a much lower pressure inside the remainder of the feedline. In the feedline, the low pressure gas was passed through a liquid nitrogen trap to remove impurities. During bakeout, the feedline was isolated and vented to a sorbent trap, a 2" diffusion pump, and a Welch model 1402 mechanical pump. The feedline pressure was approximately 10^{-7} Torr after bakeout, before any gas was admitted into the

system.

To maintain a constant drift region pressure, the gas in the feedline was slowly admitted into the drift chamber by a Granville-Phillips Automatic Pressure Controller which received its input from an MKS "Baratron" monometer. The pressure in the drift chamber could be maintained at a preset value to within $\pm 0.1\mu$. Gas had to be admitted continuously to maintain constant pressure in the drift region because of a small aperture at the bottom of the drift chamber through which the ions passed to be analyzed. The pressures used ranged from approximately 25μ to approximately 500μ.

The electric field within the drift region was maintained by 14 drift field guard rings. The potentials of the guard rings were maintained by a dc power supply connected across a string of resistors. Albritton[17] has shown the electric field to be uniform to within 0.1% within 4 cm of the axis in the drift region. To the top, middle, and bottom guard rings were attached chromel-alumel thermocouples to measure the temperature of the gas in the drift region.

The gas was differentially pumped by 4" and 6" diffusion pumps after it exited from the pin hole at the bottom of the drift region. Then the gas was pumped to the atmosphere by a Welch model 1397 mechanical pump.

Ions

The Li^+ and Na^+ ions were created in the source by thermionic emission from a filament coated with Li^7-enriched β-eucryptite. To accelerate ions away from the filament toward the drift region, the draw-out potential in Figure 2 was biased negatively with respect to the filament.

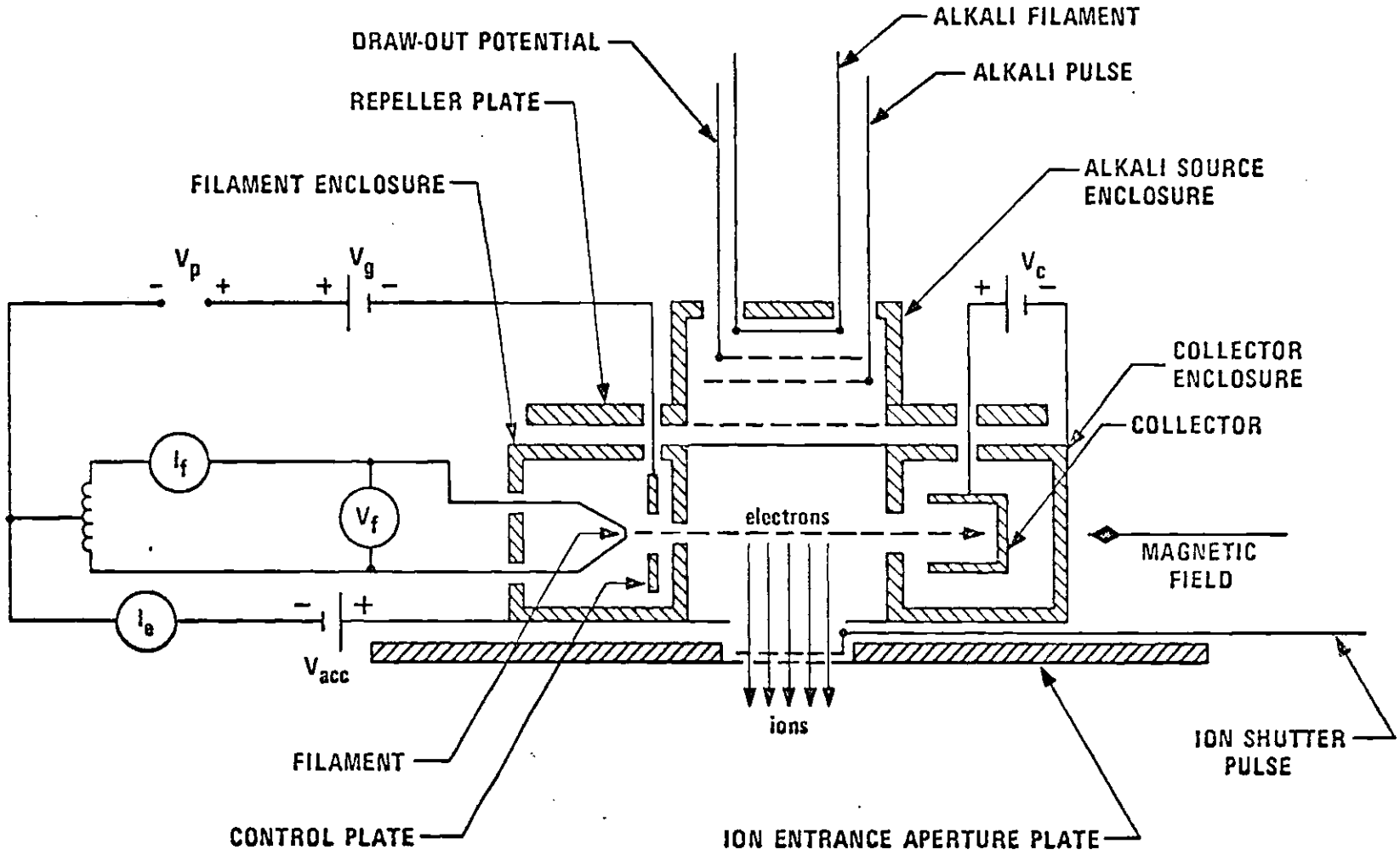

Figure 2. Schematic Diagram of the Ion Source.

Two methods of creating a pulse of ions were used. On a given run, the method used was the one which produced the greatest number of ions during a pulse, the least number of ions between pulses, and a pulse of the desired duration. The method most frequently used was to set the alkali pulse grid at a dc voltage approximately equal to the draw-out potential, thus electrically removing the alkali pulse grid. The electric field along the axis of the drift tube inside the source was maintained at the approximate value of the electric field in the drift region by properly biasing the ion entrance aperture plate, repeller plate, and magnet yoke. The Tydnall gate was biased just enough to prohibit ions from entering the drift region. At regular intervals, the Tyndall gate was pulsed to allow a burst of ions into the drift region. The second method used was to pulse the alkali pulse grid, then a few microseconds later, to pulse the Tyndall gate as described above.

The ion source was movable and could be placed at any of seven positions. The maximum drift distance, at position 7, was 43.77 cm from the Tyndall gate to the bottom plate of the drift region. The distance was approximately 6.25 cm between successive positions. For this research, only positions 4, 5, 6, and 7 were used. Four positions provided enough data so that the mobility and longitudinal diffusion coefficient could be determined. The longer drift distances were used to minimize end effects and maximize diffusion effects. Except for the case of Na^+ ions in CO_2 at low E/N, which will be discussed in a later chapter, clustering was not a problem even at the longest available drift distances.

The low E/N limit of operation was determined from the low electric field

and high pressure limits. For Na^+ in CO_2 a significant amount of clustering occurred at a pressure of 51.8 μ. This fact determined the high pressure limit for Na^+ in CO_2. For all other ion-gas combinations, no significant amount of clustering was observed at any pressure used. For these ion-gas combinations a reduced ion current at high pressures determined the high pressure operating limit. For all ion-gas combinations, as the electric field decreased, the electrostatic force on the ions decreased, reducing the number of ions that were forced out of the source and through the drift region. At low electric fields the pulse voltage on the Tyndall gate was comparable to the voltage applied to the drift region. This circumstance made it difficult to pulse the Tyndall gate without disturbing the drift field or imparting an initial velocity to the ions entering the drift region.

Operation at high E/N was limited because of the limits on high electric field strength and low gas number density. A high electric field tended to pull source ions through the Tyndall gate dc bias, so that a constant background of drifting ions was present between Tyndall pulses. At very high electric field strengths, arcing inside the drift region occurred. At low gas number density, ions receiving energy from the Tyndall gate pulse were not quickly thermalized in the drift region. Consequently, they had a higher-than-average drift velocity at the upper end of the drift region. For long drift distances, the differencing technique used to find drift velocities should cancel this effect, but for short drift distances this effect was a limiting factor. It was even more limiting on the determination of the diffusion coefficient, because the differencing technique

did not apply to the determination of the longitudinal diffusion coefficient.

After an ion swarm traveled through the drift region, most of the ions struck the grounded exit aperture plate, and the electrical charge flowed to ground. However, the ions very near the axis passed through the 0.035 cm diameter opening in the exit aperture plate. Once through, the ions were in a differentially pumped region with pressures less than 10^{-5} Torr, so that no more ion-gas diffusion occurred. The ions were accelerated and focused into an Extranuclear Lab Type 324-9 quadrupole mass filter. The ions that passed through the mass filter were detected by an Amperex Channel Electron Multiplier Type B419BL/01. The signal from the detector was fed through a Tennelec TC-L170 preamp into a Canberra 814 Preamp Amp Disc, and from there it was fed into the time-of-flight analyzer.

The time-of-flight analyzer had 256 channels. The width of each channel was adjustable by powers of two, and was set at a value that spread the arrival time spectrum over as many channels as possible. Counting of the ions ceased when any channel of the time-of-flight analyzer contained a preset value (usually 2^{12} counts). The arrival time spectrum was punched onto paper tape and fed into the computer to be analyzed. A run at one value of E/N was complete when the arrival time spectra for the four longest drift distances was obtained and analyzed. The computer results from one run gave a reduced mobility and a longitudinal diffusion coefficient for that value of pressure, E/N and temperature.

CHAPTER III

THEORY

The purpose of this chapter is to explain the four theoretical expressions for the longitudinal diffusion coefficient. These four theoretical expressions are compared with the experimental data in chapter V. The explanation is only of sufficient detail to point out the assumptions and approximations of each theory. The mathematics is covered in outline form, but it should be clear how to proceed from one step to another.

The four theories are given in chronological order. First is the Wannier theory which is based on the polarization model of the ion-neutral interaction. The Wannier longitudinal diffusion coefficient, therefore, might be expected to be valid under conditions for which the mean free time and reduced mobility are independent of E/N. Second, the Moseley and McDaniel modification of Wannier's theory replaces the constant mean free time in the Wannier theory with an experimentally determined quantity. The modification is a way of removing some of the model-dependence from the Wannier theory. Third, the Viehland-Mason correction to the longitudinal diffusion coefficient accounts for deviations from a purely polarization interaction. The correction factor is not exact, but is of second order. Fourth is an improved version of the Viehland-Mason theory incorporating high-field evaluation of collision integrals and drift velocities.

Wannier Theory

General

By integrating the Boltzmann transport equation, Wannier obtained the diffusion coefficient for the case in which the collision cross section was inversely proportional to the relative speed between ion and neutral gas molecule. First Wannier obtained an approximate differential equation for the spatially non-uniform part of the ion distribution function. Then, by comparing the integral of this equation with the definition of the diffusion coefficient, he derived an equation for the diffusion coefficient in terms of averages of the velocity components of the ion distribution. Finally, he arrived at the velocity averages by a convolution theorem which combined low field and high field velocity averages.

Theory

The Wannier theory assumes a separable solution for the ion distribution function of the form

$$n(\vec{r}, t)[f(\vec{v}) + g(\vec{v})] .$$

The spatial and temporal variation of the ion distribution is all contained in $n(\vec{r}, t)$. The velocity dependence of an assumed ion distribution moving with no spatial variation is given by $f(\vec{v})$. The correction to the velocity dependence of the ion distribution due to spatial and temporal non-uniformities is given by $g(\vec{v})$ The total ion current is the sum of the transport of the center of mass of the ion distribution and the diffusion of the ion distribution. It is straightforward to show that the ion current density due to diffusion is

$$\vec{j}(\vec{r},t) = n(\vec{r},t)\int \vec{v}\, g(\vec{v}) d^3v \quad . \tag{3-1}$$

To evaluate the integral, first write the Boltzmann transport equation for the assumed solution. Then write the Boltzmann transport equation for the assumed ion distribution moving with no diffusion. Subtracting the second equation from the first and neglecting products of small quantities gives

$$\frac{eE}{m}\frac{\partial g(\vec{v})}{\partial v_z} + \frac{N}{4\pi}\int\int [\, F(\vec{V})g(\vec{v}) - F(\vec{V}')g(\vec{v}')\,]\gamma\sigma(\gamma)\pi(\chi)\, d\Omega_{\gamma'} d^3V$$

$$= - \vec{\nabla} \ln n(\vec{r},t) \cdot (\vec{v} - \langle \vec{v} \rangle) f(\vec{v}).$$

In the above equation $F(\vec{V})$ is the assumed Maxwellian neutral gas velocity distribution, γ is the relative speed between ion and gas atom, $\sigma(\gamma)$ is the ion-neutral collision cross section, $\pi(\chi)$ is the angular dependence of the differential scattering cross section in the center of mass system, and $d\Omega_{\gamma'}$ is the differential scattering angle in the center of mass system. In the integral a primed quantity denotes that quantity after the collision. Multiplying this equation by $\vec{v}$ and integrating over ion velocity gives

$$\left(\frac{M}{M+m}\right)\left\langle\frac{1-\cos\chi}{\tau}\right\rangle\int v_i g(\vec{v})\, d^3v = -\sum_{\nu=1}^{3}\frac{\partial \ln n}{\partial \chi_\nu}\left[\langle v_i v_\nu\rangle - \langle v_i\rangle\langle v_\nu\rangle\right], \quad i = 1,2,3$$

where

$$\tau = \frac{1}{N\sigma\gamma} \tag{3-2}$$

is a constant for either polarization or isotropic scattering model. The

assumption that the collision cross section is inversely proportional to the ion-neutral relative speed is used in this step. The averages in the above equation are averages over the scattering angle in the center of mass system. Solving this equation for the integral and substituting the result into equation (3-1) gives for the ion diffusion current

$$j_i(\vec{r},t) = -\sum_{\nu=1}^{3} \frac{\partial n(\vec{r},t)}{\partial \chi_\nu} \frac{(M+m)}{M\left\langle \frac{1-\cos\chi}{\tau} \right\rangle} \left[\langle v_i v_\nu \rangle - \langle v_i \rangle \langle v_\nu \rangle \right] . \quad i = 1,2,3$$

Comparing this result with the definition in equations (1-4) and (1-5) of the diffusion coefficient gives the longitudinal and transverse diffusion coefficients in terms of averages of velocity components,

$$D_L = \frac{M+m}{m} \frac{\langle v_z^2 \rangle - \langle v_z \rangle^2}{\left\langle \frac{1-\cos\chi}{\tau} \right\rangle} \tag{3-3}$$

and

$$D_T = \frac{M+m}{m} \frac{\langle v_x^2 \rangle}{\left\langle \frac{1-\cos\chi}{\tau} \right\rangle} \tag{3-4}$$

The only difference between these equations is that the average value of the ion velocity perpendicular to the applied field is zero.

To obtain the velocity averages in equations (3-3) and (3-4), the Wannier theory uses a convolution theorem stated as follows: Let the general transport equation for constant mean free time be written

$$\frac{eE}{m}\tau\frac{\partial f(\vec{v})}{\partial v_z} + f(\vec{v}) = \frac{1}{4\pi}\iint F(\vec{V}')f(\vec{v}')\,\pi(\chi)\,d\,\Omega_{\gamma'}\,d^3V\ .$$

Let $h(\vec{v})$ and $m(\vec{v})$ denote the high field and low field solutions respectively. Then the solution $f(\vec{v})$ of the general transport equation is the convolution of the solution $h(\vec{v})$ and the solution $m(\vec{v})$;

$$f(\vec{v}) = \int h(\vec{u})\,m(\vec{v}-\vec{u})d^3u\ . \qquad (3\text{-}5)$$

The theorem is proved by constructing explicitly the equation satisfied by this convolution. The procedure is straightforward, but very involved mathematically. The proof is carried out in detail in Wannier's paper[7] and will not be repeated here.

To use the convolution theorem, the high field and the low field transport equations must be solved. In the high field limit the average velocity of the ions is so much greater than the average velocity of the neutral gas molecules that the neutral gas molecules are considered to be stationary targets. Consequently, the neutral gas distribution function reduces to a three dimensional Dirac delta function in velocity space. In terms of the angular variables χ, the scattering angle in the center of mass system, and ω, the angle between the field direction and the velocity of the ion after the collision, the high field Boltzmann transport equation can be shown to reduce to

$$\frac{eE}{m}\frac{\partial h(\vec{v})}{\partial v_z} + \frac{1}{\tau}h(\vec{v}) = \frac{(M+m)^2}{4\pi Mmv}\int_{v}^{\frac{M+m}{|M-m|}v}\frac{\pi(\chi)}{\tau}\,d^3v'\int_0^{2\pi}h(\vec{v}')d\,\omega.$$

This equation is replaced by a series of moment equations by expanding h(v) in Legendre polynomials,

$$h(\vec{v}) = \sum_{\nu=0}^{\infty} h_{\nu}(v) P_{\nu}(\text{Cos } \theta) \quad ,$$

where θ is the angle between the field direction and the velocity of the incident ion. The ω-integration can be carried out using the addition theorem for spherical harmonics. Equating coefficients of Legendre polynomials in Cos θ gives a series of integral-differential equations in h(v). Multiplying the general equation by v^{s+2} and integrating over v from zero to infinity gives the following series of moment equations

$$\frac{m}{eE}(2\nu+1)\left\langle\left[\frac{1-I_{s,\nu}(\chi)}{\tau}\right] v^{s} P_{\nu}(\text{Cos } \theta)\right\rangle = \nu(\nu+s+1)\langle v^{s-1} P_{\nu-1}(\text{Cos } \theta)\rangle$$

$$+ (\nu+1)(s-\nu)\langle v^{s-1} P_{\nu+1}(\text{Cos } \theta\rangle \quad s,\nu = 1,2,3,\ldots$$

where

$$I_{s,\nu} = \left(\frac{v}{v'}\right)^{s} P_{\nu}(\text{Cos } K) \, ,$$

and K is the angle between ion velocities before and after scattering in the lab system. Combinations of the high field moment equations with s=1, ν=1, and with s=2, ν=2 give the high field velocity averages needed for the convolution theorem,

$$\langle v_z \rangle = \left(\frac{M+m}{m}\right) \Big/ \left\langle \frac{1 - \cos\chi}{\frac{eE\tau}{m}} \right\rangle \quad ,$$

and

$$\langle v_z^2 \rangle = \frac{(M+m)^3 \left\langle \frac{M\sin^2\chi + 4m(1-\cos\chi)}{\frac{eE\tau}{m}} \right\rangle}{M^2 m \left\langle \frac{3M\sin^2\chi + 4m(1-\cos\chi)}{\frac{eE\tau}{m}} \right\rangle \left\langle \frac{1-\cos\chi}{\frac{eE\tau}{m}} \right\rangle^2} \quad .$$

Low field averages for the convolution theorem are calculated by using the Maxwell velocity distribution

$$m(\vec{v}) = \left(\frac{m}{2\pi kT}\right)^{2/3} e^{\frac{mv^2}{2kT}} \quad .$$

Applying the convolution theorem (3-5) gives

$$\begin{aligned} \langle v_z \rangle &= \iint v_z h(\vec{u}) m(\vec{v} - \vec{u})\, d^3v d^3u \\ &= \iint [u_z + (v_z - u_z)]\, h(\vec{u}) m(\vec{v} - \vec{u})\, d^3v d^3u \\ &= \int u_z h(\vec{u}) d^3u + \int p_z m(\vec{p})\, d^3p \end{aligned}$$

where $\vec{p} = \vec{v} - \vec{u}$. Thus, $\langle v_z \rangle$ at arbitrary fields can be found from a combination of high field and low field averages of v_z. Completing the high and low field integrals for $\langle v_z \rangle$ and carrying out a similar integration for $\langle v_z^2 \rangle$ gives the following averages for the diffusion coefficients:

$$\langle v_z \rangle = \frac{\left(\frac{M+m}{m}\right)}{\left\langle \frac{1-\cos\chi}{\frac{eE\tau}{m}} \right\rangle} \tag{3-6a}$$

and

$$\langle v_z^2 \rangle = \frac{kT}{m} + \frac{(M+m)^3 \left\langle \frac{M\sin^2\chi + 4m(1-\cos\chi)}{\frac{eE\tau}{m}} \right\rangle}{M^2 m \left\langle \frac{3M\sin^2\chi + 4m(1-\cos\chi)}{\frac{eE\tau}{m}} \right\rangle \left\langle \frac{1-\cos\chi}{\frac{eE\tau}{m}} \right\rangle^2} \quad . \tag{3-6b}$$

For the Maxwell model Hasse' found $\langle 1 - \cos\chi \rangle = 1.1052$, and Wannier found $\langle \sin^2\chi \rangle = 0.772$. When these numerical results are used for the velocity averages, and the velocity averages used in equation (3-3), the result is Wannier's formula for the longitudinal diffusion coefficient,

$$D_L = \left(\frac{M+m}{Mm}\right)(0.905\tau_s kT) + \frac{1}{3}\frac{(M+m)^3(M+3.72m)}{M^2 m(M+1.908m)}\left(\frac{eE}{m}\right)^2(0.905\tau_s)^3 \quad , \tag{3-7}$$

where τ_s is the mean free time for spiraling collisions.

For an elastic collision described by an attractive potential whose magnitude increases faster than r^{-2} for small r, collisions can be classified as spiraling or nonspiraling. If, for a given energy, the impact parameter b is large enough, the incident particle will be reflected at some separation distance by the effective potential consisting of the actual potential plus the centrifugal potential. In this case, the collision is a non-spiraling collision. If, for a given energy, the impact parameter b is small enough, the incident particle will continually be "sucked in" by the effective potential. In this case, the collision is a spiraling collision. If b_0 is the maximum impact parameter that produces spiraling collisions, for a given energy, a cross section for spiraling collisions, $\sigma_s = \pi b_0^2$, can be defined. The mean free time

for spiraling collisions, τ_s, is the mean free time using σ_s for the cross section, or $\tau_s = \frac{1}{N\gamma\sigma_s}$. Because D_L varies inversely as the number density N of the neutral gas, assumed to be an ideal gas, ND_L is the expression of interest. Multiplying equation (3-7) by N gives

$$ND_L = \left(\frac{M+m}{Mm}\right)(0.905N\tau_s)kT + \frac{1}{3}\frac{(M+m)^3(M+3.72m)e^2}{M^2m\,(M+1.908m)}\left(\frac{E}{N}\right)^2(0.905N\tau_s)^3. \qquad (3\text{-}8)$$

Wannier has shown that the mean free time for spiraling collisions for the polarization model is[19]

$$\tau_s = \frac{1}{N\sigma_s\gamma} = \frac{1}{2\pi Ne}\sqrt{\frac{\alpha mM}{M+m}},$$

where α is the polarizability. Thus

$$N\tau_s = \frac{1}{2\pi e}\sqrt{\frac{\alpha mM}{M+m}},$$

and therefore

$$K_0 = \frac{N}{N_0}K = \frac{e}{mN_0}\left(\frac{M+m}{M}\right)(0.905N\tau_s)$$

are independent of E/N for the polarization model. In the above equation $N_0 = 2.687 \times 10^{19}$ cm^{-3} is the number density of the neutral gas at standard temperature and pressure. To emphasize this model's independence of K_0 from E/N, the above equation will be used in the form

$$K_0(0) = \frac{e}{mN_0}\left(\frac{M+m}{M}\right)(0.905\ N\tau_s)\ . \tag{3-9}$$

Substituting equation (3-9) into equation (3-8) yields

$$ND_L = \frac{N_0 K_0(0) kT}{e} + \frac{N_0^3\, M(M+3.72m)}{3e(M+1.908m)}\left(\frac{E}{N}\right)^2 [K_0(0)]^3\ . \tag{3-10}$$

The above equation can be put into the form

$$ND_L = 2.315 \times 10^{15} K_0(0) T + 6.701 \times 10^{15} \frac{M(M+3.72m)}{(M+1.908m)}\left(\frac{E/N}{100}\right)^2 [K_0(0)]^3. \tag{3-11}$$

when T is in degrees Kelvin, E/N is in Td, the masses are in amu, $K_0(0)$ is in $cm^2/V\text{-sec}$, and ND_L is in $cm^{-1}sec^{-1}$.

Modified Wannier Theory

The original Wannier equation (3-10) has been modified[16,20] by McDaniel and Moseley to remove the dependence of that equation on the polarization model. The first term on the left in equation (3-10) needs no modification, since it is the zero field limit

$$\lim_{\frac{E}{N} \to 0} ND_L = \frac{N_0 K_0(0)\ kT}{e}$$

which is known to be correct from the Einstein relation (1-6). Therefore, the attempt to remove the model dependence from the Wannier equation deals with the second term on the left in equation (3-10). In that term $K_0(0)$ depends on the

polarization model through the mean free time for spiraling collisions, τ_s, from equation (3-9). McDaniel and Moseley remove this model dependence by evaluating K_0 at the E/N for which ND_L is to be evaluated, instead of using the polarization result of constant K_0. The modified Wannier equation is

$$ND_L(E/N) = \frac{N_0 K_0(0) kT}{e} + \frac{N_0 M(M+3.72m)}{3e(M+1.908m)} \left(\frac{E}{N}\right)^2 [K_0(E/N)]^3 . \qquad (3\text{-}12)$$

The notation $ND_L(E/N)$ emphasizes the additional field dependence in the modified Wannier equation. When $K_0(E/N)$ is in $cm^2/V\text{-}sec$, T is in degrees Kelvin, E/N is in Td, and masses are in amu, $ND_L(E/N)$ in $cm^{-1}sec^{-1}$ is given by

$$ND_L(E/N) = 2.315 \times 10^{15} K_0(0) T + 6.701 \times 10^{15} \frac{M(M+3.72m)}{(M+1.908m)} \left(\frac{E/N}{100}\right)^2 [K_0(E/N)]^3 . \qquad (3\text{-}13)$$

When the field-dependent term is expressed in terms of the measured quantities v_d and E/N, equation (3-13) becomes

$$ND_L = 2.315 \times 10^{15} K_0(0) T + 0.3455 \times 10^{17} \frac{M(M+3.72m)}{(M+1.908m)} \frac{v_d^3}{E/N} . \qquad (3\text{-}14)$$

Viehland-Mason Theory

General

In 1953 Wannier[7] noticed that for his polarization model equations (3-3) and (3-6) were equivalent to

$$D_L = \frac{v_d}{a} \left(\langle v^2 \rangle - v_d^2 \right) .$$

He reasoned that this equality was only true when v_d = KE was proportional to $a = eE/m$. However, Wannier speculated that for a more general type of interaction giving rise to a reduced mobility that varies as E/N varies, a reasonable generalization of the above equation would be

$$D_L \approx \frac{\partial v_d}{\partial a}\left(\langle v_z^2 \rangle - v_d^2\right) .$$

Using the definitions (1-1) and (1-2), Wannier's generalized equation becomes

$$D_L \approx \frac{v_d}{a}\left(\langle v_z^2 \rangle - v_d^2\right)\left\{1 + \frac{d \ln K_0}{d \ln(E/N)}\right\} .$$

Wannier's generalized D_L is thus given by a polarization-type D_L multiplied by a correction factor of the form

$$1 + \frac{d \ln K_0}{d \ln (E/N)} .$$

His generalized result has given rise to many theoretical expressions[9, 10, 21, 22] for D_L for interactions other than pure polarization, and for E/N above the low field region. In each case the result for D_L has the form of a Wannier-type D_L multiplied by a correction factor similar to that given above.

Viehland and Mason[10] solved the Boltzmann transport equation by a series method which works well in the sense of rapid convergence of the series as long as ion-neutral collisions are dominated by polarization. The series method was developed by Kihara[8] for mobilities, and extended first by Whealton and Mason[9] and then by Viehland and Mason to include diffusion effects. The method consists

of expanding the ion distribution function in a series of Burnett functions, because they are eigenfunctions for the polarization model. Therefore, they should be approximate eigenfunctions for the actual ion-neutral interaction. In these Burnett functions an ion temperature is used instead of the customary neutral gas temperature. The coefficients of the Burnett functions are used to obtain a first and a second approximation to K_0 and D_L. The first approximation yields the Kihara mobility and the Wannier diffusion coefficient. In the second approximation, by eliminating variables relating K_0 and D_L, the Viehland-Mason ND_L is the modified Wannier ND_L from equation (3-14) multiplied by the correction factor

$$1 + \frac{d \ln K_0}{d \ln (E/N)} .$$

Recently Viehland and Mason[23] have incorporated improvements in their earlier theory. They have evaluated the necessary collision integrals for the high field limit instead of using the low field polarization model. Also, they have used an empirical curve to relate the first order expression for the drift velocity to the exact drift velocity, instead of simply equating the two. With these two improvements, the most recent version of the Viehland-Mason theory gives

$$ND_L = \left\{ \frac{N_0 K_0(0) kT}{e} + \frac{N_0 K_0(E/N) M(M+3.2m)}{3e(M+1.4m)} \left[(1+\gamma) v_d \right] \right\} \left\{ 1 + \frac{d \ln K_0}{d \ln (E/N)} \right\}, \qquad (3\text{-}15)$$

where γ is the empirical factor correcting the drift velocity.

Original Viehland-Mason Theory

The Boltzmann transport equation for the ions is

$$\frac{\partial f}{\partial t} + \vec{v}\cdot\vec{\nabla} f + \frac{eE}{m}\frac{\partial f}{\partial v_z} = \int\int\left[f(\vec{v}')F(\vec{V}) - f(\vec{v})F(\vec{V})\right]\gamma\sigma\, d\Omega\, d^3V \ .$$

Here the sumbols have the same meaning as in the development of the Wannier theory with the following exceptions. $f(\vec{v})$ is the ion distribution function with diffusion effects included, in contrast to the Wannier theory where $f(\vec{v})$ was the ion distribution function excluding diffusion. Also, in contrast to the Wannier theory, σ here contains both the energy and the angular dependence of the scattering. As in the Wannier theory $F(\vec{V})$ is taken to be the Maxwellian velocity distribution for the neutral gas molecules. Multiplying the transport equation from the left by any function Ψ of ion velocity, integrating over ion velocity, and using the collision property

$$\gamma\,\sigma(\gamma)\, d^3V d^3v = \gamma'\,\sigma(\gamma')\, d^3V' d^3v'$$

gives

$$\frac{\partial}{\partial t}[n\langle\Psi\rangle] + \vec{\nabla}\cdot[n\langle\vec{v}\,\Psi\rangle] - \frac{en}{m}E\left\langle\frac{\partial\Psi}{\partial v_z}\right\rangle = -nN\langle J\Psi\rangle, \qquad (3\text{-}16)$$

where the operation J is defined by

$$J\,\Psi = \frac{1}{N}\int\int F(\vec{V})[\Psi(\vec{v}) - \Psi(\vec{v}')]\gamma\sigma\, d\Omega\, d^3V \ , \qquad (3\text{-}17)$$

and the average values are defined by

$$\langle A \rangle = \frac{1}{n} \int f A \, d^3 v \, . \tag{3-18}$$

When $\Psi = 1$ is used in equation (3-16), $\partial n/\partial t$ can be found and used in equation (3-16) to give

$$\frac{\partial \langle \Psi \rangle}{\partial t} - \langle \Psi \rangle \vec{\nabla} \cdot \langle \vec{v} \rangle + \vec{\nabla} \cdot \langle \vec{v} \Psi \rangle + [\langle \vec{v} \Psi \rangle - \langle \vec{v} \rangle \langle \Psi \rangle] \cdot \vec{\nabla} \ln n$$

$$- \frac{eE}{m} \left\langle \frac{\partial \Psi}{\partial v_z} \right\rangle = - N \langle J \Psi \rangle \, .$$

The following approximations based on time scales are made to simplify the above equation. It is assumed[24] that the time for the variation of macroscopic quantities, e. g. $\langle \Psi \rangle$, is much longer than the mean time between collisions, so that $\partial \langle \Psi \rangle / \partial t$ may be neglected in the above equation. Further, it is assumed that the moments of $\langle \vec{v} \rangle$ and $\langle \vec{v} \Psi \rangle$ are independent of position, so that the terms $\vec{\nabla} \cdot \langle \vec{v} \rangle$ and $\vec{\nabla} \cdot \langle \vec{v} \Psi \rangle$ may be neglected in the above equation. These approximations are examined in detail in Appendix IV. Using these approximations, the equation to be solved is

$$N \langle J \Psi \rangle = \frac{eE}{m} \left\langle \frac{\partial \Psi}{\partial v_z} \right\rangle - [\langle \vec{v} \Psi \rangle - \langle \vec{v} \rangle \cdot \langle \Psi \rangle] \cdot \vec{\nabla} \ln n \, . \tag{3-19}$$

If the ion-neutral collisions are dominated by polarization, then convenient function Ψ to use are eigenfunctions of the polarization model, the Burnett functions

$$\Psi_{\ell m}^{(r)} = \omega^{\ell} S_{\ell + \frac{1}{2}}^{(r)} (\omega^2) P_{\ell}^{(m)} (\text{Cos } \theta) \, e^{im\Phi}, \tag{3-20}$$

where $\omega^2 = mv^2/2kT_i$ and $\text{Cos}\,\theta = v_z/v$. The $S^{(r)}_{\ell+\frac{1}{2}}(\omega^2)$ are Sonine Polynomials.[25] T_i is defined by

$$\frac{3}{2} k T_i = \frac{1}{2} m \langle v^2 \rangle . \tag{3-21}$$

Besides being an intuitive choice for ion temperature, it will be shown after equation (3-46) that this choice for T_i leads to hopes of convergence at high E/N. Viehland and Mason's introduction of the ion temperature at this point distinguishes their work from the earlier Whealton and Mason theory.[9]

Using any of the Burnett functions $\Psi^{(r)}_{\ell m}$ in equation (3-19) yields a term $\langle J \Psi^{(r)}_{\ell m} \rangle$ which can be expanded in terms of the $\Psi^{(r)}_{\ell m}$,

$$J \Psi^{(r)}_{\ell m} = \sum_s a_{rs}(\ell)\, \Psi^{(s)}_{\ell m} , \tag{3-22}$$

where

$$a_{rs}(\ell) = \frac{\int e^{-\omega^2} \Psi^{(s)}_{\ell m}\, J \Psi^{(r)}_{\ell m}\, d^3\omega}{\int e^{-\omega^2} \Psi^{(s)}_{\ell m}\, \Psi^{(r)}_{\ell m}\, d^3\omega} . \tag{3-23}$$

Noting that $\Psi^{(0)}_{10} = \omega_z$, equation (3-19) becomes

$$\sum_s \frac{a_{rs}(\ell)}{a_{00}(1)} \langle \Psi^{(s)}_{\ell 0} \rangle = E \left[\frac{\ell(\ell + r + \frac{1}{2})}{(\ell + \frac{1}{2})} \langle \Psi^{(r)}_{\ell-1,0} \rangle - \left(\frac{\ell+1}{\ell+\frac{1}{2}} \right) \langle \Psi^{(r-1)}_{\ell+1,0} \rangle \right]$$

$$- h^{(r)}_{\ell 0} \frac{E k T_i}{eE} \frac{d \ln n}{d \ln z} , \tag{3-24}$$

where

$$E = \frac{eE}{mN} \left(\frac{m}{2kT_i} \right)^{\frac{1}{2}} \frac{1}{a_{00}(1)} , \tag{3-25}$$

and

$$h_{\ell 0}^{(r)} = \left(\frac{\ell+1}{\ell+\frac{1}{2}}\right)\left[\langle \Psi_{\ell+1,0}^{(r+1)} \rangle - \langle \Psi_{\ell+1,0}^{(r-1)} \rangle\right] + \frac{\ell(\ell+r+\frac{1}{2})}{(\ell+\frac{1}{2})} \langle \Psi_{\ell-1,0}^{(r)} \rangle$$

$$- \frac{\ell(r+1)}{(\ell+\frac{1}{2})} \langle \Psi_{\ell-1,0}^{(r+1)} \rangle - 2 \langle \Psi_{10}^{(0)} \rangle \langle \Psi_{\ell 0}^{(r)} \rangle . \qquad (3\text{-}26)$$

The first approximation consists of evaluating $\langle \Psi_{10}^{(0)} \rangle$ by retaining in the sum in equation (3-24) only those coefficients $a_{rs}(\ell)$ which are non-zero for the polarization model. For $\ell = 1$, $r = 0$, the only non-zero coefficient in the sum is $a_{00}(1)$, so that equation (3-24) reduces to

$$\langle \Psi_{10}^{(0)} \rangle = \mathcal{E} - h_{10}^{(0)} \frac{\mathcal{E} k T_i}{eE} \frac{d \ln n}{dz} . \qquad (3\text{-}27)$$

In evaluating $h_{10}^{(0)}$ from equation (3-26) density gradients are dropped to be consistent with the approximations involved in obtaining equation (3-19). Comparing equation (3-27) to the defining equation (1-8) in the form

$$\langle v_z \rangle = K\mathcal{E} - D_L \frac{d \ln n}{dz} ,$$

gives

$$K = \frac{e}{m N a_{00}(1)} , \qquad (3\text{-}28$$

and

$$\frac{e D_L}{K} = h_{10}^{(0)} k T_i . \qquad (3\text{-}29)$$

A straightforward, but detailed calculation[26] of $a_{00}(1)$ gives

$$a_{00}^{(1)} = \frac{8}{3}\left(\frac{M}{M+m}\right)\bar{\Omega}^{(1,1)}(T_{eff})\sqrt{\frac{2kT_{eff}}{\pi\mu}} \tag{3-30}$$

where μ is the ion-neutral reduced mass, and $\bar{\Omega}^{(1,1)}(T_{eff})$ is a collision integral defined by

$$\bar{\Omega}^{(\ell,s)}(T_{eff}) = \frac{1}{(s+1)!(kT_{eff})^{s+2}}\int_0^\infty e^{-\frac{E}{kT_{eff}}} E^{s+1}\bar{Q}^{(\ell)}(E)dE\,, \tag{3-31}$$

and the diffusion cross section $\bar{Q}^{(\ell)}(E)$ is defined by

$$\bar{Q}^{(\ell)}(E) = \frac{2\pi}{\left[1-\frac{1+(-1)^{\ell}}{2(\ell+1)}\right]}\int_0^\pi (1-\mathrm{Cos}^{\ell}\chi)\,\sigma\,\mathrm{Sin}\,\chi\,d\chi\,, \tag{3-32}$$

and

$$T_{eff} = \frac{mT+MT_i}{m+M}\,. \tag{3-33}$$

The integrals in equations (3-31) and (3-32) are normalized so that both $\bar{\Omega}^{(\ell,s)}(T_{eff})$ and $\bar{Q}^{(\ell)}(E)$ are πd^2 for rigid spheres of diameter d. Using equation (3-30) in equation (3-28) gives for the mobility.

$$K = \frac{3e}{16N}\sqrt{\frac{2\pi}{\mu kT_{eff}}}\;\frac{1}{\bar{\Omega}^{(1,1)}(T_{eff})}\,, \tag{3-34}$$

which is identical to the Kihara mobility[8] for low fields with T replaced by T_{eff}.

To compare the Viehland-Mason result (3-29) for D_L with Wannier's

result (3-10) for ND_L the quantity $h_{10}^{(0)}$ in the Viehland-Mason theory must be evaluated. As can be seen from equation (3-26), the moments $\langle \Psi_{20}^{(0)} \rangle$, $\langle \Psi_{10}^{(0)} \rangle$, and $\langle \Psi_{00}^{(1)} \rangle$ must be known to evaluate $h_{10}^{(0)}$. These three moments are found by solving equation (3-24). Consistent with the approximations of first order theory,[26] only terms in the sum for which $s \leq r$ are retained, and the gradient term is omitted. Under these conditions equation (3-24) reduces to

$$\langle \Psi_{10}^{(0)} \rangle = E$$

for $\ell = 1$, $r = 0$; to

$$\frac{a_{10}^{(0)}}{a_{00}^{(1)}} + \frac{a_{11}^{(0)}}{a_{00}^{(1)}} \langle \Psi_{00}^{(1)} \rangle = -2E \langle \Psi_{10}^{(0)} \rangle$$

for $\ell = 0$, $r = 1$; and to

$$\frac{a_{00}^{(2)}}{a_{00}^{(1)}} \langle \Psi_{20}^{(0)} \rangle = 2E \langle \Psi_{10}^{(0)} \rangle$$

for $\ell = 2$, $r = 0$. In addition, it will be useful later to have $\langle \Psi_{10}^{(1)} \rangle$. When $\ell = 1$, $r = 1$, equation (3-24) becomes

$$\frac{a_{10}^{(1)}}{a_{00}^{(1)}} \langle \Psi_{10}^{(0)} \rangle + \frac{a_{11}^{(1)}}{a_{00}^{(1)}} \langle \Psi_{10}^{(1)} \rangle = \frac{E}{3}\left[5 \langle \Psi_{00}^{(1)} \rangle - 4 \langle \Psi_{20}^{(0)} \rangle\right].$$

The solution of these equations is

$$<\Psi_{10}^{(0)}> = E \quad , \tag{3-35a}$$

$$<\Psi_{00}^{(1)}> = -\frac{a_{10}^{(0)}}{a_{11}^{(0)}} - 2E^2 \frac{a_{00}^{(1)}}{a_{11}^{(0)}} \quad , \tag{3-35b}$$

$$<\Psi_{10}^{(1)}> = -E\left[\frac{a_{10}^{(1)}}{a_{11}^{(1)}} + \frac{5}{3}\frac{a_{00}^{(1)}a_{10}^{(0)}}{a_{11}^{(1)}a_{11}^{(0)}}\right] - \frac{2}{3}E^3\frac{a_{00}^{(1)}}{a_{11}^{(1)}}\left[5\frac{a_{00}^{(1)}}{a_{11}^{(0)}} + 4\frac{a_{00}^{(1)}}{a_{00}^{(2)}}\right] , \tag{3-35c}$$

and

$$<\Psi_{20}^{(0)}> = 2E^2\frac{a_{00}^{(1)}}{a_{00}^{(2)}} \quad . \tag{3-35d}$$

Using these moments in equation (3-26) with $\ell = 1$, $r = 0$ yields

$$h_{10}^{(0)} = 1 + \frac{4}{3}<\Psi_{20}^{(0)}> - \frac{2}{3}<\Psi_{10}^{(1)}> - 2<\Psi_{10}^{(0)}>^2 \quad ,$$

or

$$h_{10}^{(0)} = 1 + \frac{2}{3}\frac{a_{10}^{(0)}}{a_{11}^{(0)}} - 2\left[1 - \frac{4}{3}\frac{a_{00}^{(1)}}{a_{00}^{(2)}} - \frac{2}{3}\frac{a_{00}^{(1)}}{a_{11}^{(0)}}\right]E^2 \quad .$$

A straightforward, but tedious evaluation of the matrix elements[26] yields

$$h_{10}^{(0)} = \frac{T}{T_i} - 2\left\{1 - \frac{10(m+M)}{3(5m+3MA^*)} - \frac{(m+M)}{3m}\right\}E^2$$

where

$$A^* = \frac{\bar{\Omega}^{(2,2)}(T_{eff})}{\bar{\Omega}^{(1,1)}(T_{eff})} \quad . \tag{3-36}$$

When E is used from equation (3-25), the result is

$$h_{10}^{(0)} = \frac{T}{T_i} - 2\left\{1 - \frac{10(m+M)}{3(5m+3MA^*)} - \frac{(m+M)}{3m}\right\}\left(\frac{eE}{mN}\right)^2\left(\frac{m}{2kT_i}\right)\left[\frac{1}{a_{00}(1)}\right]^2 .$$

Using this expression and equation (3-28) in equation (3-29) gives

$$\frac{eD_L}{K} = kT - \left\{1 - \frac{10(m+M)}{3(5m+3MA^*)} - \frac{(m+M)}{3m}\right\}\left[\frac{eE}{mNa_{00}(1)}\right]^2 m . \qquad (3-37)$$

From equation (3-28) it can be seen that the first order approximation to v_d is

$$v_d = \frac{eE}{mNa_{00}(1)} \qquad (3-38)$$

Using v_d from equation (3-38) in equation (3-37) and simplifying yields

$$\frac{eD_L}{K} = kT + \left[\frac{5m-(2m-M)A^*}{5m+3MA^*}\right] Mv_d^2 \qquad (3-39)$$

When the value $A^* = 0.8713$[23] for the polarization interaction is used, equation (3-39) becomes

$$\frac{eD_L}{K} = kT + \frac{M}{3}\left(\frac{M+3.72\,m}{M+1.91m}\right) v_d^2$$

or

$$ND_L = \frac{N_0 K_0 kT}{e} + \frac{N_0 K_0 M}{3e}\left(\frac{M+3.72m}{M+1.91m}\right)v_d^2 . \qquad (3\text{-}40)$$

Thus, the first order Viehland and Mason result (3-40) is identical to the Wannier result (3-10).

Second order theory corrects for small variations in mobility and diffusion coefficient at intermediate E/N. At low E/N the coefficients $a_{rs}(\ell)$ in equation (3-24) should have approximately the values for a pure polarization model. Since in the polarization model $a_{rs}(\ell) = 0$ for $s > r$,[23] the actual coefficients $a_{rs}(\ell)$ for $s > r$ are assumed small compared to the dominant terms for the polarization model. Viehland and Mason list[26] expressions for some of the $a_{rs}(\ell)$ for an arbitrary interaction and these formulae indicate that at low E/N deviations from polarization, the $|a_{rs}(\ell)|$ becomes smaller as $|s - r|$ becomes larger. Therefore, the only coefficient in equation (3-24) with $s > r$ that is retained in the second order is $a_{r\,r+1}(\ell)$.

Using $\ell = 1$, $r = 0$ in equation (3-24) gives to second order

$$\langle \Psi_{10}^{(0)} \rangle + \frac{a_{01}^{(1)}}{a_{00}^{(1)}} \langle \Psi_{10}^{(1)} \rangle = E - h_{10}^{(0)} \frac{EkT_i}{eE} \frac{d \ln n}{dz} . \qquad (3\text{-}41)$$

As before, the $h_{\ell 0}^{(r)}$ are found from equation (3-26) by determining the $\langle \Psi_{\ell 0}^{(r)} \rangle$ from equation (3-24) without the d ln n/dz terms.

To find $\langle \Psi_{10}^{(0)} \rangle$ for equation (3-41), use equation (3-24) with $\ell = 1$, $r = 1$ to get

$$\langle \Psi_{10}^{(1)} \rangle = - \frac{a_{10}^{(1)}}{a_{11}^{(1)}} \langle \Psi_{10}^{(0)} \rangle + \frac{a_{00}^{(1)}}{a_{11}^{(1)}} \left\{ \left[\frac{5}{3} \langle \Psi_{00}^{(1)} \rangle - \frac{4}{3} \langle \Psi_{20}^{(0)} \rangle \right] E \right.$$

$$\left. - h_{10}^{(1)} \frac{EkT_i}{eE} \frac{d \ln n}{dz} \right\} . \qquad (3\text{-}42)$$

$\langle \Psi_{00}^{(1)} \rangle$ is found using equation (3-24) with $\ell = 0$, $r = 1$ to give

$$\langle \Psi_{00}^{(1)} \rangle = - \frac{a_{10}^{(0)}}{a_{11}^{(0)}} - \frac{a_{00}^{(1)}}{a_{11}^{(0)}} \left[2E \langle \Psi_{10}^{(0)} \rangle + h_{00}^{(1)} \frac{EkT_i}{eE} \frac{d \ln n}{dz} \right]. \qquad (3\text{-}43)$$

$\langle \Psi_{10}^{(0)} \rangle$ is given by equation (3-27), and $\langle \Psi_{20}^{(0)} \rangle$ is found by using equation (3-24) with $\ell = 2$, $r = 0$ to give

$$\langle \Psi_{20}^{(0)} \rangle = \frac{a_{00}^{(1)}}{a_{00}^{(2)}} \left[2E \langle \Psi_{10}^{(0)} \rangle - h_{20}^{(0)} \frac{EkT_i}{eE} \frac{d \ln n}{dz} \right] \qquad (3\text{-}44)$$

with $\langle \Psi_{10}^{(0)} \rangle$ given by equation (3-27). Substituting equations (3-27), (3-43), and (3-44) into equation (3-42) and using the result in equation (3-41) gives

$$\langle \Psi_{10}^{(0)} \rangle = E \left\{ 1 + \frac{a_{11}^{(1)}}{a_{11}^{(1)}} \left[\frac{5}{3} \frac{a_{10}^{(0)}}{a_{11}^{(1)}} + \frac{2}{3} E^2 \left(5 \frac{a_{00}^{(1)}}{a_{11}^{(0)}} + 4 \frac{a_{00}^{(1)}}{a_{00}^{(2)}} \right) \right] \right\}$$

$$- \left(\frac{EkT_i}{eE} \frac{d \ln n}{dz} \right) \left\{ h_{10}^{(0)} - \frac{a_{01}^{(1)}}{a_{11}^{(1)}} \left[h_{10}^{(1)} + \frac{5}{3} \frac{a_{10}^{(0)}}{a_{11}^{(0)}} h_{10}^{(0)} \right. \right.$$

$$\left. \left. + \frac{5}{3} \frac{a_{00}^{(1)}}{a_{11}^{(0)}} E h_{00}^{(1)} - \frac{4}{3} \frac{a_{00}^{(1)}}{a_{00}^{(2)}} E h_{20}^{(0)} \right] \right\} . \qquad (3\text{-}45)$$

where only terms of order E^3 have been retained. Using the Burnett function

$$\Psi_{10}^{(0)} = \left(\frac{m}{2kT_i}\right)^{\frac{1}{2}} v_z$$

and comparing equation (3-45) with the equation

$$\langle v_z \rangle = KE - D_L \frac{d \ln n}{dz}$$

that defined K and D_L gives

$$K = \frac{e}{mNa_{00}^{(1)}} \left\{ 1 + \frac{a_{01}^{(1)}}{a_{11}^{(1)}} \left[\frac{5}{3} \frac{a_{10}^{(0)}}{a_{11}^{(1)}} + \frac{a_{10}^{(1)}}{a_{00}^{(1)}} + \frac{2}{3} E^2 \left(5 \frac{a_{00}^{(1)}}{a_{11}^{(0)}} + 4 \frac{a_{00}^{(1)}}{a_{00}^{(2)}} \right) \right] \right\}, \tag{3-46}$$

and

$$D_L = \frac{kT_i}{mNa_{00}^{(1)}} \left\{ h_{10}^{(0)} - \frac{a_{01}^{(1)}}{a_{11}^{(1)}} \left[h_{10}^{(0)} + \frac{5}{3} \frac{a_{10}^{(0)}}{a_{11}^{(0)}} h_{10}^{(0)} \right.\right.$$

$$\left.\left. + \frac{5}{3} \frac{a_{00}^{(1)}}{a_{11}^{(0)}} E h_{00}^{(1)} - \frac{4}{3} \frac{a_{00}^{(1)}}{a_{00}^{(2)}} E h_{20}^{(0)} \right] \right\}. \tag{3-47}$$

Before expanding in powers of E, a word should be said about the expansion parameter E. Combining equations (3-25) and (3-30) gives

$$E = \left(\frac{3e\pi^{\frac{1}{2}}}{16\mu^{\frac{1}{2}}}\right) \left(\frac{E}{N}\right) \left[(kT_i)^{\frac{1}{2}} (kT_{eff})^{\frac{1}{2}} \bar{\Omega}^{(1,1)} (T_{eff}) \right]^{-1}$$

At low E/N, T_i in equation (3-21) and T_{eff} in equation (3-33) are essentially T, so

that ε is proportional to E/N. However, at high E/N, T_i and T_{eff} are both proportional to v_d^2. Viehland and Mason[27] show that at high E/N $\bar{\Omega}^{(1,1)}(T_{eff})$ is proportional to v_d^{-2} E/N. Therefore, at high E/N, the expansion parameter ε reaches a constant limiting value independent of E/N. It is this finiteness of ε over the entire range of E/N that gives rise to hopes for rapid convergence of a series in powers of ε.

To see how D_L varies with ε, the $h_{\ell 0}^{(r)}$ terms in equation (3-47) are found from the definition (3-26) to be

$$h_{10}^{(0)} = 1 - 2\langle\Psi_{10}^{(0)}\rangle^2 - \frac{2}{3}\langle\Psi_{00}^{(1)}\rangle + \frac{4}{3}\langle\Psi_{20}^{(0)}\rangle ,$$

$$h_{10}^{(1)} = \frac{4}{3}\langle\Psi_{20}^{(1)}\rangle - \frac{4}{3}\langle\Psi_{20}^{(0)}\rangle + \frac{5}{3}\langle\Psi_{00}^{(1)}\rangle - \frac{4}{3}\langle\Psi_{00}^{(2)}\rangle - 2\langle\Psi_{00}^{(1)}\rangle\langle\Psi_{10}^{(1)}\rangle ,$$

$$h_{00}^{(1)} = 2\left(\langle\Psi_{10}^{(1)}\rangle - \langle\Psi_{10}^{(0)}\rangle - \langle\Psi_{10}^{(0)}\rangle\langle\Psi_{00}^{(1)}\rangle\right) , \text{ and}$$

$$h_{20}^{(0)} = \frac{6}{5}\langle\Psi_{30}^{(0)}\rangle + 2\langle\Psi_{10}^{(0)}\rangle - \frac{4}{5}\langle\Psi_{10}^{(1)}\rangle - 2\langle\Psi_{10}^{(0)}\rangle\langle\Psi_{20}^{(0)}\rangle .$$

To order ε^2, $\langle\Psi_{20}^{(1)}\rangle$, $\langle\Psi_{00}^{(2)}\rangle$, and $\langle\Psi_{30}^{(0)}\rangle$ vanish. Using the $\langle\Psi_{\ell 0}^{(r)}\rangle$ from equations (3-35) for the remaining elements gives

$$h_{10}^{(0)} = 1 + \frac{2}{3}\frac{a_{10}^{(0)}}{a_{11}^{(0)}} - 2\left[1 - \frac{4}{3}\frac{a_{00}^{(1)}}{a_{00}^{(2)}} - \frac{2}{3}\frac{a_{00}^{(1)}}{a_{11}^{(0)}}\right]\varepsilon^2 , \tag{3-48a}$$

$$h_{10}^{(1)} = -\frac{5}{3}\frac{a_{10}^{(0)}}{a_{11}^{(0)}} - \frac{2}{3}\varepsilon^2\left[4\frac{a_{00}^{(1)}}{a_{00}^{(2)}} + 5\frac{a_{00}^{(1)}}{a_{11}^{(0)}}\right] , \tag{3-48b}$$

$$h_{00}^{(1)} = -2\varepsilon\left[1 + \frac{a_{10}^{(1)}}{a_{11}^{(1)}}\right] , \text{ and} \tag{3-48c}$$

$$h_{20}^{(0)} = 2E. \tag{3-48d}$$

In using these expressions to evaluate D_L, the approximations of second order theory must be used consistently. As previously explained, each of the three quantities E^2, $a_{01}(1)$, and $a_{10}(0)$ are assumed to be small. The highest order of the three small quantities E^2, $a_{01}(1)$, and $a_{10}(0)$ that will be retained in evaluating D_L will be the product of any two of them. Using equations (3-48) and (3-47) to the order described above gives

$$D_L = \frac{kT_i}{mNa_{00}(1)}\left\{h_{10}^{(0)} + \frac{4}{3}E^2\frac{a_{01}(1)}{a_{11}(1)}\left[5\frac{a_{00}(1)}{a_{11}(0)} + 4\frac{a_{00}(1)}{a_{00}(2)}\right]\right\}. \tag{3-49}$$

To this order of E^2, no error is made by multiplying the E^2 term above by 1 in the form of $h_{10}^{(0)}$. This operation gives

$$D_L = \frac{kT_i}{mNa_{00}(1)}h_{10}^{(0)}\left\{1 + \frac{4}{3}E^2\frac{a_{01}(1)}{a_{11}(1)}\left[5\frac{a_{00}(1)}{a_{11}(0)} + 4\frac{a_{00}(1)}{a_{00}(2)}\right]\right\}. \tag{3-50}$$

The longitudinal diffusion coefficient can be related to the reduced mobility by noting that since $|a_{01}(1)/a_{11}(1)| \ll 1$, the approximation $\ln(1+x) \approx x$ for $|x| \ll 1$ can be used in equation (3-46) to give

$$\ln K \approx \ln e - \ln[mNa_{00}(1)] + \frac{a_{01}(1)}{a_{11}(1)}\left\{\frac{5}{3}\frac{a_{10}(0)}{a_{11}(1)} + \frac{a_{10}(1)}{a_{00}(1)} + \frac{2}{3}E^2\left(5\frac{a_{00}(1)}{a_{11}(0)} + 4\frac{a_{00}(1)}{a_{00}(2)}\right)\right\}.$$

Then

$$\frac{d \ln K_0}{d \ln(E/N)} \approx \frac{4}{3} \xi^2 \frac{a_{01}^{(1)}}{a_{11}^{(1)}} \left[5 \frac{a_{00}^{(1)}}{a_{11}^{(0)}} + 4 \frac{a_{00}^{(1)}}{a_{00}^{(2)}} \right].$$

Using the above relation in equation (3-50) gives the Viehland-Mason result

$$D_L = \frac{kT_i}{mNa_{00}^{(1)}} h_{10}^{(0)} \left\{ 1 + \frac{d \ln K_0}{d \ln(E/N)} \right\} \tag{3-51}$$

From equation (3-40) and the equation preceding equation (3-37),

$$\frac{kT_i}{ma_{00}^{(1)}} h_{10}^{(0)} = \frac{N_0 K_0 kT}{e} + \frac{N_0 K_0 M}{3e} \left(\frac{M+3.72m}{M+1.91m} \right) v_d^2$$

when the ratio of the collision integrals is evaluated assuming the polarization interaction. To be consistent in using second order theory, the reduced mobility in the field-dependent term is dependent on E/N. Thus, the second order Viehland-Mason expression for ND_L is

$$ND_L = \left\{ \frac{N_0 K_0(0) kT}{e} + \frac{N_0 M}{3e} \left(\frac{M+3.72m}{M+1.91m} \right) \left(\frac{E}{N} \right)^2 \left[K_0(E/N) \right]^{-3} \right\}$$

$$\times \left\{ 1 + \frac{d \ln K_0}{d \ln(E/N)} \right\}. \tag{3-52}$$

When equation (3-52) is rewritten expressing the reduced mobility in $cm^2/V\text{-}sec$, E/N in Td, temperature in ^oK, masses in amu, and ND_L in $cm^{-1}sec^{-1}$ the result is

$$ND_L = \left\{2.315 \times 10^{15} K_0(0)T + 6.701 \times 10^{15} \frac{M(M+3.72m)}{(M+1.91m)} \left(\frac{E/N}{100}\right)^2 \left[K_0(E/N)\right]^3\right\}$$

$$\times \left\{1 + \frac{d \ln K_0}{d \ln(E/N)}\right\} . \qquad (3\text{-}53)$$

Recently Viehland and Mason[23] have made further improvements in their theoretical D_L. Their improvements directly affect their old first order expression for D_L. The improved first order D_L produces an improved second order D_L, because the second order D_L is the first order D_L multiplied by the correction factor $[1 + d \ln K_0/d \ln(E/N)]$.

The first improvement is in the numerical value of A^*, the ratio of collision integrals defined by equation (3-36). Instead of using $A^* = 0.8713$ for the polarization interaction, Viehland and Mason use $A^* = 1.2$. The value 1.2 was obtained from beam data and is considered more appropriate for high E/N diffusion. Using $A^* = 1.2$ in equation (3-39) gives

$$D_L = \frac{KkT}{e} + \frac{KM}{3e}\left(\frac{M+3.2m}{M+1.4m}\right)v_d^2 . \qquad (3\text{-}54)$$

The second improvement involves the drift velocity V_d. Viehland and Mason recognize that v_d in equation (3-38) and (3-54) is not the exact drift velocity, but only the first order approximation $(v_d)_1$ to the exact drift velocity. Thus, equation (3-38) should be

$$(v_d)_1 = \frac{eE}{mNa_{00}^{(1)}} ,$$

and equation (3-54) should be

$$D_L = \frac{KkT}{e} + \frac{KM}{3e}\left(\frac{M+3.2m}{M+1.4m}\right)(v_d)_1^2 \tag{3-55}$$

In the low field region $(v_d)_1$ and v_d are essentially the same, but in the high field region $(v_d)_1$ and v_d may differ significantly. Viehland and Mason suggest making the transition from the low field region to the high field region by the following expression for $(v_d)_1$:

$$(v_d)_1 = v_d(1 + \gamma) \tag{3-56}$$

where

$$\gamma = \begin{cases} 0 , & v_d \leq v_d^0 \\ \gamma_\infty \left(\dfrac{v_d - v_d^0}{v_d^0}\right), & v_d^0 \leq v_d \leq 2v_d^0 \\ \gamma_\infty , & v_d \geq 2v_d^0 \end{cases} \tag{3-57}$$

In the above expression, v_d^0 is the drift velocity at the value of E/N for which $K_0(E/N)$ is a maximum. This value of E/N is approximately the point at which the older Viehland and Mason result in equation (3-53) begins to deviate from the experimental data. In equation (3-57), γ_∞ is the fractional difference between $(v_d)1$ and v_d in the high field limit, and it has been determined as a function of mass ratios by Viehland and Mason.[26] For the ion-gas combinations examined in this thesis, the values for γ_∞ ranged from -0.075 to 0.015. The equations (3-56) and (3-57) are of no great physical significance, but are merely a simple way to proceed

between the two limits. Thus, the most recent Viehland-Mason theory uses equation (3-56) in equation (3-55) to give

$$ND_L = \frac{N_0 K_0 kT}{e} + \frac{N_0 K_0 M}{3e}\left(\frac{M+3.2m}{M+1.4m}\right) v_d^2 (1+\gamma)^2$$

to first order. The corresponding second order result is the above ND_L multiplied by the correction factor $1 + d \ln K_0/d \ln(E/N)$, or

$$ND_L = \left\{\frac{N_0 K_0(0) kT}{e} + \frac{N_0 K_0(E/N) M}{3e}\left(\frac{M+3.2m}{M+1.4m}\right) v_d^2 (1+\gamma)^2\right\} x \left\{1 + \frac{d \ln K_0}{d \ln(E/N)}\right\}. \quad (3\text{-}58)$$

When the reduced mobility is in $cm^2/V\text{-}sec$, T is in ^oK, masses are in amu, and ND_L is in $cm^{-1}sec^{-1}$, the above equation becomes

$$ND_L = \left\{2.315 \times 10^{15} K_0(0)\, T + 6.701 \times 10^{15} \frac{M(M+3.2m)}{(M+1.4m)} \left(\frac{E/N}{100}\right)^2 \left[K_0(E/N)\right]^3 (1+\gamma)^2\right\} x \left\{1 + \frac{d \ln K_0}{d \ln(E/N)}\right\}. \quad (3\text{-}59)$$

Summary of Theoretical Results

For comparison purposes, the theoretical results in equations (3-11), (3-13), (3-14), (3-53), and (3-59) will be written together. In the summary below, the masses are in amu, temperatures are in ^oK, drift velocities are in units of 10^4 cm/sec, ND_L is in units of $10^{18} cm^{-1}sec^{-1}$ and K_0 is in $cm^2/V\text{-}sec$. These units are convenient for displaying the experimental results. The equations below are

the equations used in plotting the curves in Chapter V. Note that all quantities appearing in the equations below are measured quantities with the exception of $K_0(0)$ which is given in terms of measured quantities in equation (3-68).

The Wannier ND_L is

$$ND_L = 2.315 \times 10^{-3} K_0(0)T + 6.701 \times 10^{-3} \frac{M(M+3.72m)}{(M+1.908m)} \left(\frac{E/N}{100}\right)^2 K_0^3(0) \ . \qquad (3\text{-}60)$$

The modified Wannier ND_L is

$$ND_L = 2.315 \times 10^{-3} K_0(0)T + 6.701 \times 10^{-3} \frac{M(M+3.72m)}{(M+1.908m)} \left(\frac{E/N}{100}\right)^2 K_0^3(E/N) \qquad (3\text{-}61)$$

$$= 2.315 \times 10^{-3} K_0(0)T + 3.455 \times 10^{-2} \frac{M(M+3.72m)}{(M+1.908m)} \frac{v_d^3}{E/N} \ . \qquad (3\text{-}62)$$

The Viehland-Mason result is

$$ND_L = \left\{2.315 \times 10^{-3} K_0(0)T + 6.701 \times 10^{-3} \frac{M(M+3.72m)}{(M+1.908m)} \left(\frac{E/N}{100}\right)^2 K_0^3 (E/N)\right\} \times \left\{1 + \frac{d \ln K_0}{d \ln(E/N)}\right\} \qquad (3\text{-}63)$$

or

$$ND_L = \left\{2.315 \times 10^{-3} K_0(0)T + 3.455 \times 10^{-2} \frac{M(M+3.72m)}{(M+1.908m)} \frac{v_d^3}{E/N}\right\} \times \left\{1 + \frac{d \ln K_0}{d \ln(E/N)}\right\} \ . \qquad (3\text{-}64)$$

The improved Viehland-Mason result is

$$ND_L = \left\{2.315 \times 10^{-3} K_0(0)T + 6.701 \times 10^{-3} \frac{M(M+3.2m)}{(M+1.4m)} \left(\frac{E/N}{100}\right)^2 K_0^3 \, (E/N)(1+\gamma)^2\right\}$$

$$\times \left\{1 + \frac{d \ln K_0}{d \ln (E/N)}\right\} \tag{3-65}$$

or

$$ND_L = \left\{2.315 \times 10^{-3} K_0(0)T + 3.455 \times 10^{-2} \frac{M(M+3.2m)}{(M+1.4m)} \frac{v_d^3}{E/N} (1+\gamma)^2\right\}$$

$$\times \left\{1 + \frac{d \ln K_0}{d \ln (E/N)}\right\} \tag{3-66}$$

where

$$\gamma = \begin{cases} 0 & , \quad v_d \leq v_d^0 \\ \gamma_\infty \left(\dfrac{v_d - v_d^0}{v_d^0}\right) & , \quad v_d^0 \leq v_d \leq 2v_d^0 \\ \gamma_\infty & , \quad v_d \geq 2v_d^0 \, . \end{cases} \tag{3-67}$$

In the above equations

$$K_0 = 37.22 \frac{v_d}{E/N} \, . \tag{3-68}$$

CHAPTER IV

MOBILITIES

Method of Data Analysis

A 256 channel arrival time histogram was accumumated on paper tape for each position of a mobility run at a given temperature, pressure, and E/N. The average drift time $\bar{t}_i$ (i = 4, 5, 6, 7) for each position was determined by numerically integrating the arrival time for each channel over the 256 channels. This average drift time included both end effects and time spent in the analysis region. To eliminate the end effects a differencing technique[28] was used. The differencing technique used the drift velocity for the ions between source positions z_i and z_j to calculate v_d from the equation

$$v_d = \frac{z_i - z_j}{\bar{t}_i - \bar{t}_j} \quad . \tag{4-1}$$

In a typical run, three drift velocities were computed. The drift velocities were found between positions 4 and 5, 5 and 6, and 6 and 7. Successive positions were approximately 6.25 cm apart. Then a straight line of best fit (in the least squares sense) was constructed through these points, and v_d was set equal to the slope of this straight line. Drift velocities reported in this thesis ranged from less than 10^4 cm/sec to more than 10^6 cm/sec.

The electric field E was calculated from the equation

$$E = \frac{V}{z}$$

where V was the drift voltage read from the differential voltmeter, and z was the length of the drift region. Then the mobility was calculated from the equation

$$K = \frac{v_d}{E} . \qquad (1\text{-}1)$$

To calculate the reduced mobility, the temperature and pressure must be known. The temperature T used in the calculation of the reduced mobility was the average of all the temperature readings recorded during the run. At each source position the temperature at the top, middle, and bottom of the drift region were recorded. Usually there were four positions for each run. The pressure p used in the calculation of the reduced mobility was the pressure set and maintained by the MKS Baratron capacitance manometer multiplied by a pressure correction factor near unity. This pressure correction factor[29] was used to standardize the pressure so that the zero field reduced mobility for K^+ in N_2 was 2.54 $cm^2/V\text{-}sec$. Then the reduced mobility K_0 was obtained from the equation

$$K_0 = K\left(\frac{p}{760}\right)\left(\frac{273.16}{T}\right) . \qquad (1\text{-}2)$$

In all cases except Na^+ in CO_2, the zero field reduced mobility was found by averaging all reduced mobilities in the low field region. For Na^+ in CO_2, clustering prevented an accurate determination of the reduced mobility in the low field region.

Experimental Results

The mobility data[30] presented in this section are also given in tabular form in Appendix V. The presentation below refers to the data presented in graphical form in Figure 3 for the reduced mobilities of Na^+ in He, Ne, Ar, and CO_2, and in Figure 4 for the reduced mobilities of Li^+ in He, Ne, and Ar. In Figures 3 and 4 the numbers near the ordinate refer to the zero field reduced mobilities in $cm^2/V\text{-}sec$.

Na^+ in He

Mobility measurements were carried out for an E/N range of 1 Td to 174 Td. The corresponding ion energies ranged from essentially thermal up to 9.5 eV. The range of the Mason-Viehland effective temperatures extended from 300^oK to $11,200^oK$. The measurements used gas pressures from 493 μat the lowest value of E/N to 98.5 μ at the highest value of E/N. No clustering was observed at any pressure or at any E/N.

Allowing for scatter of experimental points, the reduced mobilities for $E/N < 4$ Td were independent of E/N. This range of E/N was the low field region for Na^+ in He. Averaging the mobilities in this region gave the zero field reduced mobility of 22.64 $cm^2/V\text{-}sec$. As E/N was increased above the low field region, the reduced mobility increased. This increased reduced mobility is thought to be due to a partial cancellation of the long range attractive polarization force by a short range repulsive force as the more energetic ion comes nearer the neutral molecule on the average. The largest reduced mobility measured was 26.1 $cm^2/V\text{-}sec$ at E/N = 30.2 Td. As E/N was increased further, the reduced mobility

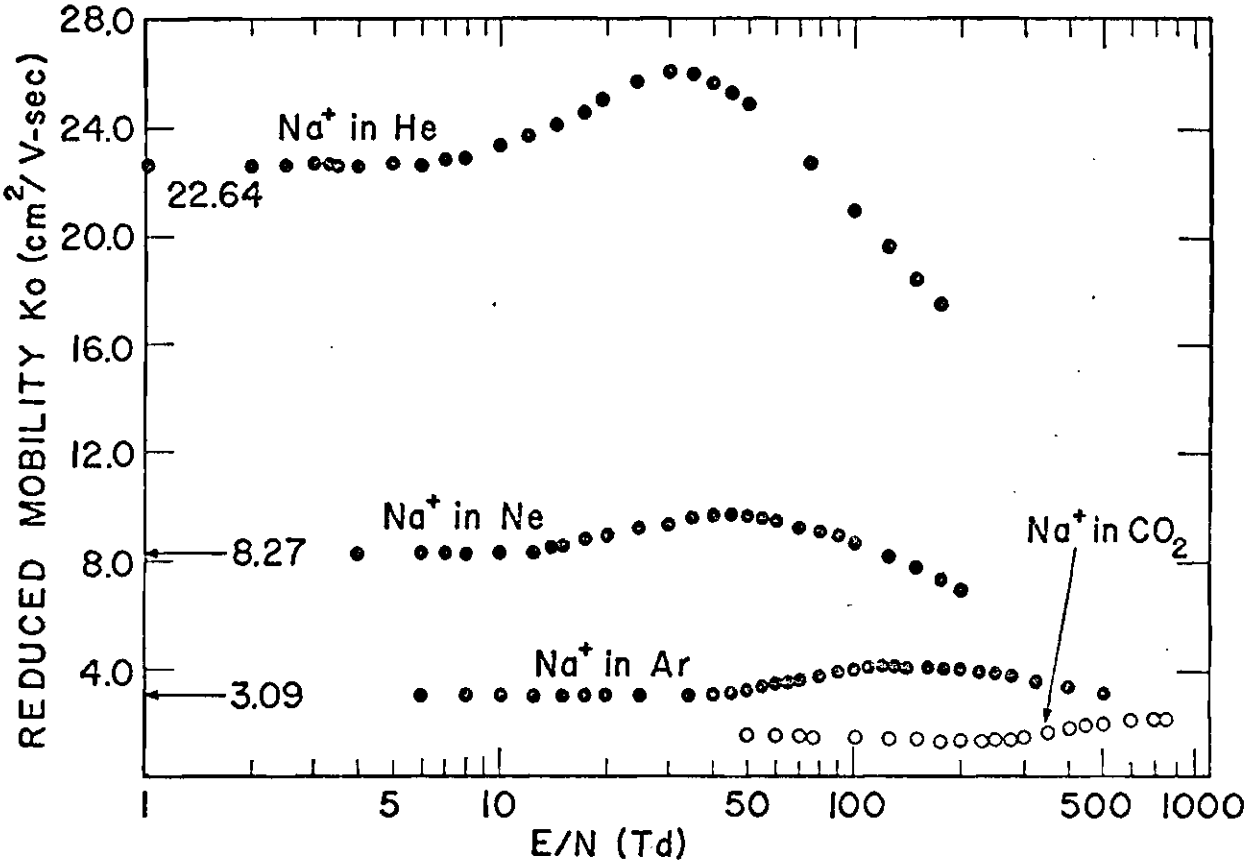

Figure 3. Reduced Mobilities for Na^+ Ions in He, Ne, Ar, and CO_2 as Functions of E/N at $300^{\circ}K$.

decreased. This decrease of reduced mobility with increasing E/N at high E/N is thought to be due to the dominance of short range repulsive forces. The lowest measured reduced mobility was 17.6 cm^2/V-sec at E/N = 174 Td.

Na^+ in Ne

The data points for the mobility of Na^+ in Ne as a function of E/N show the typical features of a non-reacting ion drifting through a neutral gas. There was a low field region below E/N = 10 Td in which the reduced mobility was independent of E/N. Averaging these data points gave the zero field reduced mobility of 8.27 cm^2/V-sec. As E/N was increased, the reduced mobility increased until it reached a maximum of 9.70 cm^2/V-sec at E/N = 45.2 Td. Increasing E/N above 45.2 Td decreased the reduced mobility. At 199 Td, the highest value of E/N used for the Na^+ in Ne measurements, the reduced mobility was 7.03 cm^2/V-sec.

The above measurements were made over a pressure range of 98.5 μ to 296 μ, and over an E/N range of 3.99 Td to 199 Td. The E/N range corresponded to effective temperatures from 305^{o}K to 11,600^{o}K, and ion energies from approximately thermal to 3.2 eV. No clustering was observed at any value of pressure or E/N.

Na^+ in Ar

Reduced mobilities were measured from E/N = 6.01 Td to E/N = 502 Td using pressures from 29.6 μ to 172 μ. The effective temperatures ranged from 305^{o}K to 29,300^{o}K. Ion energies ranged from essentially thermal to 5.9 eV. For E/N less than 18 Td, the measured reduced mobilities appeared constant, allowing for scatter of experimental data. Averaging the mobilities in this region gave

3.09 cm^2/V-sec for the zero field reduced mobility. As E/N was increased from 18 Td, the reduced mobility rose from the zero field value to the maximum of 4.18 cm^2/V-sec at E/N = 121 Td. At E/N higher than 121 Td, the reduced mobility decreased. The reduced mobility at the highest value of E/N used was 3.15 cm^2/V-sec at E/N = 502 Td. No appreciable clustering was ever observed.

Na^+ in CO_2

Reduced mobilities were measured from E/N = 51.8 Td to E/N = 762 Td with CO_2 pressures ranging from 24.6 μ to 73.9 μ. Ion energies ranged from essentially thermal to 7.7 eV. Instead of increasing from a low field value, the reduced mobility of Na^+ in CO_2 decreased from 1.63 cm^2/V-sec at 51.8 Td to 1.47 cm^2/V-sec in the region between 175 Td to 225 Td. The middle of this region, 200 Td, corresponded to an average energy in the laboratory system of 0.26 eV. The CO_2 molecule is known to have a large cross section for vibrational excitation by electron impact at electron energies on the order of 0.1 eV. Thus, it is interesting to speculate that the dip in reduced mobility between 50 Td and 250 Td is due to inelastic collisions of Na^+ with CO_2. A similar dip in reduced mobility has been observed by James[32] for K^+ in CO_2 and by Takata[33] for Li^+ in N_2. A rigorous theory of mobility as a function of E/N for inelastic collisions is needed to test this speculation.

Above 225 Td the reduced mobility increased with increasing E/N until the maximum mobility of 2.30 cm^2/V-sec was reached at E/N = 762 Td. The zero field reduced mobility could not be determined because clustering became significant at the lowest E/N reported in this work.

Clustering of Na^+ to CO_2 was observed at the lower E/N and higher pressure measurements. Clustering was determined as the ratio of the number of clustered ions counted per second to the number of unclustered ions counted per second. The highest E/N for which clustering was observed was 77.2 Td at a pressure of 49.3 μ. For that run, 0.12% clustering was observed. As E/N was reduced and pressure was increased, the amount of clustering increased. The maximum amount of clustering observed was 13% at an E/N of 51.8 Td and a pressure of 73.9 μ. Because of clustering, the mobility was not measured below an E/N of 51.8 Td.

Clustering must be accounted for in mobility measurements, since some of the ions detected as Na^+ would actually have spent part of their drift time as the cluster $Na^+ \cdot CO_2$. Using the rate coefficients $k_2 = 2 \times 10^{-29 \pm 0.5}$ cm^6/sec and $k_{-2} = 1 \times 10^{-14 \pm 0.5}$ cm^3/sec measured by Keller and Beyer[2] for the reaction

$$Na^+ + CO_2 + CO_2 \underset{k_{-2}}{\overset{k_2}{\rightleftarrows}} Na^+ \cdot CO_2 + CO_2 \ ,$$

the following calculation showed clustering was far from equilibrium. The characteristic time for the associative reaction was

$$\tau_a = \frac{1}{\alpha_2} = \frac{1}{k_2 N^2}$$

$$= \frac{1}{(2 \times 10^{-29} cm^6/sec)(2.4 \times 10^{15} cm^{-3})^2}$$

$$= 8.7 \times 10^{-3} \text{ sec.}$$

The characteristic time for the dissociative reaction was

$$\tau_d = \frac{1}{\alpha_{-2}} = \frac{1}{k_{-2}N}$$

$$= \frac{1}{(1\times10^{-14}\ cm^3/sec)(2.4\times10^{15}\ cm^3)}$$

$$= 42 \times 10^{-3}\ sec.$$

However, the longest drift time for all four positions measured at E/N = 51.8 Td and pressure of 73.9 μ was only 1.9×10^{-3} sec. Hence, the associative and dissociative reactions were both far from completion. The fraction of ion clusters that were created and broken up in the drift region must have been less than τ_a/τ_d times the number of clusters observed at the end of the drift region. To get an upper limit for the effect of clustering on the mobility, it was assumed that each of these complexes drifted the whole way in the clustered form, then broke up just before measurement. In this case the measured mobility would have differed from the mobility of Na^+ by the fraction

$$(0.13)\left(\frac{8.7ms}{42ms}\right)\left[\frac{|K_0(Na^+\cdot CO_2)-K_0(Na^+)|}{K_0(Na^+)}\right].$$

The mobility of $Na^+\cdot CO_2$ was estimated by using the square root of the reduced mass scaling factor.[34] This was only an estimate because it assumes the interaction potential between $Na^+\cdot CO_2$ and CO_2 is the same as the interaction potential between Na^+ and CO_2. Using this scaling factor approximation gave

$$\frac{K_0(Na^+ \cdot CO_2)}{K_0(Na^+)} = \sqrt{\left(\frac{67+44}{67.44}\right)\left(\frac{23.44}{23+44}\right)}$$

$$= \quad 0.569 \quad .$$

Therefore, the error between the measured reduced mobility and the true reduced mobility was no greater than

$$(0.13)\left(\frac{8.7\text{ms}}{42\text{ ms}}\right)(1 - 0.57)$$

or a maximum error of approximately 1%.

Li^+ in Ne

Reduced mobilities were measured from E/N = 2.99 Td to E/N = 125 Td using pressures from 98.5 μ to 394 μ. These values of E/N corresponded to effective temperatures ranging from approximately thermal to 16,600°K and to ion energies ranging from essentially thermal to 2.7 eV. Below E/N of 7 Td, the reduced mobilities appeared constant. Averaging the reduced mobilities for E/N below 7 Td gave the zero field reduced mobility of 10.70 cm^2/V-sec. As E/N was increased, the reduced mobility increased from the zero field value to the maximum value of 15.3 cm^2/V-sec at E/N of 45.1 Td. Increasing E/N further resulted in decreased reduced mobilities. The lowest reduced mobility measured on the high E/N side of the maximum was 13.0 cm^2/V-sec at E/N of 125 Td. No clustering was observed.

Li^+ in Ar

Reduced mobilities were measured from E/N = 5.96 Td to E/N = 201 Td,

and from pressures of 78.8 μ to 296 μ. Ion energies ranged from essentially thermal to 3.4 eV. As can be seen from Figure 4, the reduced mobility was essentially constant for E/N less than 25 Td. Averaging the reduced mobilities in this region gave the zero field reduced mobility of 4.63 cm^2/V-sec. As E/N was increased above 25 Td, the reduced mobility increased to a maximum measured value of 7.37 cm^2/V-sec at E/N = 121 Td. As E/N was further increased, the reduced mobility decreased to a final value of 6.84 cm^2/V-sec at E/N = 201 Td, the highest value of E/N used. The maximum clustering observed for Li^+ in Ar was 1%. Using the rate coefficients of Keller, et al.[4] and estimating the effects of clustering as in the case of Na^+ in CO_2, showed that clustering had a negligible effect on the mobility measurement.

Li^+ in He

Reduced mobilities for Li^+ in He were measured from E/N of 2.02 Td to 199 Td, and from pressures of 88.7 μ to 493 μ. The E/N range corresponded to effective temperatures ranging from 304°K to 28,700°K, and to ion energies ranging from essentially thermal to 10.1 eV. As can be seen from Figure 4, the reduced mobility was independent of E/N up to E/N = 4.5 Td. Averaging the reduced mobilities at values of E/N of 4.5 Td or less gave the zero field reduced mobility of 23.06 cm^2/V-sec. As E/N was increased from 4.5 Td, the reduced mobility increased from the zero field value to 32.7 cm^2/V-sec at E/N = 40.0 Td. As E/N was increased above 50.1 Td, the reduced mobility decreased to a final value of 25.0 cm^2/V-sec at E/N = 199 Td, the highest value of E/N used. No clustering was observed at any combination of pressures or E/N used in the measurements.

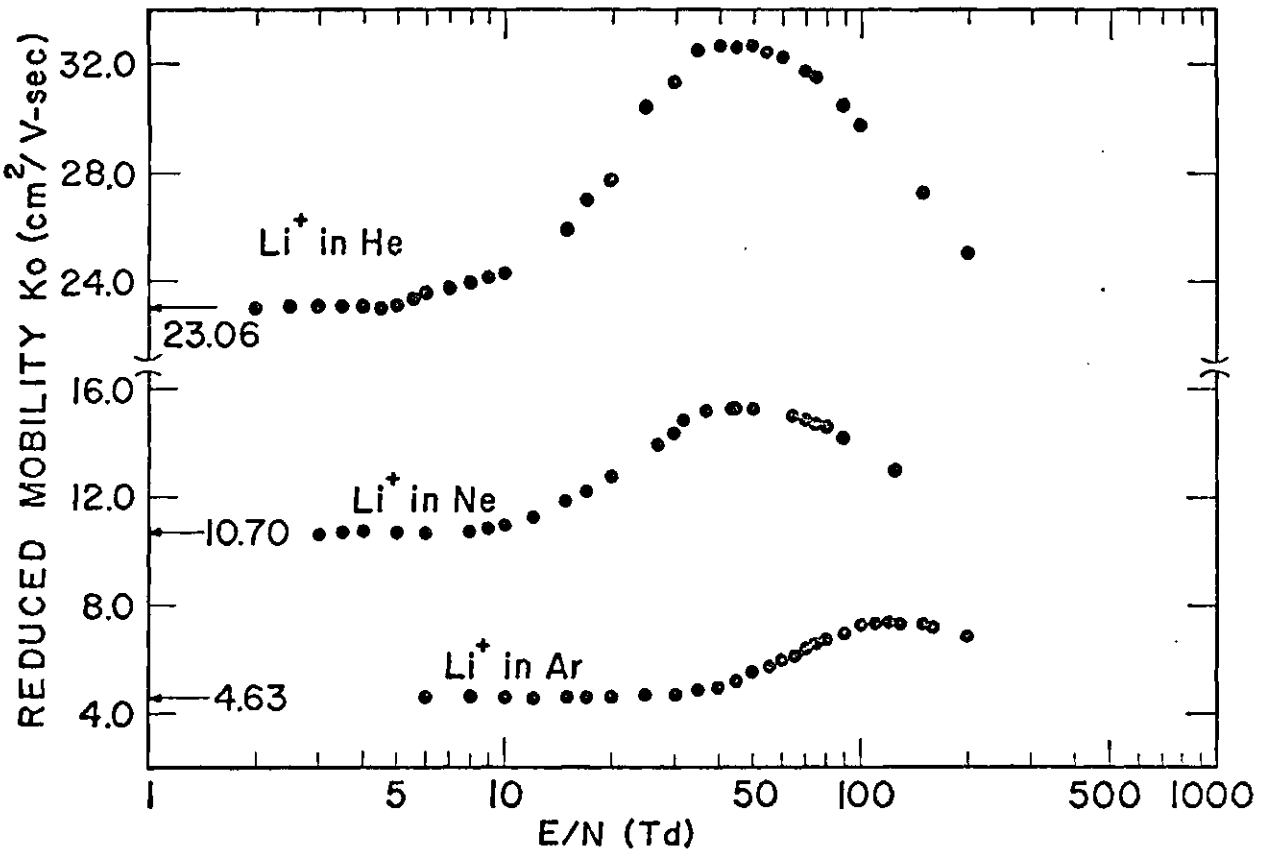

Figure 4. Reduced Mobilities for Li^+ Ions in He, Ne, and Ar as Functions of E/N at 300 ^{o}K.

The case of the mobility of Li^+ in He was especially interesting because of recent theoretical developments. Both Li^+ and He are relatively simple, two-electron, closed shell structures. Catlow et al.[35] have made an ab initio quantum mechanical calculation of the interaction potential for the Li^+-He system, and Morrison et al.[36] have used this interaction potential to calculate both the classical and the quantal $\bar{\Omega}^{(1,1)}(T_{eff})$ for Li^+ in He. The Catlow potential reproduced the general features of the experimental $\bar{\Omega}^{(1,1)}(T_{eff})$ over the entire range of T_{eff} (300 to 38,700°K) for which drift data were available. The details of the comparison between the experimental data and the theoretical predictions are discussed in Appendix I.

The general agreement between theory and experiment has far-reaching conclusions. The theory, checked by comparison with experimental data, yields the standard collision integral $\bar{\Omega}^{(1,1)}$ as a function of a single variable, T_{eff}. Solving equation (3-24) for $<\Psi_{20}^{(0)}>$ to first order, and substituting the result into equations (3-21) and (3-33) gives

$$T_{eff} = T\left(1 + \frac{Mv_d^2}{3kT}\right).$$

Thus, variation of E/N in constant T measurements is equivalent to variation of T at constant E/N. The important result is that now mobility measurements can be made at room temperature at high E/N, and those measurements converted into mobilities at temperatures far in excess of any existing drift tube temperatures.

Error Analysis

The mobility was determined from the equation

$$K = \frac{1}{V/z} \frac{\Delta z}{\Delta t} , \tag{4-2}$$

and the reduced mobility was calculated from the equation

$$K_0 = K\left(\frac{P}{760}\right)\left(\frac{273.16}{T}\right) . \tag{1-2}$$

Errors in the determination of the mobility arise from errors in the voltage V, distance z, and time t. Additional errors in determining the reduced mobility arise from errors associated with the gas pressure and temperature.

Drift Distance

The random error in the stopping position of the ion source is believed to be $\pm$ 0.003 cm. A systematic error of $\pm$ 0.008 cm is the maximum uncertainty in drift length for any one microswitch position. Each of these errors occurs twice in determining Δz, giving a random error of $\pm$ 0.006 cm and a systematic error of $\pm$ 0.016 cm for Δz. Since Δz is approximately 6.25 cm, the random and systematic errors for Δz were 0.096% and 0.26% respectively. The length z in equation (4-2) is the drift distance. An upper bound on the error in this length was found by using the shortest drift distance of approximately 25 cm, the drift distance corresponding to position 4. The random and systematic errors for this drift distance were 0.012% and 0.032% respectively. Combining the individual random errors according to the RMS rule, and adding the individual systematic errors, gave for the total errors

associated with the drift distance, 0.097% random error and 0.29% systematic error.

Time

A systematic error in $\bar{t}$ due to diffusion error was analyzed. Longitudinal diffusion caused some ions to drift for longer times than others. The ions that had drifted longer (those at the back of the pulse) were more likely to be removed from the axis due to transverse diffusion. Thus, the reduced number of late arrivals reduced the arrival time actually measured. From the discussion in Appendix II of the error introduced by diffusion into the average arrival time, the percent diffusion error for a run was less than $1.54(ND_L/v_dP)^2$, where ND_L is in units of 10^{18} $cm^{-1}sec^{-1}$, v_d is in units of 10^4 cm/sec, and P is the pressure in microns. This diffusion error varied greatly over the range of E/N covered in the mobility measurements. The maximum diffusion errors for each ion-gas combination studied were as follows: 0.019% for Li^+ in Ar, 0.037% for Li^+ in He, 0.016% for Li^+ in Ne, 0.0040% for Na^+ in He, 0.032% for Na^+ in Ar, 0.0022% for Na^+ in Ne, and 0.036% for Na^+ in CO_2. A systematic error in $\bar{t}$ of 0.037% was assigned as an upper bound on the diffusion error in $\bar{t}$.

There was a significant error in $\bar{t}$ due to reactions only in the case of Na^+ in CO_2. For the other six ion-gas combinations in this thesis, no significant reactions were observed. Physically, longitudinal diffusion causes some of the ions (those at the back of the pulse) to drift for longer times than others. Hence, those ions near the back of the pulse had a greater chance to undergo reactions and be removed than did those ions at the front of the pulse. Because of the reduced

number of late arrivals, the average arrival time would be shortened. Moseley[37] has shown that for a point source the first order arrival time $\bar{t}_i$ measured would be

$$\bar{t}_i = \frac{z_i}{v_d}\left(1 - \frac{2\alpha_2 D_L}{v_d^2}\right).$$

The differencing technique does not eliminate this reaction term. The systematic error due to reactions is $2\alpha_2 D_L / v_d^2$. Evaluating this for the worst case of E/N = 51.8 Td for Na^+ in CO_2 with Keller and Beyer's rate coefficients[2] yielded 0.029% for the largest systematic error due to reactions for a single time measurement. Since $\overline{\Delta t}$ involved two time measurements, the error in $\overline{\Delta t}$ due to reactions was 0.058%. At higher E/N and lower pressures, this effect quickly became negligible. For Na^+ in CO_2 a systematic error in the measurement of time of 0.095% was assigned to account for both reaction and diffusion errors. For the other ion-gas combinations a systematic error in the measurement of time of 0.037% was assigned.

The random experimental error was estimated by examining the differences between the mean arrival time for each position of a run and the time for that position from a least squares fit to z_i vs. $\bar{t}_i$ for that run. The standard deviations were as follows: 0.9% for Li^+ in Ar, 0.8% for Li^+ in He, 0.6% for Li^+ in Ne, 0.6% for Na^+ in He, 0.5% for Na^+ in Ar, 0.4% for Na^+ in CO_2, and 0.4% for Na^+ in Ne.

Temperature

For a given mobility run, the temperature was taken to be the average of

three thermocouple readings for each position used in that run. Usually, four positions were used per run. The overall systematic error for an individual temperature measurement was $0.5^{o}C$ or 0.17% at $300^{o}K$. The temperature gradient in the drift region usually was less than $1.5^{o}C$ about the average temperature. Therefore, a random error of 0.5% at 300% was assigned to temperature due to temperature gradients.

Pressure

The drift tube pressure was calibrated[38] by measuring the zero field reduced mobility for K^{+} in N_2, and correcting to the accepted standard value of 2.54 cm^2/V-sec for this reduced mobility. Possible error in the pressure calibration was considered to be less than 1.0%. The measured values of $K_0(0)$ for K^{+} in N_2 clustered around an average value with a standard deviation of less than 0.2%. Thus, 1.2% was assigned as the systematic error.

Random error resulted from fluctuations in the MKS Baratron. The Baratron gauge was zeroed before the drift tube was let up to pressure for the first run of the day. The error in this zeroing process was less than 5×10^{-5} Torr. During a run the pressure controller maintained the pressure to within 2×10^{-4} Torr of the preset value. The total possible random error was 2.5×10^{-4} Torr. All mobilities measured used pressures of 49.3 μ or greater except for some of the measurements on Na^{+} in Ar and Na^{+} in CO_2 for E/N > 350 Td. The lowest pressure used for any measurement was 24.6 μ. Thus, random errors associated with pressure were divided into two groups. For E/N < 350 Td, random error was never greater than 0.5%. For E/N > 350 Td, random error was never greater than 1.0%.

Voltage

The errors in voltage came from the inaccuracy of the voltmeter and from the errors in the values of the resistors determining the guard ring potentials. The Fluke 881A differential voltmeter was considered to be 0.01% accurate, and the resistors determining the guard ring potentials were manufactured to within 0.1% accuracy. In 1974 Graham[39] found these resistors to be even more accurate than the stated 0.1%. Nevertheless, a 0.1% maximum systematic error was assigned. A random error of 0.05% was assigned to the combined error in the power supply drift and the Fluke 881A differential voltmeter readings.

The errors for the low field mobility measurements on each of the ionic species are summarized in Table 1. Since the individual systematic errors were independent, the measure of the total systematic error was taken to be the sum of the individual systematic errors. Since the individual random errors were independent, the measure of the total random error was taken to be the square root of the sum of the squares of the individual random errors. The total error was then the sum of the total random error and the total systematic error.

High E/N Errors

At high E/N two other errors become important. As mentioned earlier, the lower pressures used for high E/N measurements led to larger percentage errors in pressure. For E/N > 350 Td, the random pressure error was less than 1.0%, while the systematic error in pressure remained at 1.2%.

At high E/N additional errors in determining $\bar{t}$ arise from both Fickian and non-Fickian diffusion. From the discussion in Appendix III of the correction to

Table 1. Percent Uncertainties in the Measurement of Low-field Mobilities

Type of Error		Li^+ in			Na^+ in			
		He	Ne	Ar	He	Ne	Ar	CO_2
Distance	systematic	0.27	0.27	0.27	0.27	0.27	0.27	0.27
	random	0.10	0.10	0.10	0.10	0.10	0.10	0.10
Time	systematic	0.04	0.04	0.04	0.04	0.04	0.04	0.10
	random	0.8	0.6	0.9	0.6	0.4	0.5	0.4
Temperature	systematic	0.17	0.17	0.17	0.17	0.17	0.17	0.17
	random	0.5	0.5	0.5	0.5	0.5	0.5	0.5
Pressure	systematic	1.2	1.2	1.2	1.2	1.2	1.2	1.2
	random	0.5	0.5	0.5	0.5	0.5	0.5	0.5
Voltage	systematic	0.1	0.1	0.1	0.1	0.1	0.1	0.1
	random	0.05	0.05	0.05	0.05	0.05	0.05	0.05
Total Error		2.9	2.7	2.9	2.7	2.6	2.7	2.7

the drift velocity due to non-Fickian effects, the percentage error in determining $\bar{t}$ is

$$P.e = \frac{100}{z\,\bar{t}}\left(\frac{D_L^2}{v_d^3} - \frac{2Q}{v_d^2}\right) \tag{4-3}$$

where Q, the quantity controlling non-Fickian diffusion, is defined by equation (III-5) of Appendix III. Using equation (IV-16) from Appendix IV in which a theoretical expression for Q is derived and equation (3-10), and replacing the numerical factors 3.72 and 1.908 in equation (3-10) by the isotropic scattering values of 4 and 2 respectively, the high E/N percent error in $\bar{t}$ is given by

$$P.e. = 100\,\frac{(M^2-8m^2)}{M(M+4m)}\left(\frac{D_L}{zv_d}\right)^2. \tag{4-4}$$

Expressing masses in amu, ND_L in units of 10^{-18} cm^{-1} sec^{-1}, E/N in Td, K_0 in cm^2/V-sec, and P in μ, the percent error by which $\bar{t}$ is decreased due to the inclusion of non-Fickian effects at high E/N is given by

$$P.e = \frac{0.177(M^2-8m^2)}{M(M+4m)}\left(\frac{ND_L}{K_0 P\,E/N}\right)^2.$$

The maximum errors for each ion-gas combination are as follows: 0.0013% for Li^+ in Ar, 0.65% for Li^+ in He, 0.032% for Li^+ in Ne, 0.15% for Na^+ in He, 0.062% for Na^+ in Ar, 0.015% for Na^+ in Ne, and 0.034% for Na^+ in CO_2.

In calculating the above errors, the minimum value of z = 25 cm was used to insure an upper bound on the error estimate. For all ion-gas combinations except

for Li^+ in Ne and Na^+ in Ar, the run at the lowest pressure was used to determine ND_L, K_0, E/N, and P. The Wannier ND_L, being larger than the measured ND_L, was used to insure an upper bound on the error estimate. The errors were then calculated from equation (4-4). In the cases of Li^+ in Ne and Na^+ in Ar, the measured values of Q were available from Appendix IV. For these two cases the errors were calculated directly from equation (4-3) in the form

$$P.e = \frac{100}{z^2}\left(\frac{D_L^2}{v_d^2} - \frac{2Q}{v_d}\right).$$

Comparison with Existing Data

Zero field reduced mobilities for some of the ion-gas combinations studied in this thesis have been measured by Tyndall,[1] Johnsen et al.,[3] and Keller et al.[4] Before comparing these results, a further understanding of Tyndall's meausrements is necessary.

In the 1930's, Tyndall made the first accurate measurements of zero field reduced mobility. His measurements differed from the measurements carried out in this work in three ways. First, his gas pressures were higher than those used in this work. Tyndall used pressures of several Torr, and the pressures used in this investigation ranged from 0.025 Torr to 0.493 Torr. However, in calculating reduced mobilities, all data were normalized to a pressure of 760 Torr. Thus, pressure differences would not appear in the reduced mobility unless clustering were a factor. Although Tyndall might have had clustering at his higher pressures, this circumstance would seem unlikely for work on Na^+ and Li^+ in He, Ne, and Ar.

As has been shown earlier, clustering was a factor only in the reduced mobility of Na^+ in CO_2, but Tyndall did not measure this mobility. Thus, Tyndall's higher pressures should not be a factor in producing differences between his reduced mobilities and the reduced mobilities measured in this work.

Tyndall's measurements were normalized to 18^oC or 291.16^oK, whereas the measurements of this work were normalized to the modern standard of 0^oC or 273.16^oK. Therefore, Tyndall's reduced mobilities were renormalized to the standard of 273.16^oK to be reasonably compared with the reduced mobilities measured in this work. The values quoted below as Tyndall's reduced mobilities are actually Tyndall's values multiplied by the temperature correction factor $(273.16/297.16) = 0.93818$.

Also of importance was the value of E/N at which Tyndall believed he had reached the zero field region, the region in which reduced mobility was independent of E/N. Unfortunately, Tyndall did not quote the value of E/N at which his measurements were made. From his papers[1,40] it appears that the measurements he quoted as zero field reduced mobilities were made at an E/N of approximately 12 Td for Li^+, because his reduced mobility for Li^+ in N_2 was constant below about 12 Td, but above 12 Td his reduced mobility increased with increasing E/N. Actually, the reduced mobility had a zero field region that was characteristic of the gas as well as the ion. As can be seen from Figure 4, Tyndall would have been above the zero field region for Li^+ in He and for Li^+ in Ar. For Na^+, Tyndall used lower E/N values to determine zero field reduced mobilities, because his data on Na^+ in N_2 indicated that the reduced mobility for that combination should be

measured at approximately 4 to 8 Td to be independent of E/N. From Figure 3, it appears that Tyndall was actually within, or nearly within, the zero field region for measurements on Na^+ in He, Ne, and Ar.

In summary, the zero field reduced mobilities listed as those of Tyndall, are actually Tyndall's values multiplied by a temperature correction factor to account for a different temperature normalization. Also, Tyndall's zero field reduced mobilities should be in agreement with those of this work except for the case of Li^+ in He and Li^+ in Ar. For those two cases, Tyndall's zero field reduced mobilities should be close to the reduced mobilities measured in this work at approximately 12 Td.

The zero field reduced mobility for Na^+ in He has been measured by two other investigators. Tyndall obtained 22.70 cm^2/V-sec, and Johnsen et al. obtained (21.0 $\pm$ 1.0) cm^2/V-sec. Tyndall's value agreed well with the value of (22.64 $\pm$ 0.61) cm^2/V-sec obtained in this work. The drift tube of Johnsen et al., as mentioned in Chapter I, was built primarily for measuring reaction rates, and can be expected to give only approximate values for the reduced mobility.

Except for this work, only Tyndall has measured the zero field reduced mobility for Na^+ in Ne. Tyndall's value of 8.16 cm^2/V-sec agreed well with the value of (8.27 $\pm$ 0.22) cm^2/V-sec measured in this work.

The only other investigator to measure the reduced mobility of Na^+ in Ar was Tyndall. Tyndall's zero field reduced mobility of 3.02 cm^2/V-sec agreed fairly well with the zero field reduced mobility of (3.09 $\pm$ 0.08) cm^2/V-sec obtained here.

For the zero field reduced mobility of Li^+ in He, Tyndall obtained 24.20 cm^2/V-sec compared to (23.06 $\pm$ 0.62) cm^2/V-sec measured in this research. As explained, it appeared that Tyndall's measurements were made at an E/N of approximately 12 Td. In that case, Tyndall's value of 24.20 cm^2/V-sec agreed well with the value of approximately (24.30 $\pm$ 0.66) cm^2/V-sec which was the interpolated value of the reduced mobility measured here at 12 Td. Also, the theoretical predictions of the omega integral, essentially the reciprocal of reduced mobility, for the case of Li^+ in He, agreed well with the data obtained in this research. The theoretical predictions and the experimental data appear in Figure 13 in Appendix I.

Tyndall obtained 11.12 cm^2/V-sec for the zero field reduced mobility of Li^+ in Ne. If, as suspected, Tyndall's measurements on Li^+ were taken at approximately 12 Td, his 11.12 cm^2/V-sec agreed well with the value of (11.20 $\pm$ 0.30) cm^2/V-sec, the interpolated value of the reduced mobility measured in this work at 12 Td.

The reduced mobility of Li^+ in Ar has been measured by two other investigators. Tyndall obtained a zero field reduced mobility of 4.68 cm^2/V-sec. For this ion-gas combination, Tyndall's measurements were within the zero field range. Keller, et al., obtained (4.57 $\pm$ 0.12) cm^2/V-sec. Both of the above values compared favorably with the (4.63 $\pm$ 0.13) cm^2/V-sec measured in this work.

CHAPTER V

LONGITUDINAL DIFFUSION COEFFICIENTS

Method

The shape of the arrival time spectrum is determined by three quantities: α the reaction frequency, D_T the transverse diffusion coefficient, and D_L the longitudinal diffusion coefficient. Moseley[28] showed that two of these three quantities have relatively little effect upon the shape of the arrival time spectrum. He showed that the transverse diffusion coefficient D_T could be varied from $0.01D_T$ to $10D_T$, and that the reaction frequency α could be varied from zero up to 10^6 sec^{-1} without appreciably changing the shape of the arrival time spectrum. The shape of the arrival time spectrum is almost completely determined by the value of the longitudinal diffusion coefficient D_L. Basically, the longitudinal diffusion coefficient determines the width of the arrival time spectrum.

Gatland[34] solved the transport equation for the geometry of the drift tube used in this thesis. He found that the number of ions per second passing through the exit aperture at the end of the drift tube on the axis for depleting reactions only was

$$\Phi = \frac{ase^{-\alpha\tau}}{4(\pi D_L t)^{\frac{1}{2}}} \left(v_d + \frac{z}{\tau}\right)\left(1 - e^{-\frac{r_s^2}{4D_T\tau}}\right) e^{-\frac{(z-v_d\tau)^2}{4D_L\tau}}, \qquad (5\text{-}1)$$

in which a was the area of the exit aperture at the bottom of the drift tube, s was the number of ions per cm^2 admitted by the source into the drift region, and r_s was

the radius of the source. The other terms in equation (5-1) have the usual meaning.

A run usually consisted of obtaining an arrival time spectrum for each of four positions. From these data, the drift velocity v_d was determined as described in Chapter IV. Because the shape of the arrival time spectrum was essentially independent of the reaction frequency α, and since few reactions occurred in the drift region, the reaction frequency was set equal to zero.

In work on nitrogen ions in nitrogen[28] the transverse diffusion coefficient did not vary more than a factor of five from the value of the diffusion coefficient as calculated from the Einstein equation (1-6). Using this observation as a guideline, and recalling that the shape of the arrival time spectrum was relatively unaffected by the transverse diffusion coefficient within these limits, the value for the transverse diffusion coefficient used in equation (5-1) in this work was the value D calculated from the Einstein equation (1-6).

The dependence of Φ on a and s was eliminated by normalizing the height of the theoretical arrival time spectrum to the height of the experimental arrival time spectrum. The time the ions spent from admission into the drift region until detection by a given channel in the 256 channel time-of-flight analyzer was recorded. From this time, the time spent in the analysis region was subtracted. In the computer program used, this analysis time was the average time for the four spectra, and slight adjustments in the time in the analysis region were made to obtain the best fit for each spectrum. Finally, the longitudinal diffusion coefficient calculated from the Einstein equation (1-6) was used as a trial fit to equation (5-1). Starting from this initial value for D_L, the computer program arrived at a best fit value for

the longitudinal diffusion coefficient in the least squares sense. This was the value of D_L for one position for that run. The four longitudinal diffusion coefficients for a run usually clustered around an average value with a spread of less than 4%. In most cases, this average value was quoted as the value of D_L for that particular combination of E/N, pressure, and temperature. In a few cases of high E/N and low pressure, only the longest drift distances were used to arrive at a value for D_L. In obtaining data at high E/N and low pressure, the ions entered the drift region with speeds higher than thermal, and had to drift a short distance before being thermalized. The shorter the total drift distance, the more pronounced this effect became.

Comparison with Theory

Since ND_L was found to be independent of N, gas number density, ND_L, was the quantity examined, rather than D_L. In the low field limit, the ions were approximately in thermal equilibrium with the neutral gas molecules. In this case the Einstein relation

$$\frac{D}{K} = \frac{kT}{e} \tag{1-6}$$

held. In the above equation, D represented either the longitudinal or the transverse diffusion coefficient, since both had the same value in this limit. Both K and D were inversely proportional to N, so that the ideal gas law yielded a simple relation between ND and the zero field reduced mobility $K_0(0)$. Multiplying equation (1-6) by NK gave

$$ND(0) = NK\frac{kT}{e} \quad ,$$

or

$$ND(0) = 2.315 \times 10^{-3}\ T\ K_0(0) \quad . \tag{5-2}$$

In equation (5-2) ND(0) is in units of $10^{-18} cm^{-1} sec^{-1}$, T is in ^oK, and $K_0(0)$ is in $cm^2/V\text{-}sec$. It is to be emphasized that equation (5-2) was valid only in the low field limit. By substituting the zero field reduced mobilities from Chapter IV into equation (5-2), the zero field limits of the ND_L's were calculated. The numerical values for the zero field limit of each ND_L appear near the ordinate on Figures 5 and 8.

When the average ion energy was significantly above thermal, a non-equilibrium solution to the transport equation was used to describe ion diffusion. The non-equilibrium solutions examined in this chapter were the original Wannier ND_L, the modified Wannier ND_L, the Viehland-Mason ND_L, and the improved Viehland-Mason ND_L. The original Wannier ND_L given by equation (3-60) was described by the dashed curves in Figures 5 and 8. The modified Wannier ND_L given by equation (3-62) was described by the solid curves in Figures 5, 6, 8, and 9. The Viehland-Mason ND_L given by equation (3-64) was described by the dashed curves in Figures 6 and 9. The improved Viehland and Mason ND_L given by equation (3-66) was described by the solid curves in Figures 7 and 10. To obtain the derivative for the correction factor

$$c.f. = 1 + \frac{d \ln K_0}{d \ln (E/N)} \tag{5-3}$$

used in both Viehland-Mason ND_L's, a parabola was fitted in the least squares sense to the two values of reduced mobility on either side of the value at which the derivative was to be evaluated. Then the derivative was computed from the parabola. Inaccuracies may have arisen from this procedure at the extreme high values of E/N, because the two data points needed to fit the curve at even higher E/N were absent.

Experimental Results

The experimental data[41] for Li^+ in He, Ne, and Ar were plotted in Figures 5, 6, and 7. Separate figures for the same data were needed to clearly display the different theoretical predictions. The experimental data for Na^+ in He, Ne, Ar, and CO_2 were plotted in Figures 8, 9, and 10. Again, the same experimental data appear in different figures to clearly display the different theoretical predictions.

Li^+ in Ne

Measurements of ND_L were carried out from E/N of 2.99 Td to E/N of 125 Td. The experimental data appear in Figures 5, 6, and 7. From equation (5-2), the predicted value of ND_L in the zero field limit was 7.43×10^{18} cm^{-1} sec^{-1}. This zero field limit was based on the value of $K_0(0) = 10.70$ $cm^2/V\text{-}sec$ from Chapter IV. The dashed curve in Figure 5 was the Wannier ND_L from equation (3-60). At the lowest values of E/N the second term in equation (3-60) was small compared to the zero field value, and the curve approached the constant limiting value of 7.43×10^{18} cm^{-1} sec^{-1}. At intermediate values of E/N, the two terms were comparable, and the result was the curved portion of the Wannier ND_L. For the highest values of E/N used, the second term of equation (3-60)

dominated, and the Wannier ND_L was proportional to $(E/N)^2$. On the log axes used in displaying the diffusion data, the resulting Wannier ND_L at high E/N appeared as a straight line with slope 2. Agreement was good at low E/N, but the Wannier ND_L fell below the measured values at intermediate E/N. At the highest values of E/N, the Wannier ND_L approached the experimental data, but only to cross it. Based on the behavior of the Wannier ND_L in some of the other ion-gas combinations, it would seem that after the Wannier ND_L crossed the data, it would again deviate from the data. Thus, rather than agreement at high E/N, this coincidence of Wannier ND_L and experimental data was in the nature of an accidental crossing.

The solid curve in Figures 5 and 6 represented the modified Wannier ND_L. The dependence of the modified Wannier ND_L on E/N was apparent from the dependence of $K_0(E/N)$ on E/N, from Figure 4 in Chapter IV. As E/N was increased from the lowest values, the reduced mobility increased above the zero field limit. Equation (3-62) shows that this increased reduced mobility resulted in a modified Wannier ND_L which was larger than the original Wannier ND_L. This difference was greatest where the reduced mobility was the largest, at E/N = 45 Td. At E/N above 45 Td, the reduced mobility decreased, and the difference between the modified Wannier ND_L and the original Wannier ND_L decreased. As can be seen from Figure 5, the modified Wannier ND_L gave better agreement with experimental data over the entire range of E/N than did the original Wannier ND_L. However, there was still considerable difference between the experimental data and the modified Wannier ND_L.

The dashed curve in Figure 6 gave the Viehland-Mason ND_L. The dependence

of this curve on E/N was seen from equation (3-64). At the lowest values of E/N, from Figure 4 in Chapter IV, the reduced mobility was independent of E/N, so that the derivative in equation (5-3) was zero. In this region, the Viehland-Mason ND_L was the same as the modified Wannier ND_L, the solid curve. However, at intermediate E/N, the reduced mobility increased with increasing E/N. The slope of the reduced mobility curve was positive, and the Viehland-Mason correction factor given by equation (5-3) was greater than unity. Thus, from the low field region up to the E/N at which the reduced mobility was a maximum, the Viehland-Mason ND_L was larger than the modified Wannier ND_L. At the E/N for which the reduced mobility was a maximum, the slope of the reduced mobility curve was zero, and the Viehland and Mason ND_L was identical to the modified Wannier ND_L. The two curves could be seen to cross at E/N = 45 Td. For E/N above 45 Td, the slope of the reduced mobility curve was negative, and the correction factor given by equation (5-3) was less than unity. Thus, for E/N greater than 45 Td, the Viehland-Mason ND_L fell below the modified Wannier ND_L. From Figure 6, it was clear that the Viehland-Mason ND_L agreed better with the experimental data over the entire range of E/N than did the modified Wannier ND_L.

The solid curve in Figure 7 was the improved Viehland-Mason ND_L given by equation (3-66). The low field behavior of the improved Viehland-Mason ND_L was the same as the low field behavior of the other theories, since they all reduced to essentially the same low field limit. In the moderate field region from 10 Td to 40 Td, the improved Viehland-Mason ND_L lay below the experimental data. In this region the improved Viehland and Mason ND_L did not agree as well with the

experimental data as the original Viehland-Mason ND_L did, because the improved Viehland and Mason ND_L used the high field $A^* = 1.2$ in a region of E/N below the high field region. In this medium field region, the original Viehland and Mason ND_L, using the polarization value of $A^* = 0.8713$ would be expected to give better results. In the high field region above 40 Td, the high field value $A^* = 1.2$ was realistic, and the correction to v_d in equation (3-56) became significant. In the high field region, the improved Viehland-Mason ND_L gave excellent agreement with the experimental data. The values[23] $v_d^0 = 1.8 \times 10^5$ cm/sec and $\gamma_\infty = 0.015$ were used in equation (3-67) to plot the improved Viehland-Mason ND_L from equation (3-66).

Li^+ in He

Measurements of ND_L were made from E/N = 2.03 Td to E/N = 1.99 Td. The results were presented graphically in Figures 5, 6, and 7. The 16.01×10^{18} $cm^{-1}sec^{-1}$ zero field value for ND_L was obtained from the Einstein relation, equation (5-2). In that equation the value of $K_0(0) = 23.06$ $cm^2/V\text{-sec}$ from Chapter IV was used. The dashed curve in Figure 5 was the original Wannier ND_L from equation (3-60). This curve approached the zero field value at low E/N. For moderate E/N, the second term in equation (3-60) dominated, and the curve on the log-log axes used became a straight line of slope 2. The original Wannier curve agreed fairly well with the experimental data at very low E/N, but the agreement was poor at both intermediate and high E/N.

The solid curve in Figures 5 and 6 was the modified Wannier ND_L from equation (3-62). The modified Wannier curve lay higher than the original Wannier

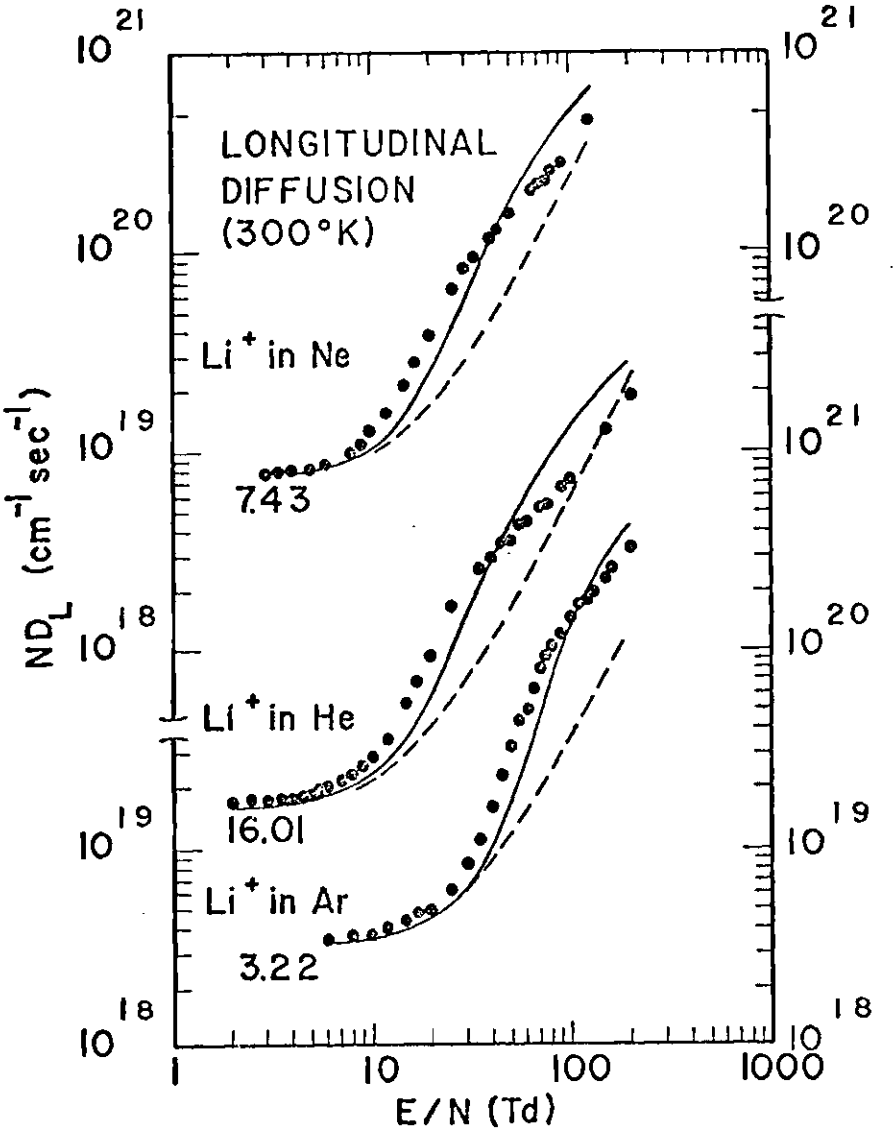

Fig. 5. Longitudinal Diffusion Coefficients for Li^+ in Ne, He, and Ar Compared to the Wannier Predictions. The Experimental Data are Represented by Dots, the Wannier Theory Using Constant Mean Free Time is Represented by the Dashed Curve, and the Wannier Theory Modified to Take Account of Variation in Reduced Mobility with E/N is Represented by the Solid Curve.

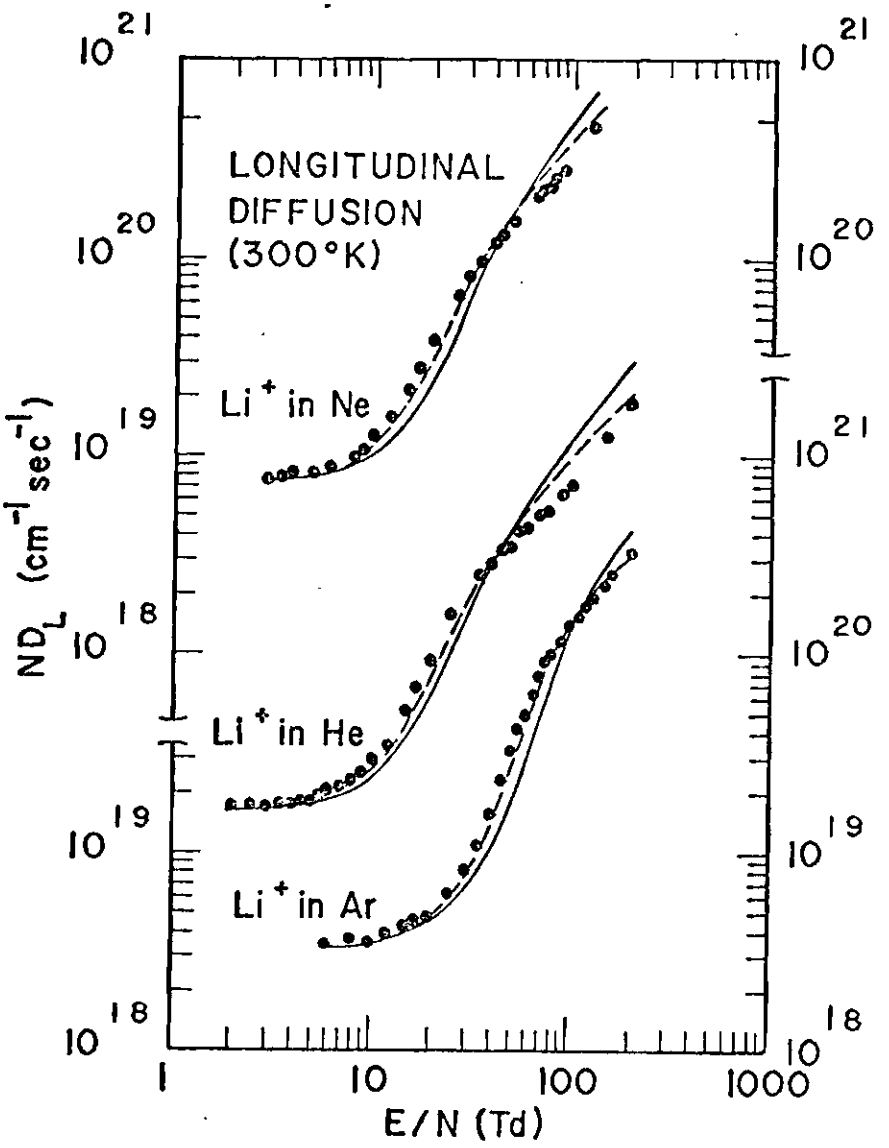

Fig. 6. Longitudinal Diffusion Coefficients for Li^+ in Ne, He, and Ar Showing the Modified Wannier Predictions with the Viehland-Mason Correction. The Experimental Data are Represented by Points, the Wannier Theory Modified to Take Account of Variations in Reduced Mobility with E/N is Represented by the Solid Curve, and the Modified Wannier Theory with the Viehland-Mason Second Order Correction is Represented by the Dashed Curve.

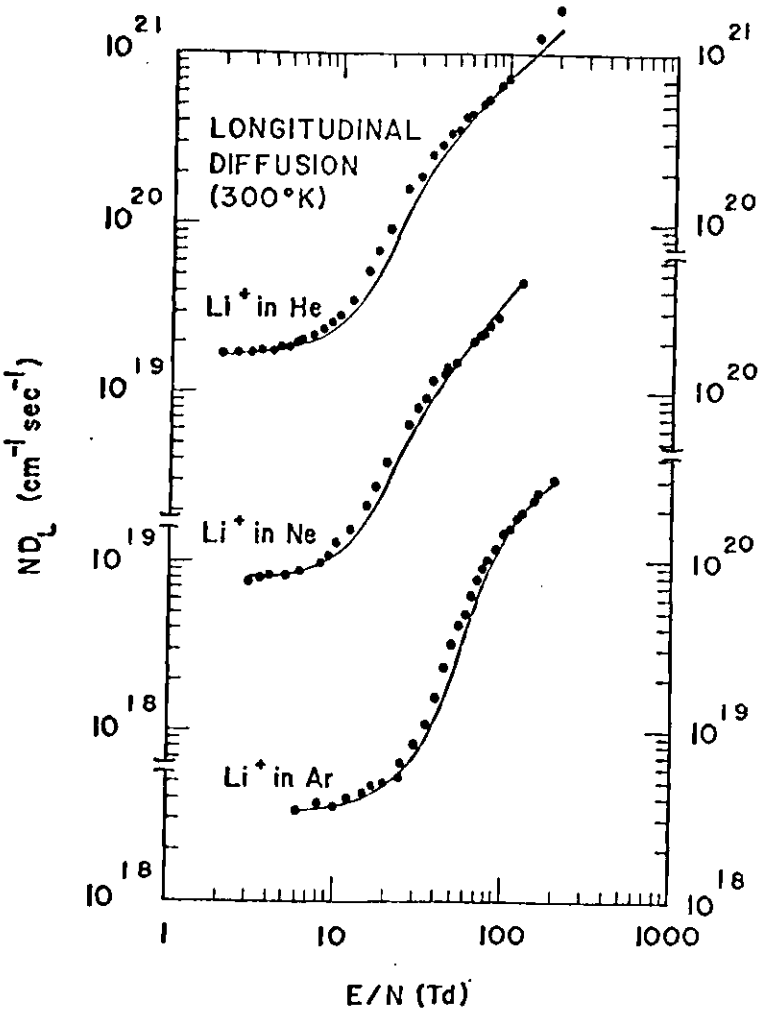

Fig. 7. Longitudinal Diffusion Coefficients for Li^+ in He, Ne, and Ar Showing the Improved Viehland-Mason Prediction. The Experimental Data are Represented by Points, and the Modified Wannier Theory with the Viehland-Mason Second Order Correction and the High E/N Modification to Drift Velocity and Collision Integrals is Represented by the Solid Curve.

curve above the zero field region, because the reduced mobility was larger than the zero field reduced mobility in this region. As in the case of Li^+ in Ne, the modified Wannier ND_L agreed better with the experimental data than the original Wannier ND_L did. However, there was still considerable difference between the modified Wannier ND_L and the experimental data except at the crossover point.

The dashed curve in Figure 6 was the Viehland-Mason ND_L from equation (3-64). The Viehland-Mason ND_L was identical to the modified Wannier ND_L in the low field region, because the reduced mobility was independent of E/N, and the correction factor given by equation (5-3) was unity. At intermediate values of E/N, the reduced mobility increased with increasing E/N as can be seen from Figure 4 in Chapter IV. In this region the slope of the reduced mobility curve was positive, and the correction factor was greater than unity. Hence, at intermediate E/N, the Viehland-Mason ND_L lay above the modified Wannier ND_L. The maximum value of the reduced mobility occurred at approximately E/N = 50 Td. Here the slope of the reduced mobility was zero, and the Viehland-Mason ND_L was identical to the modified Wannier ND_L. For E/N above 50 Td, the reduced mobility decreased with increasing E/N. Thus, above 50 Td, the correction factor was negative, and the Viehland-Mason ND_L was less than the modified Wannier ND_L. Figure 6 showed that the Viehland-Mason ND_L agreed fairly well with the experimental values over the entire range of E/N examined. However, a significant deviation from the experimental data occurred between 70 Td and 100 Td.

The solid curve in Figure 7 was the improved Viehland-Mason ND_L from equation (3-66). The improved Viehland-Mason ND_L gave good agreement with the

experimental data at low fields, since it reduced to essentially the same low field limit the other three theories did. For moderate fields ranging from 8 to 30 Td, the improved Viehland-Mason ND_L did not agree as well with the experimental data as the original Viehland-Mason ND_L did, because the improved Viehland-Mason ND_L used the high field value of $A^* = 1.2$ in a moderate field region. For high fields (E/N greater than 30 Td), the improved Viehland and Mason ND_L agreed better with the experimental data than did any of the other theoretical ND_L's. In this region, the high field value of $A^* = 1.2$ was reasonable. The values[23] $v_d^0 = 4.0 \times 10^5$ cm/sec and $\gamma_\infty = -0.075$ were used to calculate the improved Viehland-Mason ND_L.

Li^+ in Ar

Values of ND_L were measured from E/N = 5.96 Td to E/N = 201 Td. The experimental data appeared graphically in Figures 5, 6, and 7. Using the Einstein relation, equation (5-2) gave the zero field value for ND_L of 3.22×10^{13} $cm^{-1}sec^{-1}$ that appeared near the ordinate in Figure 5. The dashed curve in Figure 5 was the original Wannier ND_L. This curve approached the zero field value at low E/N and then increased, approaching a straight line of slope 2 on the log-log axes used. The original Wannier curve agreed fairly well at low E/N, but differed significantly with the experimental data at intermediate and high E/N.

The solid curve in Figures 5 and 6 represented the modified Wannier ND_L from equation (3-62). The difference between the modified Wannier ND_L and the original Wannier ND_L reflected the variation of the reduced mobility with E/N shown in Figure 4 of Chapter IV. The modified Wannier curve had the general

shape of the experimental data, but agreement with the data was only fair above the low field region.

The dashed curve in Figure 6 represented the Viehland-Mason ND_L from equation (3-64). The difference between this curve and the modified Wannier ND_L reflected the slope of the reduced mobility curve. The two curves were identical in the low field region in which the reduced mobility was independent of E/N. At intermediate values of E/N, the reduced mobility curve had a positive slope; the correction factor, equation (5-3), was greater than unity; and the Viehland-Mason ND_L lay above the modified Wannier ND_L. The two curves crossed at approximately E/N = 120 Td where the reduced mobility was a maximum. At higher E/N, the reduced mobility had a negative slope, the correction factor, equation (5-3), was less than unity, and the Viehland-Mason ND_L lay below the modified Wannier ND_L. The Viehland-Mason ND_L agreed well with the experimental data over the entire range of E/N.

The solid curve in Figure 7 was the improved Viehland-Mason ND_L from equation (3-66). The improved Viehland-Mason ND_L did not agree as well with the experimental data at moderate fields from 30 Td to 80 Td as did the original Viehland and Mason ND_L. For E/N greater than 80 Td, the improved Viehland and Mason ND_L agreed better with the experimental data than did any of the other theories. The values[23] $v_d^0 = 2.3 \times 10^5$ cm/sec and $\gamma_\infty = +0.01$ were used in equation (3-67) to calculate the improved Viehland-Mason ND_L from equation (3-66).

Na^+ in He

From equation (5-2) the expected value for ND_L in the zero field limit was

15.72×10^{12} $cm^{-1}sec^{-1}$, using the value of $K_0(0) = 22.64$ $cm^2/V\text{-sec}$ from Chapter IV. The experimental values of ND_L appeared as points in Figures 8, 9, and 10. The measured ND_L increased from the zero field limit with increasing E/N up to the highest value of E/N used, 174 Td. The dashed curve in Figure 8 was the original Wannier ND_L from equation (3-60). The original Wannier ND_L increased from the zero field value at low E/N to a curve of slope 2 at high E/N on the log-log axes used. As can be seen from Figure 8, the original Wannier ND_L deviated significantly from the experimental data except for the crossing at approximately 50 Td.

The solid curve in Figures 8 and 9 represented the modified Wannier ND_L from equation (3-62). For E/N between approximately 5 Td and 75 Td, $K_0(E/N)$ was larger than $K_0(0)$, causing the modified Wannier ND_L to lie above the original Wannier ND_L. At approximately 75 Td, the reduced mobility was equal to the zero field reduced mobility, and the two values of ND_L agreed. For E/N greater than 75 Td, the reduced mobility was less than the zero field reduced mobility, causing the modified Wannier ND_L to lie below the original Wannier ND_L. The modified Wannier ND_L agreed with the experimental data fairly well below approximately 30 Td. At higher E/N, the modified Wannier ND_L lay significantly above the experimental data. However, it appeared that the modified Wannier ND_L followed the profile of the experimental data at intermediate and high E/N much better than the original Wannier ND_L did.

The dashed curve in Figure 9 represented the Viehland-Mason NDL from equation (3-64). The Viehland-Mason ND_L lay above the modified Wannier ND_L

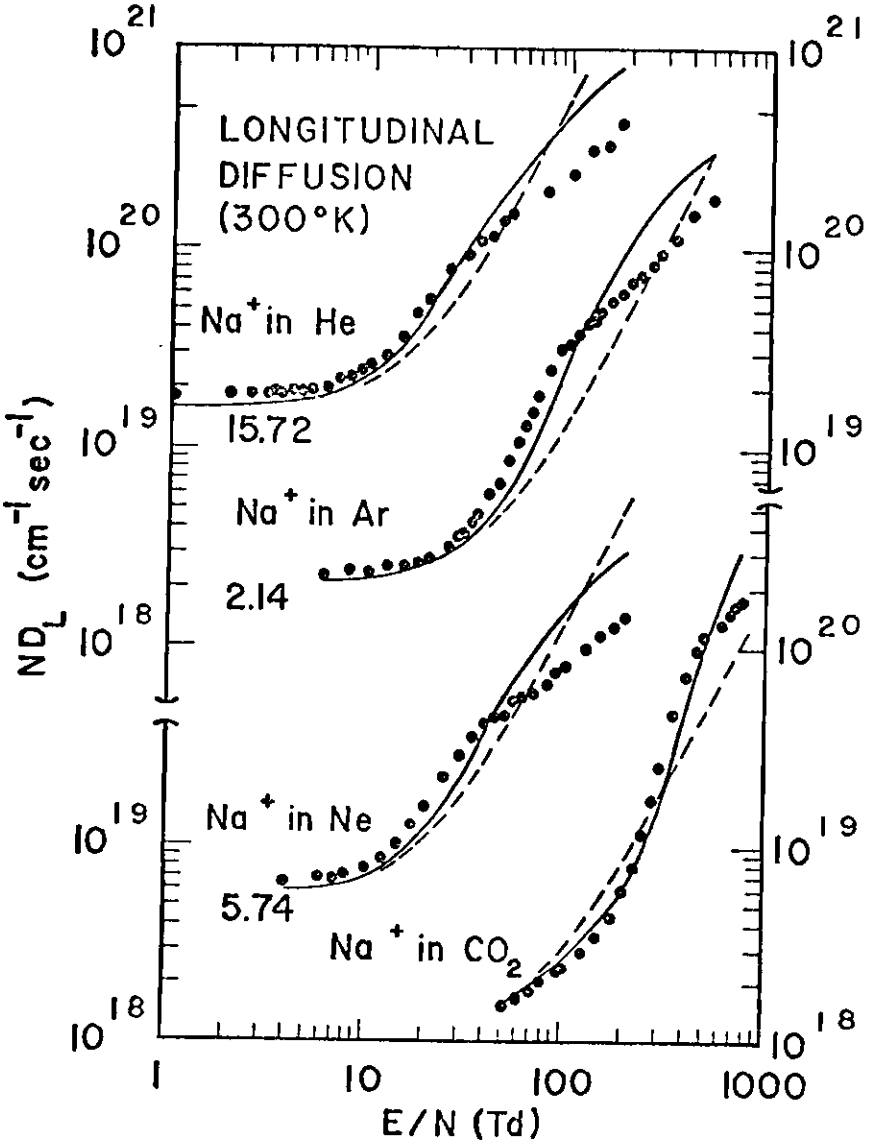

Fig. 8. Longitudinal Diffusion Coefficients for Na^+ in He, Ne, Ar, and CO_2 Compared to the Wannier Predictions. The Experimental Data are Represented by Dots, the Wannier Theory Using Constand Mean Free Time is Represented by the Dashed Curves, and the Wannier Theory Modified to Take Account of Variations in the Reduced Mobility with E/N is Represented by the Solid Curve.

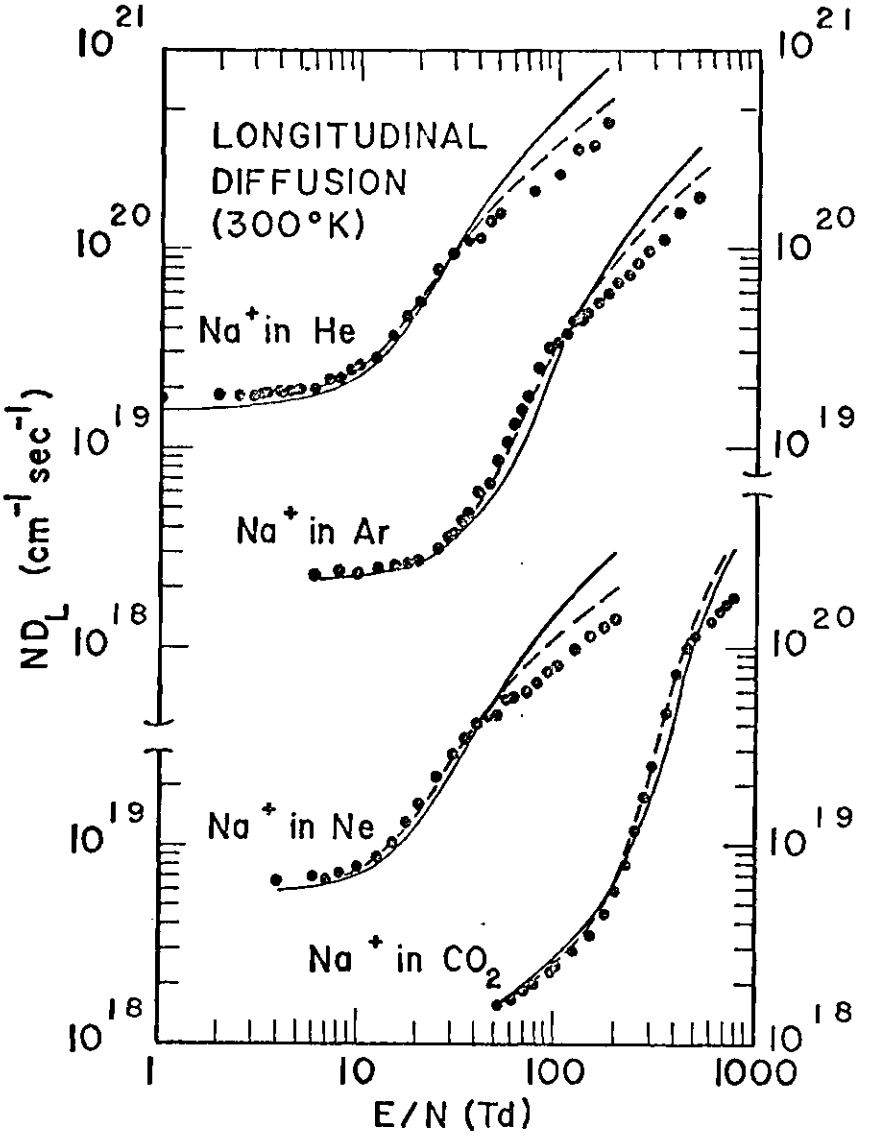

Fig. 9. Longitudinal Diffusion Coefficients for Na^+ in He, Ne, Ar, and CO_2 Showing the Modified Wannier Predictions with the Viehland-Mason Correction. The Experimental Data are Represented by Points, the Wannier Theory Modified to Take Account of Variations in the Reduced Mobility with E/N is Represented by the Solid Curve, and the Modified Wannier Theory with the Viehland-Mason Second Order Correction is Represented by the Dashed Curve.

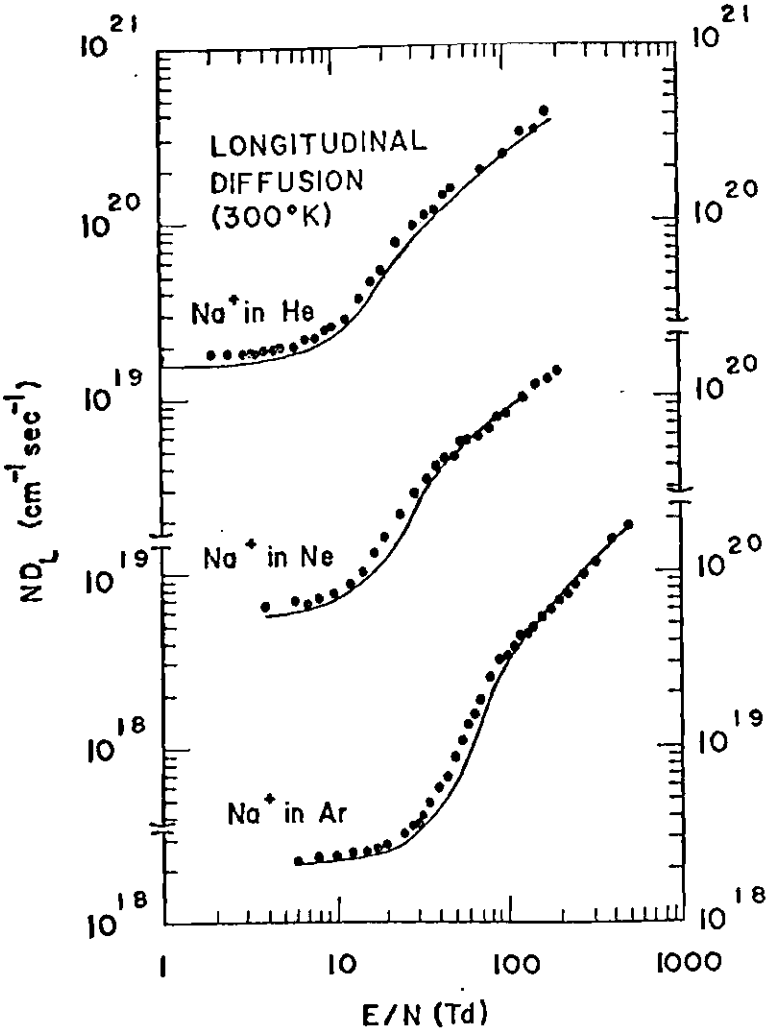

Fig. 10. Longitudinal Diffusion Coefficients for Na^+ in He, Ne, and Ar Showing the Improved Viehland-Mason Predictions. The Experimental Data are Represented by Points, and the Modified Wannier Theory with the Viehland-Mason Second Order Correction and the High E/N Modifications to the Drift Velocity and Collision Integrals is Represented by the Solid Curves.

for E/N greater than the low field region up to approximately 30 Td at which $K_0(E/N)$ was a maximum. For these values of E/N, the reduced mobility had positive slope as can be seen from Figure 3 in Chapter IV, and the correction factor given by equation (5-3) was greater than unity. For E/N greater than approximately 30 Td, the reduced mobility decreased from its maximum. The negative slope of the reduced mobility made the correction factor less than unity. The resulting Viehland-Mason ND_L lay below the modified Wannier ND_L for E/N greater than 30 Td. Figure 9 showed good agreement between Viehland-Mason ND_L and the experimental ND_L below approximately 30 Td. At higher E/N the Viehland-Mason ND_L agreed better with the experimental data than did either the original or the modified Wannier ND_L, but still differed significantly from the experimental data.

The solid curve in Figure 10 was the improved Viehland and Mason ND_L from equation (3-66). The improved Viehland and Mason ND_L gave fair agreement with the experimental data below 70 Td. However, for E/N greater than 70 Td, the improved Viehland-Mason ND_L agreed better with the experimental data than did any other theory. The values[23] of $v_d^0 = 2.1 \times 10^5$ cm/sec and $\gamma_\infty = -0.01$ were used in equation (3-67) to plot the improved Viehland-Mason ND_L from equation (3-66).

Na^+ in Ar

Experimental values for ND_L were obtained from E/N = 6.01 Td to E/N = 502 Td. The experimental values appeared as points in Figures 8, 9, and 10. The zero field limit of $ND_L = 2.14 \times 10^{18}$ $cm^{-1}sec^{-1}$ was obtained from the Einstein relation, equation (5-2) where $K_0(0) = 3.09$ $cm^2/V\text{-sec}$ from Chapter IV.

The dashed curve in Figure 8 represented the original Wannier ND_L equation (3-60). The original Wannier ND_L increased from the zero field value to a line of slope 2 on the log-log axes used. This curve agreed with the experimental data at very low E/N. At higher E/N, the original Wannier ND_L differed significantly from the experimental data except at the crossing point near E/N = 300 Td.

The solid curve in Figures 8 and 9 represented the modified Wannier ND_L, equation (3-62). The modified Wannier ND_L lay above the original Wannier ND_L from E/N of approximately 20 Td up to E/N of approximately 500 Td, because in this region, the reduced mobility was greater than the zero field reduced mobility, as can be seen from Figure 3 in Chapter IV. The modified Wannier ND_L lay closer to the experimental data at intermediate E/N than did the original Wannier ND_L, but agreement was still not good. At E/N above 200 Td, neither the original Wannier ND_L nor the modified Wannier ND_L agreed well with the experimental data.

The dashed curve in Figure 9 represented the Viehland-Mason ND_L from equation (3-64). Above the low field region, the Viehland and Mason ND_L lay above the modified Wannier ND_L, because the reduced mobility as a function of E/N had positive slope, making the correction factor given by equation (5-3) greater than unity. The Viehland-Mason ND_L equaled the modified Wannier ND_L at approximately 120 Td, since the reduced mobility was a maximum there. Above 120 Td, the reduced mobility had negative slope, the correction factor was less than unity, so that the Viehland-Mason ND_L lay below the modified Wannier ND_L. Figure 9 showed that the Viehland and Mason ND_L gave good agreement with the experimental data below approximately 100 Td. Above 100 Td, the Viehland-Mason ND_L gave

better agreement with the experimental data than did the modified Wannier ND_L, but significant differences still appeared.

The solid curve in Figure 10 was the improved Viehland-Mason ND_L from equation (3-66). For E/N less than 120 Td, the improved Viehland-Mason ND_L did not agree as well with the experimental data as the original Viehland-Mason ND_L did. However, for E/N greater than 120 Td, the improved Viehland-Mason ND_L gave very good agreement with the experimental data over a considerable range of E/N (from approximately 120 Td to 502 Td). The values[23] of $v_d^0 = 1.3 \times 10^5$ cm/sec and $\gamma_\infty = -0.035$ were used in equation (3-67) to plot the improved Viehland-Mason ND_L from equation (3-66).

Na^+ in Ne

Experimental values for ND_L were obtained from E/N = 3.99 Td to E/N = 199 Td. These values appeared as points in Figures 8, 9, and 10. The zero field limit of $ND_L = 5.74 \times 10^{18}$ cm^{-1} sec^{-1} was calculated from equation (5-2) using $K_0(0) = 8.27$ cm^2/V-sec from Chapter IV. The dashed curve in Figure 8 represented the original Wannier ND_L from equation (3-60). The original Wannier ND_L increased from the zero field limit to a line of slope 2 on the log-log axes used. Except for very low E/N, and the crossing point, the original Wannier ND_L gave poor agreement with the experimental data.

The solid curve in Figures 8 and 9 represented the modified Wannier ND_L from equation (3-62). The modified Wannier ND_L lay above the original Wannier ND_L from approximately 12 Td up to approximately 110 Td, because in this region the reduced mobility was greater than the zero field reduced mobility. At E/N

above 110 Td, the modified Wannier ND_L lay below the original Wannier ND_L, because the reduced mobility was less than the zero field reduced mobility. Figure 8 showed that at intermediate values of E/N, the modified Wannier ND_L lay closer to the experimental data than did the original Wannier ND_L, but agreement with the experimental data was still not good. At higher values of E/N, neither the original Wannier ND_L nor the modified Wannier ND_L gave good agreement with the experimental data.

The dashed curve in Figure 9 represented the Viehland-Mason ND_L from equation (3-64). From the low field E/N up to E/N of approximately 45 Td, the Viehland-Mason ND_L lay above the modified Wannier ND_L, because $K_0(E/N)$ had positive slope, making the correction factor, equation (5-3), greater than unity. At E/N greater than 45 Td, the Viehland-Mason ND_L lay below the modified Wannier ND_L, because $K_0(E/N)$ had negative slope, making the correction factor less than unity. The Viehland and Mason ND_L gave good agreement with the experimental data below E/N of 45 Td. At higher E/N, the Viehland-Mason ND_L lay closer to the experimental data than did either the original Wannier ND_L or the modified Wannier ND_L, but agreement with experimental data was not good.

The solid curve in Figure 10 was the improved Viehland-Mason ND_L from equation (3-66). For E/N less than 50 Td, the improved Viehland-Mason ND_L did not agree as well with the experimental data as the original Viehland-Mason ND_L did. However, for E/N greater than 50 Td, the improved Viehland-Mason ND_L agreed much better with the experimental data than did any other theory. The values[23] of $v_d^0 = 1.15 \times 10^5$ cm/sec and $\gamma_\infty = -0.06$ were used in equation (3-67)

to plot the improved Viehland-Mason ND_L from equation (3-66).

$\underline{Na^+ \text{ in } CO_2}$

Values of ND_L were measured for E/N from 51.8 Td to 762 Td. The zero field limit of ND_L was not found in this case, because clustering prevented an accurate measurement of $K_0(0)$ as explained in Chapter IV. However, using the reduced mobility at the lowest value of E/N measured in place of $K_0(0)$ in equation (5-2) gave a zero field limit of ND_L of 1.14×10^{18} $cm^{-1}sec^{-1}$. The dashed curve in Figure 8 gave the original Wannier ND_L from equation (3-60). This curve approached a straight line of slope 2 on the log-log axes used. There was good agreement between the original Wannier ND_L and the experimental data at very low E/N, and fair agreement even at higher E/N. Only for this ion-gas combination did the Wannier ND_L lie above the experimental ND_L at intermediate values of E/N.

The solid curve in Figures 8 and 9 was the modified Wannier ND_L from equation (3-62). Unlike the other six ion-gas combinations, the reduced mobility plotted in Figure 3 decreased with increasing E/N for intermediate E/N. This decreased reduced mobility gave a modified Wannier ND_L which lay below the original Wannier ND_L at intermediate E/N. However, as E/N was further increased, the reduced mobility increased. Thus, at high E/N, the modified Wannier ND_L from equation (3-62) lay above the original Wannier ND_L. Except for the cour highest E/N data points, the modified Wannier ND_L gave good agreement with the experimental data.

The dashed curve in Figure 9 gave the Viehland and Mason ND_L from

equation (3-64). The correction factor from equation (5-3) was less than unity below approximately 200 Td, because the reduced mobility decreased to a minimum value in the neighborhood of 200 Td. Thus, the Viehland and Mason ND_L lay below the modified Wannier ND_L for E/N less than 200 Td. In the neighborhood of 200 Td, the Viehland and Mason ND_L was identical to the modified Wannier ND_L, because the reduced mobility passed through a minimum there. For E/N greater than 200 Td, the reduced mobility increased with increasing E/N, giving a Viehland-Mason ND_L which lay above the modified Wannier ND_L. Except for the highest E/N data, the Viehland-Mason ND_L gave excellent agreement with the experimental data. However, for E/N greater than 500 Td, the Viehland-Mason ND_L differed significantly from the experimental data.

Generalizations

The following general conclusions were drawn from Figures 5, 6, 7, 8, 9, and 10. For a given ion-gas combination, there was a low field region in which all theories agreed well with the experimental data, approaching the zero field limit of ND_L given by the Einstein equation (5-2). There was a moderate field region in which agreement between theory and experiment improved in going from the original Wannier equation (3-60) to the modified Wannier equation (3-62) to the Viehland-Mason equation (3-64) which gave very good agreement with the experimental data for moderate field. In the moderate field region, the improved Viehland-Mason ND_L did not agree as well with the experimental data as the original Viehland-Mason ND_L did. There existed a high field region in which

agreement between theory and experiment improved steadily in going from the original Wannier equation (3-60) to the modified Wannier equation (3-62) to the Viehland-Mason ND_L equation (3-64) to the improved Viehland-Mason ND_L equation (3-66). In the high field region, the improved Viehland-Mason ND_L gave excellent agreement with the experimental data.

Error Analysis

Drift Velocity

Errors in determining the drift velocity arose from errors in determining $\overline{\Delta t}$ and Δz. These errors have already been discussed in Chapter IV. The systematic and random errors in a single determination of Δz were found to be 0.26% and 0.10% respectively. The error in determining $\Delta \bar{t}$ was bounded by the maximum error in $\Delta \bar{t}$ for any ion-gas combination, or 0.04% systematic error and 0.9% random error. Thus, the error in v_d for any ion-gas combination was bounded by the error estimate of 1.2% formed in adding the systematic errors to the RMS of the random errors. This error in drift velocity gave rise to an error in D_L for the following reason. Before fitting the theoretical arrival time spectrum given by equation (5-1) to the data recorded by the time-of-flight analyzer, the drift velocity was found by methods outlined in Chapter IV. Fitting a theoretical arrival time spectrum, incorporating an incorrect drift velocity, to the data recorded by the time-of-flight analyzer, would yield an incorrect value for D_L. Schummers[42] has shown that small variations in the drift velocity resulted in variations in the longitudinal diffusion coefficient that were approximately three

times as large as the variations in the drift velocity. Therefore, the error in D_L due to errors in the drift velocity was assigned a value three times the error in drift velocity given above, or 3.6%.

Temperature

In the high field region, the average ion energies were well above thermal. Equation (3-60) showed that the high field term was independent of temperature, except for the weak temperature dependence of the reduced mobility. Therefore, variations in gas temperature had little effect upon the energies involved in the ion-gas collision at high E/N.

In the low field region, the error in ND_L due to an error in temperature was significant. In the low field region Equation (3-60) reduced to

$$ND_L = 2.315 \times 10^{-3} K_0(0) T.$$

Since $K_0(0)$ varied only weakly with variations in temperature, ND_L varied directly with temperature. The error in a measurement of temperature was determined to be 0.67% by adding the systematic and random errors in temperature from Table 1 in Chapter IV. Hence, the same error of 0.67% was assigned to the variation in ND_L due to an error in temperature.

E/N

Errors in ND_L due to errors in E/N were very small in the low field region, because ND_L was nearly independent of E/N in the low field region. However, at high E/N, equation (3-60) showed that ND_L varied as $(E/N)^2$. Since the quantity E/N was directly or inversely proportional to z, V, T, and P, the error

in a measurement of E/N was taken to be the sum of the individual systematic errors in z, V, T, and P, plus the RMS random error in z, V, T, and P, or 1.4% for E/N less than 350 Td, and 1.7% for E/N greater than 350 Td. The error introduced into the determination of ND_L was twice the error in E/N. Thus, the maximum error in ND_L due to errors in E/N was assigned the high field value of 3.4% for E/N greater than 350 Td, and the low field value of 2.8% for E/N less than 350 Td.

Other Errors

The value of the longitudinal diffusion coefficient was determined fitting the theoretical arrival time spectrum given by equation (5-1) to the experimental arrival time spectrum. A reasonable error involved in the curve fitting was the root mean square value of the difference between the theoretical and experimental arrival time spectra. Random scatter of data in the experimental arrival time spectra was thought to be small due to the large number of ions detected in each position of each run. For each experimental arrival time spectrum, the time-of-flight analyzer was set to record a maximum of 2^{12} or 4096 ions in the peak channel. The indication of random scatter in measurements of ND_L was the scatter among the values of ND_L measured at the different distances during a run. The scatter among the values of ND_L for one run averaged less than 4.0% for each ion-gas combination.

Another source of error at high E/N resulted from the assumption of Fickian diffusion. The experimental arrival time spectrum was fitted to the theoretical arrival time spectrum Φ, that assumed only Fickian diffusion, i.e.,

$$j_z = nv_d - D_L \frac{\partial n}{\partial z} \quad .$$

Appendix IV showed that at high E/N, non-Fickian diffusion, i.e.

$$j_z = nv_d - D_L \frac{\partial n}{\partial z} + Q \frac{\partial^2 n}{\partial z^2}$$

was important, and it examined the effect that the inclusion of non-Fickian diffusion had on the value of D_L. From that Appendix, the systematic error in ND_L due to non-Fickian diffusion was estimated at 5.0% or less at high E/N. At low E/N, the error in ND_L due to non-Fickian diffusion was negligible compared to the other errors listed above.

These individual sources of error were considered to be independent, and the best estimate of probable error was obtained by combining them in a square root of the sum of the squares fashion. Combining the above errors yielded an error bound of 5.6% in the low field (E/N less than 350 Td) region, and 7.8% in the high field region (E/N greater than 350 Td).

Comparison with Existing Data

The only other known measurements of the longitudinal diffusion coefficient for any of the ion-gas combinations studied in this thesis were those made by Keller et al.[4] for Li^+ in Ar. A comparison of the ND_L measured in this work to the ND_L measured by Keller et al. is presented in Figure 11. In that figure, an "x" indicated the value of the ratio of ND_L measured in this work to the value of

ND_L given by the Einstein equation (5-2), and a point indicated the value of the same ratio as determined by Keller, et al. The measurements of Keller, et al. covered only the limited range of E/N from 9 Td to 24 Td, so that no firm conclusions could be drawn from the comparison. However, considering the 7.2% error in ND_L estimated by this lab, and the fact that the ion source of Keller, et al. did not approximate a point source pulse of ions, the two sets of data compare favorably.

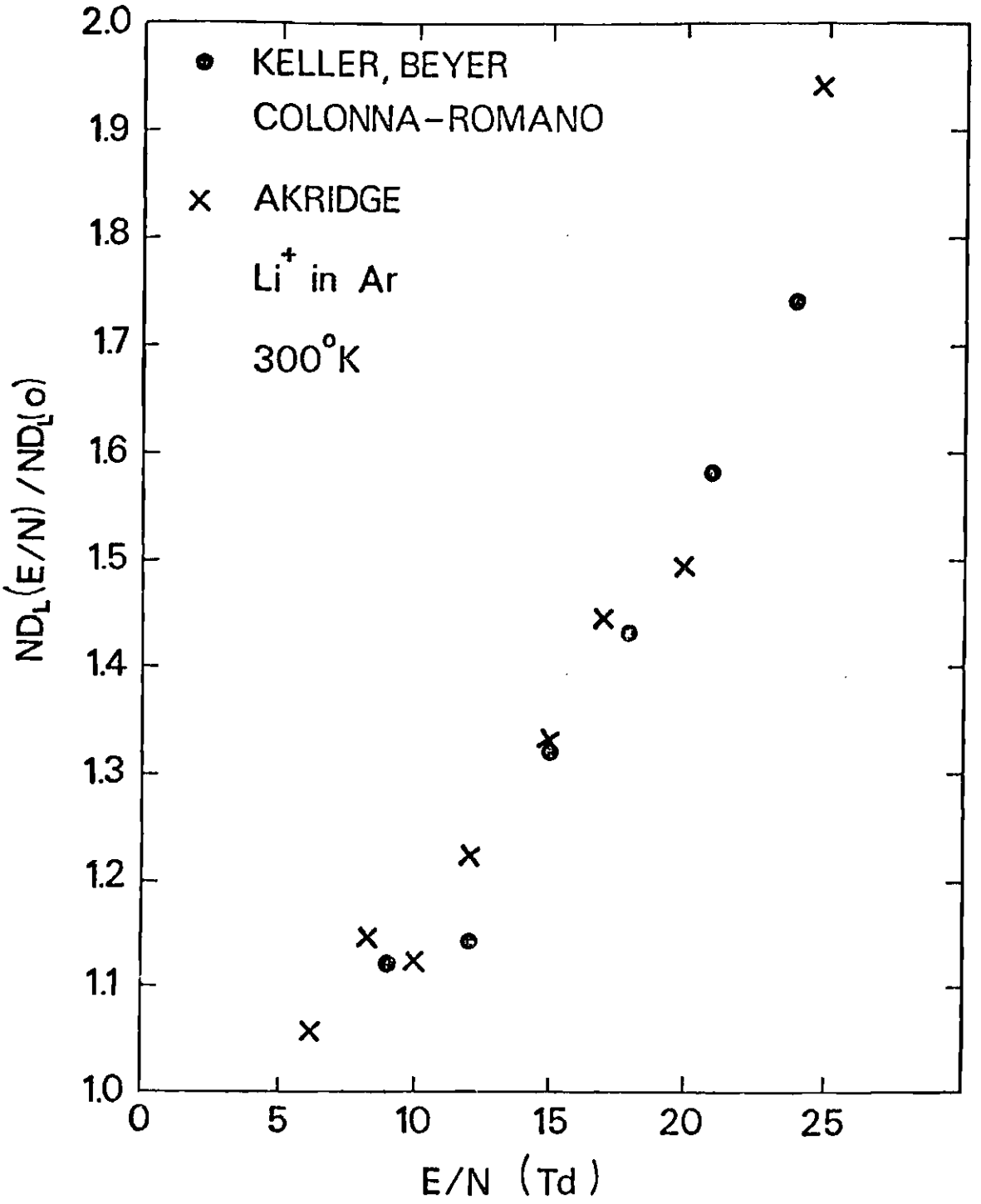

Fig. 11. Comparison of the Longitudinal Diffusion Coefficients for Li^+ in Ar with the Results of Keller, et al.

CHAPTER VI

CONCLUSIONS

The reduced mobilities of seven ion-gas combinations were measured over a much wider range of E/N and pressure than had been done previously. All measurements were made at approximately 300 ^{o}K.

The reduced mobilities of Li^+ and Na^+ in He, Ne, and Ar exhibited the usual features of alkali ions in a monatomic gas. There was a low field region in which the reduced mobility was independent of E/N. The zero field reduced mobilities unambiguously measured in this work were 23.06 cm^2/V-sec for Li^+ in He, 10.70 cm^2/V-sec for Li^+ in Ne, 4.63 cm^2/V-sec for Li^+ in Ar, 22.64 cm^2/V-sec for Na^+ in He, 8.27 cm^2/V-sec for Na^+ in Ne, and 3.09 cm^2/V-sec for Na^+ in Ar. As E/N was increased above the low field region, the reduced mobility increased to a maximum. As E/N was further increased, the reduced mobility decreased continually up to the highest values of E/N used. No significant clustering was observed for any of the above ion-gas combinations.

The reduced mobility of Na^+ in CO_2 was not measured for E/N less than 51.8 Td, so that an accurate zero field reduced mobility was not obtained. The reduced mobility at the lowest E/N used was 1.63 cm^2/V-sec. As E/N was increased from 51.8 Td to 200 Td, the reduced mobility decreased. As E/N was further increased, the reduced mobility increased up to the maximum value of E/N used, 762 Td. It was interesting to speculate that inelastic collisions were

responsible for the dip in the reduced mobility of Na^+ in CO_2 in the neighborhood of 200 Td.

The zero field reduced mobilities of all the ion-gas combinations measured compared favorably with earlier measurements.[1,3,4] The reduced mobility of Na^+ in CO_2 had not been measured before for any value of E/N.

The values of ND_L were measured for Li^+ in He, Ne, and Ar, and for Na^+ in He, Ne, Ar, and CO_2 over as wide a range of E/N and pressure as possible. With the exception[4] of measurements of ND_L over a limited range of E/N for Li^+ in Ar, these are the only measurements of ND_L existing for the above seven ion-gas combinations. At low enough E/N, the measured ND_L values approached the Einstein values from equation (5-2), except for Na^+ in CO_2, because clustering limited the minimum E/N used in that case. The values of the Einstein ND_L's measured were 7.43×10^{18} cm^{-1} sec^{-1} for Li^+ in Ne, 16.01×10^{18} cm^{-1} sec^{-1} for Li^+ in He, 3.22×10^{18} cm^{-1} sec^{-1} for Li^+ in Ar, 15.72×10^{18} cm^{-1} sec^{-1} for Na^+ in He, 2.14×10^{18} cm^{-1} sec^{-1} for Na^+ in Ar, and 5.74×10^{18} $cm^{-1}sec^{-1}$ for Na^+ in Ne. Increasing E/N resulted in a steeply increasing ND_L up to the highest values of E/N used, 762 Td.

The measured values of ND_L were compared with the predictions of four theories. The original Wannier theory assumed a polarization interaction. The modified Wannier theory attempted to remove the model dependence from the Wannier theory by using $K_0(E/N)$ instead of $K_0(0)$ in the expression for ND_L. The Viehland-Mason theory corrected for higher order terms in E/N. The improved Viehland-Mason theory used a drift velocity and a ratio of collision integrals

that should give good high field results. In the low field region, each of the four theories approached the Einstein ND_L, as did the experimental data. For moderate fields, agreement between theory and experiment improved in going from the Wannier ND_L to either the modified Wannier ND_L or the improved Viehland-Mason ND_L, to the Viehland-Mason ND_L which gave excellent agreement for moderate fields. For high fields, agreement between theory and experiment steadily improved in going from the Wannier ND_L, to the modified Wannier ND_L, to the Viehland-Mason ND_L, to the improved Viehland-Mason ND_L, which gave excellent agreement for high fields.

For the case of Li^+ in He,[36] the experimentally determined collision integral $\bar{\Omega}^{(1,1)}$ was compared to the same collision integral obtained from theory. This comparison of experimental data and theoretical predictions was of great importance. The Catlow Li^+ - He interaction potential[35] was the result of an ab initio quantum mechanical derivation. The Li^+ -He system has only four electrons and is one of the simplest systems to treat theoretically, and the Catlow potential is the result of the most accurate calculations to date for this system. The Li^+ - He system has no excited states available to it at the energies encountered in the drift tube, because both Li^+ and He are closed shell structures. Finally, beam data are available at high E/N, but the Li^+ -He drift tube data filled in the gap corresponding to the wide range of ion-atom separations from long range attractions, through the potential minimum, to the hard core repulsion.

Deviations from Fickian diffusion were examined. A theoretical expression was derived for the parameter Q controlling longitudinal non-Fickian diffusion.

This expression was compared with the measured values of Q at high E/N for two ion-gas combinations, and was found to be in fair agreement with the experimental data. Although the deviations from Fickian diffusion were of minor numerical importance in the range of E/N and pressures used in this thesis, non-Fickian diffusion could make an interesting theoretical and experimental problem for the future.

APPENDICES

APPENDIX I

COMPARISON OF Li^+-HE DATA WITH THEORETICAL PREDICTIONS

This Appendix compares the theoretically determined and experimentally measured transport properties of Li^+ in He. It is basically the text of a paper[36] published by this author and others.

In the last few years ab initio quantal calculations of the Li^+-He interaction potential which are in substantial agreement have been reported.[35,43] This "Catlow" potential appears in Fig. 12. Reported here is a new kind of test of the Catlow potential, the first to cover a wide range of ion-atom separation distances using a single type of experimental data.

The work is based on the recently developed Viehland and Mason theory.[10] The primary conditions required by the theory are that the ions be present only in trace amounts and that only binary, elastic ion-atom collisions occur; these conditions are always met in experimental measurements of Li^+ mobility in He. Unlike previous approaches,[16] this theory is not restricted to a specific ion-atom mass ratio or interaction potential, and it applies at arbitrarily high values of E/N. In the first approximation, the drift velocity v_d is found by combining equations (3-34) and (1-1) to be given by

$$v_d = \frac{3eE}{8N}\left[\frac{\pi}{2\mu kT_{eff}}\right]^{\frac{1}{2}} \frac{1}{\overline{\Omega}^{(1,1)}(T_{eff})} , \qquad (I-1)$$

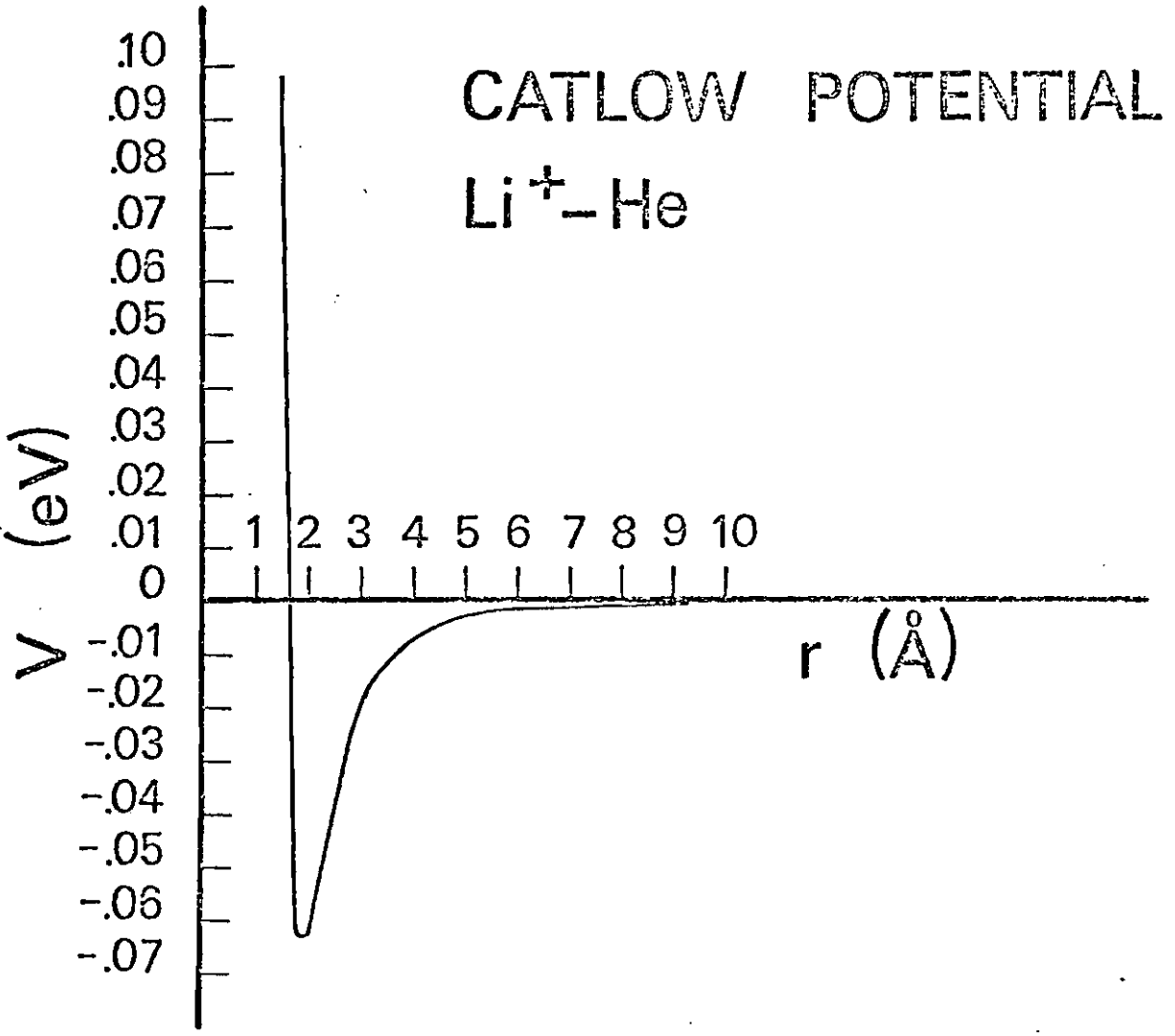

Figure 12. Catlow Interaction Potential for the Li^+-He System.

where the effective temperature T_{eff} is given in terms of the gas temperature T and the atomic mass M by

$$T_{eff} = T\left[1 + \frac{Mv_d^2}{3kT}\right]. \qquad \text{(I-2)}$$

Equation (I-1) shows that the ion-atom potential affects v_d only through the collision integral $\bar{\Omega}^{(1,1)}(T_{eff})$ defined by equations (3-31) and (3-32).

The important feature of this new theory of ion mobility is that it shows that v_d depends only upon T_{eff}, so that the variation of E/N at constant T in mobility measurements is equivalent to variation of T at constant E/N. This is important because much higher average ion energies can be achieved by operating at high values of E/N than can be obtained by heating the drift tube to the highest possible T. In summary, ion mobility measurements as a function of E/N at constant T can be used to obtain $\bar{\Omega}^{(1,1)}(T_{eff})$ as a function of T_{eff} over a wide range of effective temperature, and these values can then be used to test the accuracy of an ab initio potential over a wide range of ion-atom separation.

Using the Li^+ in He data reported in this thesis, $\bar{\Omega}^{(1,1)}(T_{eff})$ has been calculated as a function of T_{eff}, which ranged from 304 ^{o}K at the lowest value of E/N to 28,700^{o}K at the highest value. The results are plotted in Fig. 13, where the short-dash curve has been drawn through the many drift tube data points. For T_{eff} less than 4650 ^{o}K the data points were many and had little scatter. At large values of E/N (i.e., high T_{eff}), fewer data were collected because of the lower counting rates resulting from increased transverse diffusion in the drift tube, so that the uncertainty in the data increases above about 4650 ^{o}K. The point

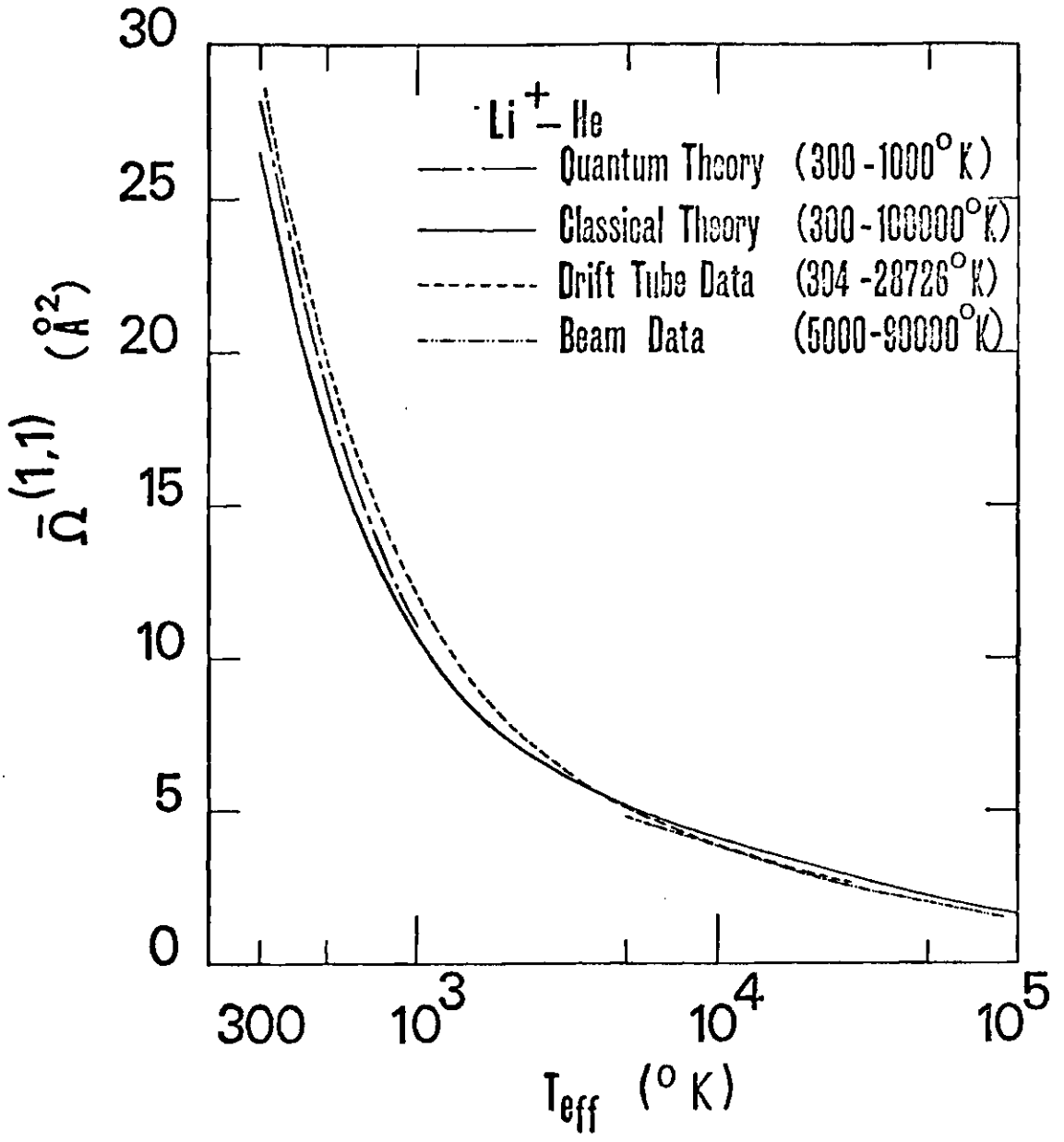

Fig. 13. Comparison of the Experimental and Theoretical $\bar{\Omega}^{(1,1)}$ over the T_{eff} Range 300 to 60,000°K. The curves labeled "Drift Tube Data" and "Beam Data" were obtained by analysis of experimental results, while those labeled "Classical Theory" and "Quantum Theory" were obtained by calculations based on the Catlow potential.

near 28,700 ^{o}K exhibits an especially large uncertainty. Here the small cross section for the Li^{+}-He system and the correspondingly small number of collisions are probably only marginally consistent with the swarm model used to analyze the experimental data, in spite of the very long ionic drift distance (up to 44 cm).

Because the ionic theory of Viehland and Mason[10] has been used only in its first approximation, the $\bar{\Omega}^{(1,1)}(T_{eff})$ curve is more inaccurate than the 2% inaccuracy attributable to most of the mobility measurements. Based on the considerations given in the Viehland and Mason theory,[10] it is estimated that, compared with the true results that would be obtained by using an infinite order approximation, the "Drift Tube Data" $\bar{\Omega}^{(1,1)}(T_{eff})$ values shown in Fig. 13 are between 1.5% too low and 2.5% too high at temperatures near 300 ^{o}K and between 4% and 8% too high at high temperatures (i.e. greater than 10,000 ^{o}K).

Li^{+} beam scattering experiments with He targets[44] have led to the short-range repulsive interaction potential

$$V(r) = 15.73 \exp(-2.704r) \qquad 1.47 < r < 2.29 \qquad \text{(I-3)}$$

where the energy V and the separation distance r are expressed in atomic units (27.210 eV and 5.2917×10^{-9} cm, respectively). Using this potential and the tabulations available in the literature,[45] the $\bar{\Omega}^{(1,1)}(T_{eff})$ curve shown in Fig. 13 that is labeled "Beam Data" was obtained. Since the potential given by equation (I-3) was claimed[44] to be accurate to 10%, the accuracy of this curve is 4%. Note that the $\bar{\Omega}^{(1,1)}(T_{eff})$ curve can be valid only over a range of temperature

(estimated[46] to be 6,000 ^{o}K to 60,000 ^{o}K) because the potential given by equation (I-3) is restricted to a small range of Li^{+}-He separation. Comparison of the two sets of "experimental" $\bar{\Omega}^{(1,1)}(T_{eff})$ data, one derived from ion mobility measurements and the other from beam scattering studies, shows them to be in excellent agreement over the range 10,000-20,000 ^{o}K.

In order to facilitate the theoretical calculation of $\bar{\Omega}^{(1,1)}(T_{eff})$ from equations (3-31) and (3-32), the Catlow potential was fitted by the expression

$$V(r) = \begin{cases} 16.93 \exp(-2.6306r) + (3.476 \times 10^{-7}),\ r^{-12} & r \leq 1.29 \\ 24.69 \exp(-2.6325r) - 0.7152\ r^{-4}, & 1.29 \leq r \leq 8 \\ -(2.923 \times 10^{-4}) \exp(-0.4933r) - 0.692\ r^{-4} & r \geq 8 \end{cases} \quad (I\text{-}4)$$

in atomic units. A classical calculation of $\bar{\Omega}^{(1,1)}(T_{eff})$ from this potential was made by using the Smith-O'Hara computer program.[47] The results, with a numerical accuracy of 0.1%, are shown in Fig. 13. The quantal calculation of $\bar{\Omega}^{(1,1)}(T_{eff})$ from the potential given by equation (I-4) involved the evaluation of $Q^{(1)}(E)$, given by equation (3-32), by the phase-shift method according to the equation

$$Q^{(1)}(E) = \left(\frac{4\pi}{K^2}\right) \sum_{\ell=0}^{\infty} (\ell + 1) \sin^2(\delta_\ell - \delta_{\ell+1}), \quad (I\text{-}5)$$

where δ_ℓ is the ℓ-th order phase shift and K is the wave number associated with E. The phase shifts were evaluated by integration of the Schrödinger equation using a Numerov technique, the criterion for convergence being that two successive evaluations agree within 10^{-3} radians. The effect of the long-range polarization

tail of the potential was taken into account[49] by using the JWKB approximation. The momentum-transfer cross section $Q^{(1)}$ was evaluated for K in the range 10^{-3}-30 atomic units, convergence being assumed when the ratio of the ℓ-th partial cross section to the sum was less than 10^{-5} for ten successive terms. In general, fewer than 100 phase shifts were required to achieve convergence, except at the highest energies where up to 200 were needed. The overall numerical accuracy of the quantal $\bar{\Omega}^{(1,1)}$ calculations is 0.2%.

It should be noted from Fig. 13 that the classical and quantal $\bar{\Omega}^{(1,1)}(T_{eff})$ curves computed from the Catlow potential are still distinguishable at 1,000 ^{o}K. In way of contrast, He-He interaction potentials give indistinguishable results above room temperature. The enhanced persistence of the classical-quantal difference in ion-atom systems is a direct result of the presence of the long-range polarization tail of the potential.[36]

A comparison of $\bar{\Omega}^{(1,1)}(T_{eff})$ over an extremely wide range of temperatures appears in Fig. 14. In Fig. 14, the quantal predictions are denoted by the letter "Q", and the classical predictions by the letter "C." A smooth curve was drawn through the beam data, and the curve was labeled with the letter "B." A smooth curve was drawn through the drift tube data reported in this thesis, and that curve labeled with the letter "D." Hoselitz's temperature-dependent data[50] appear as points. Using equation (3-34) and the definition of the reduced mobility, the comparisons of $\bar{\Omega}^{(1,1)}(T_{eff})$ in Fig. 14 are given in terms of reduced mobilities in Fig. 15. The generally good agreement of all theories and measurements over such a wide range of effective temperatures should be noted.

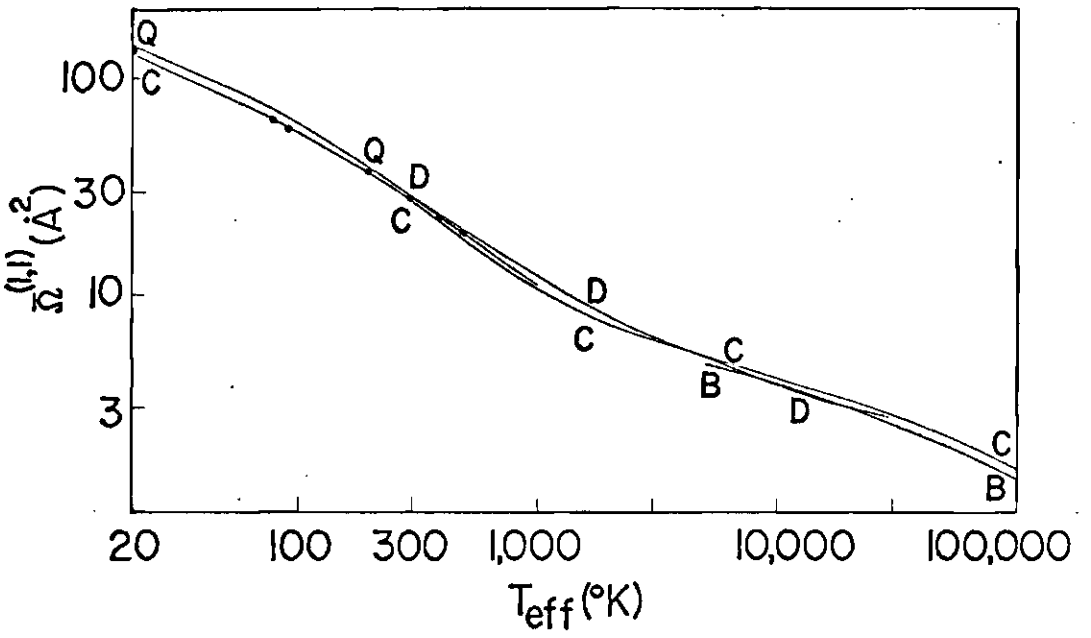

Fig. 14. Comparison of the Experimental and the Theoretical $\bar{\Omega}^{(1,1)}$ over the T_{eff} Range 20 to 100,000 °K. The Points give Hoselitz's Temperature-dependent Data. Q indicates Quantal Prediction, G indicates Classical Prediction, B indicates Beam Data, and D indicates Drift Tube Data.

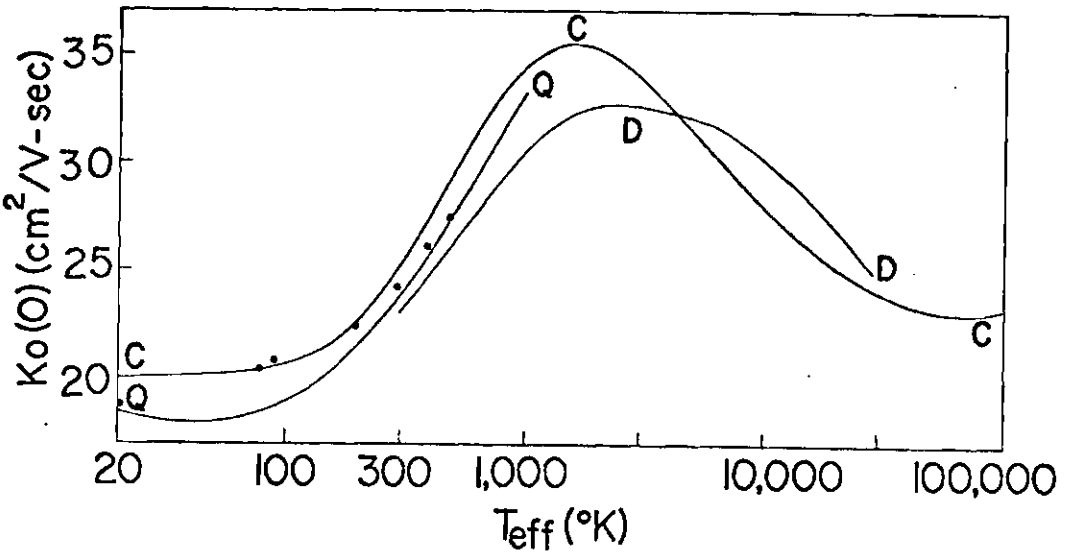

Fig. 15. Comparison of the Experimental and Theoretical Zero Field Reduced Mobilities over the Temperature Range 20 to 100,000°K. The Points give Hoselitz's Temperature-dependent Data. Q indicates Quantal Predictions, C indicates Classical Predictions, B indicates Beam Data, and D indicates Drift Tube Data.

The ability of the Catlow potential, demonstrated in Fig. 13, to reproduce the general features of the "experimental" $\bar{\Omega}^{(1,1)}(T_{eff})$ dependence on T_{eff} over the full range from 300 ^{o}K to 60,000 ^{o}K is impressive. However, close examination reveals some problems, which will now be discussed.

First, the theoretical and experimental $\bar{\Omega}^{(1,1)}(T_{eff})$ curves above 10,000 ^{o}K will be compared using Fig. 16, the ordinate of which is in units that bring out the differences between the various results. Note that in the range 10,000 ^{o}K to 20,000 ^{o}K, both sets of experimental data lie about 8% lower than the curve calculated from the Catlow potential. This discrepancy cannot be attributed to classical-quantal deviations in the theoretical curve, estimated to be less than 1% above 10,000 ^{o}K. Next, note that between 20,000 ^{o}K and 60,000 ^{o}K, the discrepancy between the $\bar{\Omega}^{(1,1)}(T_{eff})$ values calculated from the beam data and the Catlow potential persists at the level of 8-10%. For reasons mentioned earlier, at high E/N, the uncertainty in measurements of the reduced mobility, and therefore of $\bar{\Omega}^{(1,1)}(T_{eff})$, increases. Consequently, great weight should not be given to the drift tube data point at T_{eff} = 28,700 ^{o}K. Since both the magnitude and the direction of the 8-10% discrepancy between the theoretical and experimental $\bar{\Omega}^{(1,1)}(T_{eff})$ curves above 10,000 ^{o}K conflict with the error limits for these curves previously discussed, this discrepancy at high temperatures is considered to be significant. It could be eliminated by making a substantial modification in the Catlow potential at small r. For small r, the potentials given by equations (I-3) and (I-4) differ by as much as 23%.

Next, note from Fig. 16 that the theoretical and experimental $\bar{\Omega}^{(1,1)}(T_{eff})$

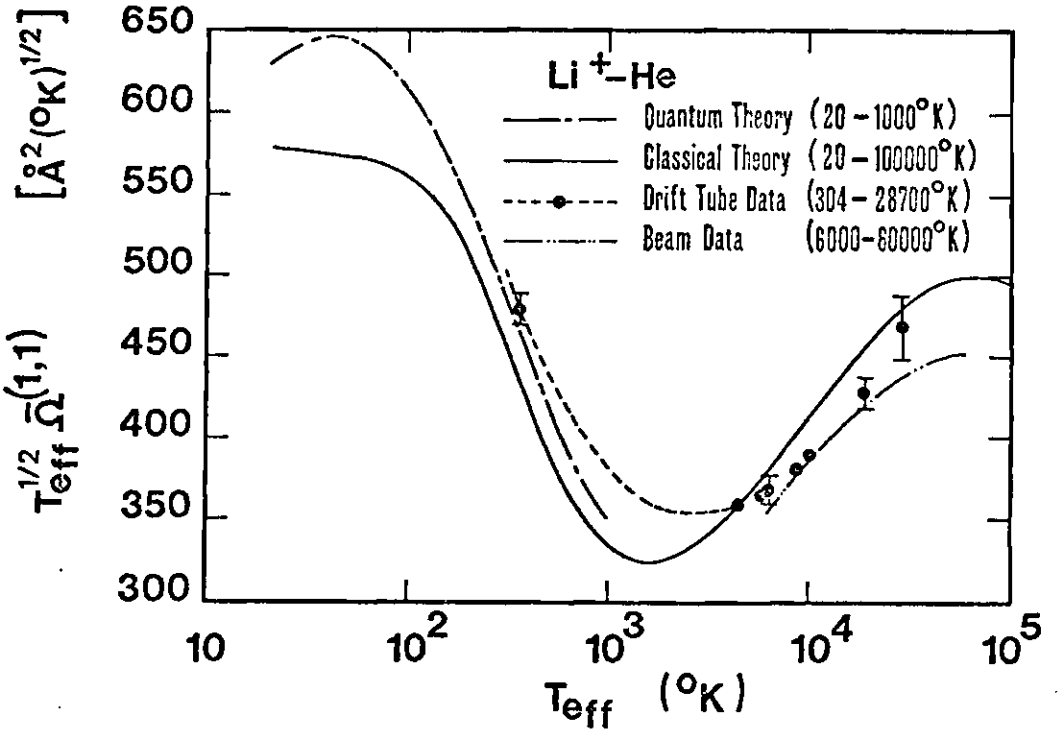

Fig. 16. $T_{eff}^{\frac{1}{2}}\,\bar{\Omega}^{(1,1)}$ as a Function of T_{eff}. The curves labeled "Drift Tube Data" and "Beam Data" were obtained by analysis of experimental results, while those labeled "Classical Theory" and "Quantum Theory" were obtained by calculations based on the Catlow Potential. Many drift tube data were taken for $T_{eff} \leq 4650^{\circ}$K; they are represented by the short-dash curve extending from 304 to 4650°K. Above 4650°K, drift tube data were taken at six values of T_{eff}: 6030, 9070, 10400, 19500, and 28700°K. Data points are shown for these six temperatures. The error bars on the data points reflect only the experimental error associated with the drift velocity measurements. Additional error arises from the use of the first-order expression [equation (I-1)] rather than an exact expression for $\bar{\Omega}^{(1,1)}$ in terms of v_d.

show a slight discrepancy at 300 ^{o}K. To be specific, using the quantal, theoretical value for $\bar{\Omega}^{(1,1)}(T_{eff})$ at 300 ^{o}K in equation (I-1) gives a value for the reduced mobility[16] of 23.78 cm^2/V-sec, which on the basis of the error analysis given previously should be too low (by no more than 0.5%, or 0.12 cm^2/V-sec). The experimental value is (23.06 $\pm$ 0.37) cm^2/V-sec. Therefore, the experimental and theoretical values lie just outside the combined error limits. This discrepancy is interpreted as reflecting an inaccuracy in the Catlow potential in the region of the potential minimum.

In conclusion, this test of the Catlow potential indicates that this potential is inaccurate at the short ion-atom separations, and may also be slightly inaccurate in the region of the potential minimum. Since the Li^+-He system has only four electrons and is one of the simplest systems to treat theoretically, and since the Catlow potential is the result of the most accurate calculations to date for this system, it is concluded that experimental measurements still contain more detailed information about ion-atom interaction potentials than can readily be obtained from ab initio calculations.

APPENDIX II

DIFFUSION ERROR INTRODUCED INTO TIME MEASUREMENTS

This Appendix examines the diffusion error introduced into the measurements of the average arrival time $\bar{t}$ made by using the differencing technique. This diffusion error has already been examined, but only in an approximate fashion, by Moseley.[29] In this Appendix, first an exact expression for the average arrival time is derived. This exact arrival time turns out to be identical to Moseley's first order approximate expression. Second, an expression for the diffusion error in measurements of drift velocity v_d is derived. Previous estimates[51] of this diffusion error for various ion-gas combinations were quotes of Moseley's value of 0.1%, arrived at by a computer simulation for N_2^+ ions in N_2.

The average arrival time $\bar{t}$, during which an ion pulse travels the distance z is given by

$$\bar{t} = \frac{\int_0^\infty t\,\Phi(0,z,t)dt}{\int_0^\infty \Phi(0,z,t)dt} \qquad \text{(II-1)}$$

where $\Phi(0,z,t)$ is the flux of ions leaving the drift region through the exit aperture on the axis of the drift tube a distance z from the ion source. In the above equation, r = 0, because in the experiment, the ions are detected on the axis of the drift region. There are two limiting geometries for the ion source, the point

source and the plane source. Moseley examined both of these geometries to a first order expansion in D_L. However, for both geometries, the calculation of $\bar{t}$ in equation (II-1) could have been done exactly.

For the infinite plane source, it can be shown[16] that for a non-reacting ion-gas combination;

$$\Phi(0,z,t) = \frac{As(v_d + z/t)}{(4\pi D_L t)^{\frac{1}{2}}} \; e^{-\frac{(z-v_d t)^2}{4D_L t}} , \qquad \text{(II-2)}$$

where s is the source strength, A is the area of the exit aperture, and v_d is the actual drift velocity. Substituting equation (II-2) into equation (II-1) and using the change of variable

$$t = \frac{z}{v_d} y^2 , \qquad \text{(II-3)}$$

equation (II-1) becomes

$$\bar{t} = \frac{v_d I_1 + z I_0}{v_d I_0 + z I_{-1}} , \qquad \text{(II-4)}$$

where

$$I_n = \left(\frac{z}{v_d}\right)\sqrt{\frac{zv_d}{D_L}} \; e^{\frac{zv_d}{2D_L}} \int_0^\infty y^{2n} \, e^{-\frac{zv_d}{4D_L}\left(y^2 + \frac{1}{y^2}\right)} dy . \qquad \text{(II-5)}$$

The integral expression I_n was approximated by Moseley, but can be evaluated exactly[52] for the cases n = 1, 0, -1, and -2 to give

$$I_1 = \frac{z}{v_d}\left(1 + \frac{2D_L}{zv_d}\right), \tag{II-6}$$

$$I_0 = 1, \tag{II-7}$$

$$I_{-1} = \frac{v_d}{z}, \tag{II-8}$$

and

$$I_{-2} = \left(\frac{v_d}{z}\right)^2\left(1 + \frac{2D_L}{zv_d}\right). \tag{II-9}$$

Using I_1, I_0, and I_{-1}, as given above, in equation (II-4), $\bar{t}$ becomes

$$\bar{t} = \frac{z}{v_d} + \frac{D_L}{v_d^2}, \tag{II-10}$$

which is identical to Moseley's first order expression for t.

For a point source, it can be shown[16] that for a non-reacting ion-gas combination

$$\Phi(0, z, t) = \frac{Ab(v_d + z/t)}{2(4\pi t)^{3/2}\, D_T D_L^{1/2}}\, e^{-\frac{(z - v_d t)^2}{4D_L t}} \tag{II-11}$$

where b is the point source strength. Using this expression for Φ in equation (II-1), $\bar{t}$ becomes

$$\bar{t} = \frac{v_d I_0 + z I_{-1}}{v_d I_{-1} + z I_{-2}}. \tag{II-12}$$

Using equations (II-7), (II-8), and (II-9) for I_0, I_{-1}, and I_{-2} yields

$$\bar{t} = \frac{z}{v_d}\left(1 + \frac{D_L}{z v_d}\right). \qquad \text{(II-13)}$$

The $D_L/v_d z$ term is typically much less than one. As an example, for the Li^+ in Ar run at 5.96 Td, $D_L/v_d z = 0.0019$ for the shortest drift distance. When $D_L/v_d z << 1$, the term in parenthesis in equation (II-13) can be expanded to give

$$\bar{t} = \frac{z}{v_d} - \frac{D_L}{v_d^2 z} + \frac{D_L^2}{v_d^3 z} - \ldots \qquad \text{(II-14)}$$

As expected, the first two terms of this expansion are identical to Mosesey's first order expression for $\bar{t}$ when reactions are absent. However, to evaluate the diffusion error involved when using the differencing technique, the $D_L^2/v_d^3 z$ term in equation (II-14) must be retained, because differencing eliminates the first order term, $D_L/v_d z$. Calculating v_d' by the differencing technique gives

$$v_d' = \frac{z_i - z_j}{t_i - t_j},$$

or

$$v_d' = \frac{v_d}{\left(1 - \dfrac{D_L^2}{v_d^2 z_i z_j}\right)}. \qquad \text{(II-15)}$$

The $D_L^2/v_d^2 z_i z_j$ term is typically small. As an example, for the Li^+ in Ar run at

5.96 Td between positions 5 and 6, $D_L^2/v_d^2\ z_i z_j = 2.9 \times 10^{-6}$. Thus, equation (II-15) may be written, to first order in $D_L^2/v_d^2\ z_i z_j$,

$$v_d' = v_d \left(1 + \frac{D_L^2}{v_d^2\ z_i\ z_j}\right) . \qquad \text{(II-16)}$$

The fractional error between v_d and v_d' from the above equation is $D_L^2/v_d^2\ z_i z_j$. Because v_d is approximately equal to v_d', the fractional error can also be written as $D_L^2/v_d'^2 z_i z_j$. As an upper bound on this error term, both z_i and z_j can be replaced by the minimum drift distance used, z_{min}, giving

$$\text{Fractional Diffusion Error} \leq (D_L/v_d' \text{ min})^2 . \qquad \text{(II-17)}$$

Expressing ND_L in units of 10^{18} cm^{-1} sec^{-1}, v_d' in units of 10^4 cm/sec, and pressure P in microns gives

$$\text{Percent Diffusion Error} \leq 1.54\ (ND_L/v_d'P)^2 , \qquad \text{(II-18)}$$

using a temperature of 300 ^{o}K and a minimum drift distance of 25 cm corresponding to position 4.

APPENDIX III

NON-FICKIAN ERROR IN THE DRIFT VELOCITY

This Appendix investigates non-Fickian longitudinal diffusion. In the first half of this Appendix, an expression is derived for ion current from a point source. In the second half, an expression is derived for the drift velocity as measured by the differencing technique.

The diffusion equation for non-reacting ions from a point source is

$$\vec{\nabla}\cdot\vec{j} + \frac{\partial n}{\partial t} = \beta(\vec{r}, t) , \qquad \text{(III-1)}$$

where

$$\beta(\vec{r}, t) = s\,\delta^3(\vec{r})\,\delta(t) = \frac{s}{(2\pi)^4}\int e^{i(\vec{k}\cdot\vec{r}-\omega t)}\, d^3k\, d\omega, \qquad \text{(III-2)}$$

represents the point source, $\vec{j}$ is the ion current density, and n is the ion number density. Since the ions drift longitudinally, deviations from Fickian diffusion should be noticed first in the longitudinal direction. Therefore, the components of the ion current density will be taken as[9]

$$j_x = -D_T \frac{\partial n}{\partial x} , \qquad \text{(III-3)}$$

$$j_y = -D_T \frac{\partial n}{\partial z} , \qquad \text{(III-4)}$$

and

$$j_z = nv_d - D_L \frac{\partial n}{\partial z} + Q \frac{\partial^2 n}{\partial z^2} \quad , \tag{III-5}$$

modifying equation (1-8).

Expanding

$$n(\vec{r}, t) = \frac{1}{(2\pi)^4} \int u(\vec{k}, \omega) e^{i(\vec{k}\cdot\vec{r} - \omega t)} d^3k d\omega \quad , \tag{III-6}$$

the diffusion equation (III-1) becomes

$$\left[D_T(k_x^2 + k_y^2) + D_L k_z^2 + iv_d k_z - iQ k_z^3 - i\omega\right] u(\vec{k}, \omega) = 1.$$

Substituting the solution for $u(\vec{k}, \omega)$ back into equation (III-6) gives

$$n(\vec{r}, t) = \frac{i}{(2\pi)^4} \int e^{i\vec{k}\cdot\vec{r}} d^3k \int_{-\infty}^{+\infty} \frac{e^{-i\omega t} du}{\omega + Qk_z^3 - v_d k_z + i\left[D_T(k_x^2 + k_y^2) + D_L k_z^2\right]} \quad .$$

The integral in braces can be evaluated by standard methods of complex analysis to yield for $t > 0$,

$$n(\vec{r}, t) = \frac{1}{(2\pi)^3} \int e^{i(k_x x + k_y y + k_z z) - i(v_d k_z - Qk_z^3)t - D_T t(k_x^2 + k_y^2) - D_L t k_z^2} d^3k \quad .$$

The integrals over k_x and k_y are well known,[52] and the ion number density reduces to

$$n(\vec{r},t) = \frac{s\,e^{-\frac{r^2}{4D_T t}}}{(4\pi D_T t)} \quad \frac{1}{2\pi}\int_{-\infty}^{+\infty} e^{-D_L t k_z^2 + i\left[(z - v_d t)\,k_z + Q t k_z^3\right.} \qquad \text{(III-7)}$$

Note that, if the diffusion were purely Fickian, Q would be zero, and equation (III-7) would reduce to

$$n_0(\vec{r},t) = \frac{se^{-\left[\frac{r^2}{4D_T t} + \frac{(z-v_d t)^2}{4D_L t}\right]}}{(4\pi D_T t)(4\pi D_L t)^{\frac{1}{2}}}, \qquad \text{(III-8)}$$

a familiar expression in diffusion theory.[16]

To find the longitudinal ion current density, substitute equation (III-7) into equation (III-5) to get

$$j_z = \frac{se^{-\frac{r^2}{4D_T t}}}{(4\pi D_T t)} \quad \frac{1}{2\pi}\int_{-\infty}^{+\infty} e^{-D_L t k_z^3 + i\left[(z - v_d t)k_z + Q t k_z^3\right.} \quad (v_d - ik_z D_L - Q k_z^3)\,dk_z \qquad \text{(III-9)}$$

This expression will be evaluated only to first order in Q, i. e.

$$j_z = j_z^{(0)} + Q j_z^{(1)} + \ldots . \qquad \text{(III-10)}$$

The zero order term is found by setting Q equal to zero in equation (III-9) and carrying out the integration to get

$$j_z^{(0)} = \frac{1}{2}\left(v_d + \frac{z}{t}\right) n_0(r, z, t) \quad . \tag{III-11}$$

The first order term $j_z^{(1)}$ is

$$j_z^{(1)} = \left.\frac{\partial jz}{\partial Q}\right|_{Q=0} ,$$

or

$$j_z^{(1)} = \frac{se^{-\frac{r^2}{4D_T t}}}{(4\pi D_T t)} \left[\frac{1}{2\pi} \int_{-\infty}^{+\infty} e^{(-k_z^2 + i t v_d k_z^3 + D_L t k_z^4)} e^{-D_L t k_z^2 + i(z - v_d t)k_z} \, dk_z \right] .$$

Evaluating the integral[52] gives

$$j^{(1)} = \frac{n_0}{4D_L t}\left[(4\xi^4 - 8\xi^2 + 1) + \frac{2v_d t}{\sqrt{D_L t}}\,\xi(2\xi^2 - 3)\right] , \tag{III-12}$$

where

$$\xi = \frac{z - v_d t}{\sqrt{D_L t}} \quad . \tag{III-13}$$

Combining equations (III-10), (III-11), and (III-12), the ion current density to first order in Q is

$$j_z(r, z, t) = j_z^{(0)}(r, z, t)\left\{1 + \frac{Q}{2D_L\sqrt{D_T t}} \left[\frac{(4\xi^4 - 8\xi^2 + 1) + \frac{2v_d t}{\sqrt{D_L t}}\,\xi(2\xi^2 - 3)}{\frac{(z + v_d t)}{\sqrt{D_L t}}} \right] \right\} . \tag{III-14}$$

Equation (III-14) is the desired expression for the longtiduinal ion current density with non-Fickian diffusion. The constant Q is determined by trial and error as that value which gives the best fit to the experimentally determined arrival time spectrum. The determination of a value for Q is the subject of Appendix IV.

The rest of this Appendix examines the problem of determining the drift velocity using the differencing technique when non-Fickian diffusion is present. For each position of a run, the average arrival time $\bar{t}$ is determined by numerical integration from

$$\bar{t} = \frac{\int_0^\infty t j_z(0, z, t)dt}{\int_0^\infty j_z(0, z, t)dt} \quad . \tag{III-15}$$

Using equation (III-5) in equation (III-15 yields

$$\bar{t} = \frac{\left(v_d - D\frac{\partial}{\partial z} + Q\frac{\partial^2}{\partial z^2}\right)\int_0^\infty tn(0, z, t)dt}{\left(v_d - D\frac{\partial}{\partial z} + Q\frac{\partial^2}{\partial z^2}\right)\int_0^\infty n(0, z, t)dt} \quad .$$

When equation (III-7) is used for $n(0, z, t)$, and the numerator and denominator are expanded to first order in Q, the result is

$$\bar{t} = \frac{\int_0^{\infty} \left\{ \left(v_d - D_L \frac{\partial}{\partial z} \right) + Q \frac{\partial^2}{\partial z^2} - t \left(v_d - D_L \frac{\partial}{\partial z} \right) \frac{\partial^3}{\partial z^3} \right\} dt \int_{-\infty}^{+\infty} e^{-D_L t k_z^2 + i(z - v_d t) k_z} dk_z}{\int_0^{\infty} \left\{ \left(v_d - D_L \frac{\partial}{\partial z} \right) + Q \frac{\partial^2}{\partial z^2} - t \left(v_d - D_L \frac{\partial}{\partial z} \right) \frac{\partial^3}{\partial z^3} \right\} \frac{dt}{t} \int_{-\infty}^{+\infty} e^{-D_L t k_z^2 + i(z - v_d t) k_z} dk_z}$$

Using the integral

$$\frac{1}{2\pi} \int_{-\infty}^{+\infty} e^{-D_L t k_z^2 + i(z - v_d t) k_z} dkz = \frac{e^{-\frac{(z - v_d t)^2}{4 D_L t}}}{(4\pi D_L t)^{\frac{1}{2}}} ,$$

the expression for $\bar{t}$ may be written as

$$\bar{t} = \frac{\left(v_d - D_L \frac{\partial}{\partial z} \right) \int_0^{\infty} t^{-\frac{1}{2}} e^{-\frac{(z + v_d t)^2}{4 D_L t}} dt + Q \left[\frac{\partial^2}{\partial z^2} \int_0^{\infty} t^{-\frac{1}{2}} e^{-\frac{(z - v_d t)^2}{4 D_L t}} dt - \left(v_d - D_L \frac{\partial}{\partial z} \right) \frac{\partial^3}{\partial z^3} \int_0^{\infty} t^{\frac{1}{2}} e^{-\frac{(z - v_d t)^2}{4 D_L t}} dt \right]}{\left(v_d - D_L \frac{\partial}{\partial z} \right) \int_0^{\infty} t^{-3/2} e^{-\frac{(z - v_d t)^2}{4 D_L t}} dt + Q \left[\frac{\partial^2}{\partial z^2} \int_0^{\infty} t^{-3/2} e^{-\frac{(z - v_d t)^2}{4 D_L t}} dt - \left(v_d - D_L \frac{\partial}{\partial z} \right) \frac{\partial^3}{\partial z^3} \int_0^{\infty} t^{-\frac{1}{2}} e^{-\frac{(z - v_d t)^2}{4 D_L t}} dt \right]} . \qquad \text{(III-16)}$$

Using the change of variable

$$t = \frac{z}{v_d}\, y^2 \ ,$$

all three integrals above may be evaluated.[52]

$$\int_0^\infty t^{-3/2} e^{-\frac{(z-v_d t)^2}{4D_L t}}\, dt = 2\frac{\sqrt{D_L}}{v_d} I_{-1} = \frac{2\sqrt{D_L}}{v_d}\left(\frac{v_d}{z}\right) , \qquad \text{(III-17)}$$

$$\int_0^\infty t^{-\frac{1}{2}} e^{-\frac{(z-v_d t)^2}{4D_L t}}\, dt = \frac{2\sqrt{D_L}}{v_d} I_0 = \frac{2\sqrt{D_L}}{v_d} \ , \qquad \text{(III-18)}$$

and

$$\int_0^\infty t^{-3/2} e^{-\frac{(z-v_d t)^2}{4D_L t}}\, dt = \frac{2\sqrt{D_L}}{v_d} I_1 = \frac{2\sqrt{D_L}}{v_d}\left[\frac{z}{v_z}\left(1+\frac{2D_L}{z v_d}\right)\right] \qquad \text{(III-19)}$$

where

$$I_n = \left(\frac{z}{v_d}\right)^n \left(\frac{z v_d}{D_L}\right)^{\frac{1}{2}} e^{\frac{z v_d}{2D_L}} \int_0^\infty y^{2n} e^{-\frac{z v_d}{4D_L}\left(y^2+\frac{1}{y^2}\right)}\, dy \ . \qquad \text{(III-20)}$$

Using equations (III-17), (III-18), and (III-19) in equation (III-16) gives

$$\bar{t} = \frac{z/v_d}{\left(1+\frac{D_L}{z v_d}+\frac{2Q}{z^2 v_d}\right)} \ . \qquad \text{(III-21)}$$

Assuming the terms in the denominator are small compared to unity,

$$\bar{t} \approx \frac{z}{v_d} - \frac{D_L}{v_d^2} + \frac{1}{z}\left(\frac{D_L^2}{v_d^3} - \frac{2Q}{v_d^2}\right) . \qquad \text{(III-22)}$$

Let v_d' represent the drift velocity determined by the differencing technique from the equation

$$v_d' = \frac{z_i - z_j}{\bar{t}_i - \bar{t}_j} \qquad \text{(III-23)}$$

The subscripts in equation (III-23) refer to different positions of a run. Using equation (III-22) in equation (I-23) yields

$$v_d' = \frac{v_d}{1 - \frac{1}{z_i z_j}\left(\frac{D_L}{v_d^2} - \frac{2Q}{v_d}\right)} . \qquad \text{(III-24)}$$

This is the desired equation for the drift velocity v_d' as measured from the differencing techniques, in terms of the true drift velocity v_d.

APPENDIX IV

DETERMINATION OF NON-FICKIAN COEFFICIENT Q

The purpose of this Appendix is to estimate the error in the determination of the value of ND_L at high E/N due to non-Fickian diffusion. Li^+ in Ne and Na^+ in Ar are used to arrive at an error assumed to be reasonable for all seven ion-gas combinations examined in this thesis. This Appendix first derives equation (IV-17) as an approximate formula to calculate the quantity N^2Q controlling non-Fickian diffusion, and it compares the results of the formula with the measured values of N^2Q. Agreement between the theoretical N^2Q and the measured N^2Q seen in Fig. 18 and Fig. 19 is reasonable, considering that the derivation of the theoretical expression for N^2Q contains the same restrictions as the derivations of the Wannier ND_L--the assumption that polarization is the dominant interaction. Agreement between the theoretical N^2Q and the measured N^2Q serves as a check on the concept of non-Fickian diffusion. Finally, this Appendix shows that ND_L at high E/N is lowered by approximately 5% when non-Fickian diffusion is taken into account.

A word about the importance of non-Fickian diffusion is in order. Since Q is proportional to N^{-2}, non-Fickian diffusion is relatively unimportant at low E/N. However, at high E/N, non-Fickian diffusion should be taken into account. A full theoretical treatment of non-Fickian diffusion similar to the Viehland and Mason theory[10] of Fickian diffusion would be very interesting as an independent study.

The resulting theory should then be carefully compared with experimental data taken only at high E/N.

To arrive at a theoretical expression for Q, it will be sufficient for the purpose of this Appendix to solve the transport equation assuming that polarization is the dominant interaction. The moment form of the transport equation (3-16) divided by n is

$$\frac{1}{n}\left[\frac{\partial}{\partial t}(n\langle\Psi\rangle)+\frac{\partial}{\partial z}(n\langle v_z\Psi\rangle)\right]-\frac{eE}{m}\left\langle\frac{\partial\Psi}{\partial v_z}\right\rangle = -N\langle J\Psi\rangle, \qquad \text{(IV-1)}$$

where only the longitudinal density gradients are considered. The iteration procedure developed by Whealton and Mason[9] will be used to solve this equation. Their iteration procedure assumes the spacial and temporal derivatives in equation (IV-1) are a lower order than the other two terms. The order of the approximation will be denoted by a superscript. The first approximation neglects spacial and temporal derivates to get

$$-\frac{eE}{m}\left\langle\frac{\partial\Psi}{\partial v_z}\right\rangle^{(1)} = -N\langle J\Psi\rangle^{(1)} . \qquad \text{(IV-2)}$$

This equation describes the problem of mobility without diffusion. The solution of this equation by an expansion in Burnett functions is the Kihara theory.[8] The solution for the moments of the first few Burnett functions for the polarization model is given in equations (3-35).

In the second approximation, the spacial and temporal derivatives of

equation (IV-1) are taken only to the first order to get

$$\frac{1}{n^{(1)}}\left[\frac{\partial}{\partial t}(n<\Psi>)^{(1)}+\frac{\partial}{\partial z}(n<v_z\,\Psi>)^{(1)}\right]-\frac{eE}{m}<\frac{\partial\Psi}{\partial v_z}>^{(2)}=N<J\Psi>^{(2)} \quad . \tag{IV-3}$$

This equation describes the Fickian diffusion problem. The solution of this equation by an expansion in Burnett functions is the Viehland and Mason theory[10] outlined in Chapter III. In Chapter III, equation (IV-3) was reduced to

$$N<J\Psi>^{(2)}=\frac{eE}{m}<\frac{\partial\Psi}{\partial v_z}>^{(2)}-\left[<v_z\,\Psi>^{(1)}-<v_z>^{(1)}<\Psi>^{(1)}\right]\frac{\partial \ln n^{(1)}}{\partial z} \quad . \tag{IV-4}$$

The above equation is identical with equation (3-19), except that the superscripts have been added to clarify the order of approximation. It should be noted that to this order, the quantities $h_{\ell 0}^{(r)}$, defined in Chapter III, are expressed in terms of first order moments, and are therefore independent of space and time. To be consistent with the notation of Chapter III, the superscripts on the quantities $h_{\ell 0}^{(r)}$ will not refer to the order of approximation, but will be consistent with the defining equation (3-26). All $h_{\ell 0}^{(r)}$ terms used here are of first order. The first few $h_{\ell 0}^{(r)}$ are given by equations (3-48).

Expanding equation (IV-4) in Burnett functions gives equations (3-24), (3-25), and (3-26) which are more clearly written to show the order of the approximation as

$$\sum_{s} \frac{a_{rs}^{(\ell)}}{a_{00(1)}} \langle \Psi_{\ell 0}^{(s)} \rangle^{(2)} = E\left[\frac{\ell(\ell+r+\frac{1}{2})}{(\ell+\frac{1}{2})} \langle \Psi_{\ell-1,0}^{(r)} \rangle^{(2)} - \left(\frac{\ell+1}{\ell+\frac{1}{2}}\right) \langle \Psi_{\ell+1,0}^{(r-1)} \rangle^{(2)}\right.$$

$$\left. -h_{\ell 0}^{(r)} \left(\frac{EkT_i}{eE}\right) \frac{\partial \ln n^{(1)}}{\partial z}\right] \quad , \tag{IV-5}$$

and

$$h_{\ell 0}^{(r)} = \left(\frac{\ell+1}{\ell+\frac{1}{2}}\right)\left[\langle \Psi_{\ell+1,0}^{(r)} \rangle^{(1)} - \langle \Psi_{\ell+1,0}^{(r-1)} \rangle^{(1)}\right] + \frac{\ell(\ell+r+\frac{1}{2})}{(\ell+\frac{1}{2})} \langle \Psi_{\ell-1,0}^{(r)} \rangle^{(1)}$$

$$- \frac{\ell(r+1)}{(\ell+\frac{1}{2})} \langle \Psi_{\ell+1,0}^{(r)} \rangle^{(1)} - 2 \langle \Psi_{1,0}^{(0)} \rangle^{(1)} \langle \Psi_{\ell,0}^{(r)} \rangle^{(1)} \quad . \tag{IV-6}$$

In the third approximation, the spacial and temporal derivatives in equation (IV-1) are taken to a second approximation, and are known from the preceding stage. To third order, equation (IV-1) is

$$\frac{1}{n^{(2)}}\left[\frac{\partial}{\partial t}(n \langle \Psi \rangle)^{(2)} + \frac{\partial}{\partial z}(n \langle v_z \Psi \rangle)^{(2)}\right] - \frac{eE}{m} \left\langle \frac{\partial \Psi}{\partial v_z} \right\rangle^{(3)} = - N \langle J \Psi \rangle^{(3)} \quad . \tag{IV-7}$$

When $\Psi = 1$, equation (IV-7) becomes

$$\frac{\partial \ln n^{(2)}}{\partial t} + \langle v_z \rangle^{(2)} \frac{\partial \ln n^{(2)}}{\partial z} + \frac{\partial \langle v_z \rangle^{(2)}}{\partial z} = 0 \quad , \tag{IV-8}$$

the second order continuity equation. Using $\Psi = \Psi_{10}^{(0)}$ in equation (IV-7) gives

$$<\Psi_{10}^{(0)}>^{(2)} \frac{\partial \ln n^{(2)}}{\partial t} + \frac{\partial <\Psi_{10}^{(0)}>^{(2)}}{\partial t} + <v_z \Psi_{10}^{(0)}>^{(2)} \frac{\partial \ln n^{(2)}}{\partial z}$$

$$+ \frac{\partial <v_z \Psi_{10}^{(0)}>^{(2)}}{\partial z} - \frac{eE}{m} < \frac{\partial \Psi}{\partial v_z} >^{(3)} = -N < J \Psi >^{(3)} \quad .$$

Using equation (IV-8) to eliminate $\partial \ln n^{(3)}/\partial t$, the above equation becomes

$$N < J \Psi_{10}^{(0)}>^{(3)} = \frac{eE}{m} < \frac{\partial \Psi_{10}^{(0)}}{\partial v_z} >^{(3)} - \left[<v_z \Psi_{10}^{(0)}>^{(2)} - <v_z>^{(2)} <\Psi_{10}^{(0)}>^{(2)} \right] \frac{\partial \ln n^{(2)}}{\partial z}$$

$$+ <\Psi_{10}^{(0)}>^{(2)} \frac{\partial <v_z>^{(2)}}{\partial z} - \frac{\partial <\Psi_{10}^{(0)}>^{(2)}}{\partial t} - \frac{\partial <v_z \Psi_{10}^{(0)}>^{(2)}}{\partial z} \quad . \qquad \text{(IV-9)}$$

Comparing equation (IV-9) with equation (IV-4) shows three additional terms appearing in the third order. These additional terms give rise to non-Fickian diffusion.

Evaluation of $\partial <v_z>^{(2)}/\partial z$ proceeds as follows:

From equation (3-20),

$$\frac{\partial <v_z>^{(2)}}{\partial z} = \left(\frac{2kT_i}{m} \right)^{\frac{1}{2}} \frac{\partial <\Psi_{10}^{(0)}>^{(2)}}{\partial z} \quad .$$

Using equation (IV-5) to find $<\Psi_{10}^{(0)}>^{(2)}$, the above equation becomes

$$\frac{\partial <v_z>^{(2)}}{\partial z} = \left(\frac{2kT_i}{m} \right)^{\frac{1}{2}} \frac{\partial}{\partial z} \left[E - h_{10}^{(0)} \left(\frac{EkT_i}{eE} \right) \frac{\partial \ln n^{(1)}}{\partial z} \right]$$

$$= - \left(\frac{2kT_i}{m} \right)^{\frac{1}{2}} h_{10}^{(0)} \left(\frac{EkT_i}{eE} \right) \frac{\partial^2 \ln n^{(1)}}{\partial z^2} \quad .$$

Using $<\Psi_{10}^{(0)}>^{(2)}$ from equation (IV-5), and neglecting products of derivatives gives

$$<\Psi_{10}^{(0)}>^{(2)} \frac{\partial <v_z>^{(2)}}{\partial z} = - E\left(\frac{2kT_i}{m}\right)^{\frac{1}{2}} h_{10}^{(0)} \left(\frac{EkT_i}{eE}\right) \frac{\partial^2 \ln n^{(1)}}{\partial z^2} \quad . \tag{IV-10}$$

Evaluation of $\partial <\Psi_{10}^{(0)}>^{(2)}/\partial t$, the second additional term in equation (IV-9) proceeds as follows. From equation (IV-5)

$$\frac{\partial <\Psi_{10}^{(0)}>^{(2)}}{\partial t} = \frac{\partial}{\partial t}\left[E - h_{10}^{(0)}\left(\frac{E\,kT_i}{eE}\right) \frac{\partial \ln n^{(1)}}{\partial z}\right] ,$$

or

$$\frac{\partial <\Psi_{10}^{(0)}>^{(2)}}{\partial t} = - h_{10}^{(0)}\left(\frac{E\,kT_i}{eE}\right) \frac{\partial}{\partial z}\left(\frac{\partial \ln n^{(1)}}{\partial t}\right) . \tag{IV-11}$$

The term $\partial \ln n^{(1)}/\partial t$ can be evaluated from equation (IV-3) with $\Psi = 1$ to get

$$\frac{\partial \ln n^{(1)}}{\partial t} = - <v_z>^{(1)} \frac{\partial \ln n^{(1)}}{\partial z} \quad .$$

Substituting this equation into equation (IV-11), and using equation (3-20), gives

$$\frac{\partial <\Psi_{10}^{(0)}>^{(2)}}{\partial t} = E\left(\frac{2kT_i}{m}\right)^{\frac{1}{2}} h_{10}^{(0)}\left(\frac{E\,kT_i}{eE}\right) \frac{\partial^2 \ln n^{(1)}}{\partial z^2} \quad . \tag{IV-12}$$

Evaluation of $\partial <v_z \Psi_{10}^{(0)}>^{(2)}/\partial t$, the last additional term in equation (IV-9), proceeds as follows. From equation (3-20)

$$v_z \Psi_{10}^{(0)} = \left(\frac{2kT_i}{m}\right)^{\frac{1}{2}} \Psi_{10}^{(0)} \Psi_{10}^{(0)} \quad .$$

Also, from equation (3-20), by finding $\Psi_{00}^{(0)}$, $\Psi_{10}^{(0)}$, and $\Psi_{20}^{(0)}$, it can be shown[16] that

$$\Psi_{10}^{(0)} \Psi_{10}^{(0)} = \frac{2}{3} \Psi_{20}^{(0)} + \frac{1}{3} \quad .$$

Therefore,

$$\frac{\partial < v_z \Psi_{10}^{(0)} >^{(2)}}{\partial z} = \frac{2}{3} \left(\frac{2kT_i}{m}\right)^{\frac{1}{2}} \frac{\partial < \Psi_{20}^{(0)} >^{(2)}}{\partial z}$$

Using equation (IV-5) to find $< \Psi_{20}^{(0)} >^{(2)}$ gives

$$\frac{\partial < v_z \Psi_{10}^{(0)} >^{(2)}}{\partial z} = \frac{2}{3} \left(\frac{2kT_i}{m}\right)^{\frac{1}{2}} \frac{\partial}{\partial z} \left[2\mathcal{E}^2 - \left(2\mathcal{E} h_{10}^{(0)} + h_{20}^{(0)} \right) \frac{\partial \ln n^{(1)}}{\partial z} \left(\frac{\mathcal{E} kT_i}{eE}\right) \right] ,$$

or

$$\frac{\partial < v_z \Psi_{10}^{(0)} >^{(2)}}{\partial z} = - \frac{2}{3} \left(\frac{2kT_i}{m}\right)^{\frac{1}{2}} \left(2\mathcal{E} h_{10}^{(0)} + h_{20}^{(0)}\right) \left(\frac{\mathcal{E} kT_i}{eE}\right) \frac{\partial^2 \ln n^{(1)}}{\partial z^2} \quad . \qquad \text{(IV-13)}$$

Substituting equations (IV-10), (IV-12), and (IV-13) into equation (IV-9) gives

$$< \Psi_{10}^{(0)} >^{(3)} = \mathcal{E} - \left(\frac{\mathcal{E} kT_i}{2eE}\right) \left[< v_z \Psi_{10}^{(0)} >^{(2)} - < v_z >^{(2)} < \Psi_{10}^{(0)} >^{(2)} \right] \frac{\partial \ln n^{(2)}}{\partial z}$$

$$+ \frac{2}{3Na_{00}^{(1)}} \left(\frac{\mathcal{E} kT_i}{eE}\right) \left(\frac{2kT_i}{m}\right)^{\frac{1}{2}} \left(h_{20}^{(0)} - \mathcal{E} h_{10}^{(0)} \right) \frac{\partial^2 \ln n^{(1)}}{\partial z^2} \quad . \qquad \text{(IV-14)}$$

This equation shows that the additional terms in third order give rise to non-Fickian diffusion. Comparing equation (IV-14) to

$$\langle v_z \rangle = v_d - D_L \frac{\partial \ln n}{\partial z} + Q \frac{\partial^2 \ln n}{\partial z^2}$$

defining the non-Fickian coefficient Q shows

$$Q = \frac{2}{3Na_{00}(1)} \left(\frac{\mathcal{E} kT_i}{eE}\right)\left(\frac{2kT_i}{m}\right)\left(h_{20}^{(0)} - h_{10}^{(0)}\right) . \qquad \text{(IV-15)}$$

Consider the first non-vanishing terms in $\mathcal{E}$ in equation (IV-15). In this limit $h_{20}^{(0)} \approx 2\mathcal{E}$ and $h_{10}^{(0)} \approx 1$, and equation (IV-15) becomes

$$Q = \frac{2\mathcal{E}}{3Na_{00}(1)} \left(\frac{\mathcal{E} kT_i}{eE}\right)\left(\frac{2kT_i}{m}\right) h_{10}^{(0)} .$$

Multiplying by N^2, using equations (3-25), (3-28), (3-29), the ideal gas law, the definition of reduced mobility, and the above equation, the result is

$$N^2 Q = \frac{2}{3} \frac{m}{e} (ND_L) N_0^2 K_0^2 \frac{E}{N} . \qquad \text{(IV-16)}$$

Expressing ND_L in units of 10^{17} cm^{-1} sec^{-1}, K_0 in cm^2/V-sec, E/N in Td, m in amu, and N^2Q in units of 10^{33} cm^{-3} sec^{-1}, the above equation becomes

$$N^2 Q = 0.523\ m \left(\frac{ND_L}{1000}\right) K_0^2 \frac{E}{N} . \qquad \text{(IV-17)}$$

Equation (IV-17) is plotted in Fig. 18 and Fig. 19. In those figures the circles represent equation (IV-17) when the Wannier ND_L was used, and the triangles represent equation (IV-17) when the measured ND_L was used. The dots in Fig. 18 and Fig. 19 are the measured values of N^2Q. The method of measuring Q will be described later in this Appendix. Equation (IV-17) with the Wannier ND_L gives fair agreement in both Fig. 18 and Fig. 19.

The derivation of a more exact expression for N^2Q from equation (IV-15) could be completed using equation (IV-6) to get

$$h_{20}^{(0)} = \frac{6}{5}\langle\Psi_{30}^{(0)}\rangle^{(1)} + 2\langle\Psi_{10}^{(0)}\rangle^{(1)} - \frac{4}{5}\langle\Psi_{10}^{(1)}\rangle^{(1)} - 2\langle\Psi_{10}^{(0)}\rangle^{(1)}\langle\Psi_{20}^{(0)}\rangle^{(1)} \quad \text{(IV-18)}$$

Equation (IV-5) without the gradient term can be used to find $\langle\Psi_{30}^{(0)}\rangle^{(1)}$. The other moments can be found from equation (3-35). Using these moments in equation (IV-18) gives

$$h_{20}^{(0)} = E\left\{2 + \frac{4}{5}\frac{a_{10}^{(1)}}{a_{11}^{(1)}} + \frac{4}{3}\frac{a_{00}^{(1)}a_{10}^{(0)}}{a_{11}^{(1)}a_{11}^{(0)}}\right\}$$

$$+ E^3\left\{\frac{2a_{00}^{(1)}}{a_{00}^{(2)}}\left[\frac{18}{5}\frac{a_{00}^{(1)}}{a_{00}^{(3)}} - 2\right] + \frac{8}{15}\frac{a_{00}^{(1)}}{a_{11}^{(1)}}\left[5\frac{a_{00}^{(1)}}{a_{11}^{(0)}} + 4\frac{a_{00}^{(1)}}{a_{00}^{(2)}}\right]\right\} \quad \text{(IV-19)}$$

The elements $a_{rs}(\ell)$ have been tabulated by Viehland and Mason.[10] The ratios of elements necessary for equation (IV-19) are

$$\frac{a_{10}^{(1)}}{a_{11}^{(1)}} = -\left(\frac{T_i - T}{T_i}\right)\frac{\left[5m+(4A^*-5)M\right]m}{\left[3m^2+\frac{8}{5}A^*mM+M^2\right]}$$

$$= -\frac{\left[5m+(4A^*-5)M\right]m}{\left[3m^2+\frac{8}{5}A^*mM+M^2\right]}\ \frac{(m+M)v_d^2}{3kT_i} \quad ,$$

$$\frac{a_{00}^{(1)}}{a_{11}^{(1)}} = \frac{(m+M)^2}{\left[3m^2+\frac{8}{5}A^*mM+M^2\right]} \quad ,$$

$$\frac{a_{10}^{(0)}}{a_{11}^{(0)}} = -\frac{2}{3}\left(\frac{T_i - T}{T_i}\right) = -\frac{2(m+M)v_d^2}{9\,kT_i} \quad ,$$

$$\frac{a_{00}^{(1)}}{a_{00}^{(2)}} = \frac{5}{2}\left(\frac{m+M}{5m+3MA^*}\right) \quad ,$$

$$\frac{a_{00}^{(1)}}{a_{00}^{(3)}} = \frac{2}{3}\ \frac{(m+M)^2}{\left[2m^2+\frac{12}{5}A^*mM+\left(\frac{16}{7}F^*-1\right)M^2\right.} \quad ,$$

and

$$\frac{a_{00}^{(1)}}{a_{11}^{(0)}} = \frac{(M+m)}{2m} \quad .$$

A^* is defined by equation (3-36), and F^* is defined by the equation

$$F^* = \frac{\bar{\Omega}^{(3,3)}}{\bar{\Omega}^{(1,1)}} \tag{IV-20}$$

Using these ratios in equation (IV-19), and using the expression for $h_{10}^{(0)}$ from Chapter III, equation (IV-15) can be written in the form

$$N^2Q = \frac{2}{3}\frac{m}{e}(ND_L')N_0^2 K_0^2 \frac{E}{N} \quad , \tag{IV-21}$$

where D_L' is given by

$$D_L' = \frac{K}{e}\left[kT + q\, Mv_d^2\right] \tag{IV-22}$$

similar to equation (3-39) for ND_L.

At this point, it should be noted that the incorporation of an effective ion temperature T_i into the derivation has yielded a result for Q different from the Whealton and Mason result[9]

$$Q_{zzz} = \frac{2kTmK^2 v_d}{e^2}\left(-2 + q_1 E^2\right) . \tag{1-14}$$

The Whealton and Mason result was arrived at by a similar derivation, but without the inclusion of an effective ion temperature T_i.

In equation (IV-22), q is a lengthy combination of ratios of masses and collision integrals. The final expression for N^2Q given by equations (IV-21) and (IV-22) would be of little use for two reasons. First, the collision integrals at high E/N will depend on the interaction energy. From a practical point of view,

they are very difficult to calculate numerically. Second, equation (IV-21) was derived assuming polarization was the dominant interaction. At the high E/N for which non-Fickian diffusion becomes important, polarization is dominated by other interactions. Thus, completing the derivation of equation (IV-21) is not practical at this stage.

The numerical value of Q for a given ion-gas combination, E/N, and pressure was measured by fitting equation (III-14) to the arrival time histogram recorded on the TMC. A value of Q was chosen, the mobility program was executed, and the sum of the squares of the differences between equation (III-14) and the arrival-time histogram was computed. Then another value of Q was chosen, and the calculation repeated. The value of Q for which the sum of the squared differences was the smallest was assigned the numerical value of Q for that position.

The average of the Q's for all positions of a run was taken to be the measured value of Q for that ion-gas combination, pressure, and E/N. Multiplying that value by N^2 gave the points in Fig. 18 and Fig. 19.

The difference between the best fit of the theoretical ion current with non-Fickian diffusion, equation (III-14), and the theoretical ion current with only Fickian diffusion, can be seen in Fig. 17. In Fig. 17 the points represent the measured arrival-time histogram, the solid line represents the ion current given by equation (III-14) including non-Fickian diffusion, and the dashed line represents the ion current given by equation (III-11) with only Fickian diffusion.

It should be noted that the curve-fitting procedure used actually adjusts two parameters to arrive at a best fit. For each trial value of Q, the computer program

finds the value of D_L which produces the best fit for that value of Q. Therefore, when the non-Fickian ion current given in equation (III-14) is fitted to the arrival-time histogram, D_L differs from the value found when the purely Fickian ion current, given by equation (III-11), is used. Both values of ND_L for Na^+ in Ar and for Li^+ in Ne are listed in the tables below.

From the tables, it is evident that including non-Fickian diffusion in the analysis of the arrival-time histogram leads to a smaller value of ND_L at high E/N by an average of 4.6% for Li^+ in Ne, and by an average of 4.3% for Na^+ in Ar. Based on the analyses of these two ion-gas combinations, an error of -5.0% due to non-Fickian diffusion at high E/N is assigned to the value of ND_L, when a purely Fickian analysis is used to determine the value of ND_L.

Table 2. Non-Fickian Measurements of ND_L and Q for Na^+ in Ar

E/N (Td)	$ND_L \times 10^{17}$ ($cm^{-1} sec^{-1}$) Purely Fickian Diffusion	$ND_L \times 10^{17}$ ($cm^{-1} sec^{-1}$) Fickian and Non-Fickian Diffusion	% Difference In ND_L Values	Q (cm^3/sec)
249	842	809	-3.9%	16,500
276	951	951	0	16,800
326	1120	1059	-5.4%	34,000
402	1515	1413	-6.7%	65,500
502	1800	1704	-5.3%	124,000

Table 3. Non-Fickian Measurements of ND_L and Q for Li^+ in Ne

E/N (Td)	$ND_L \times 10^{17}$ ($cm^{-1} sec^{-1}$) Purely Fickian Diffusion	$ND_L \times 10^{17}$ ($cm^{-1} sec^{-1}$) Fickian and Non-Fickian Diffusion	% Difference In ND_L Values	Q (cm^3/sec)
74.3	2234	2140	-4.2%	60,700
80.0	2504	2414	-3.6%	33,600
89.7	2719	2607	-4.1%	17,800
125	4549	4259	-6.4%	72,300

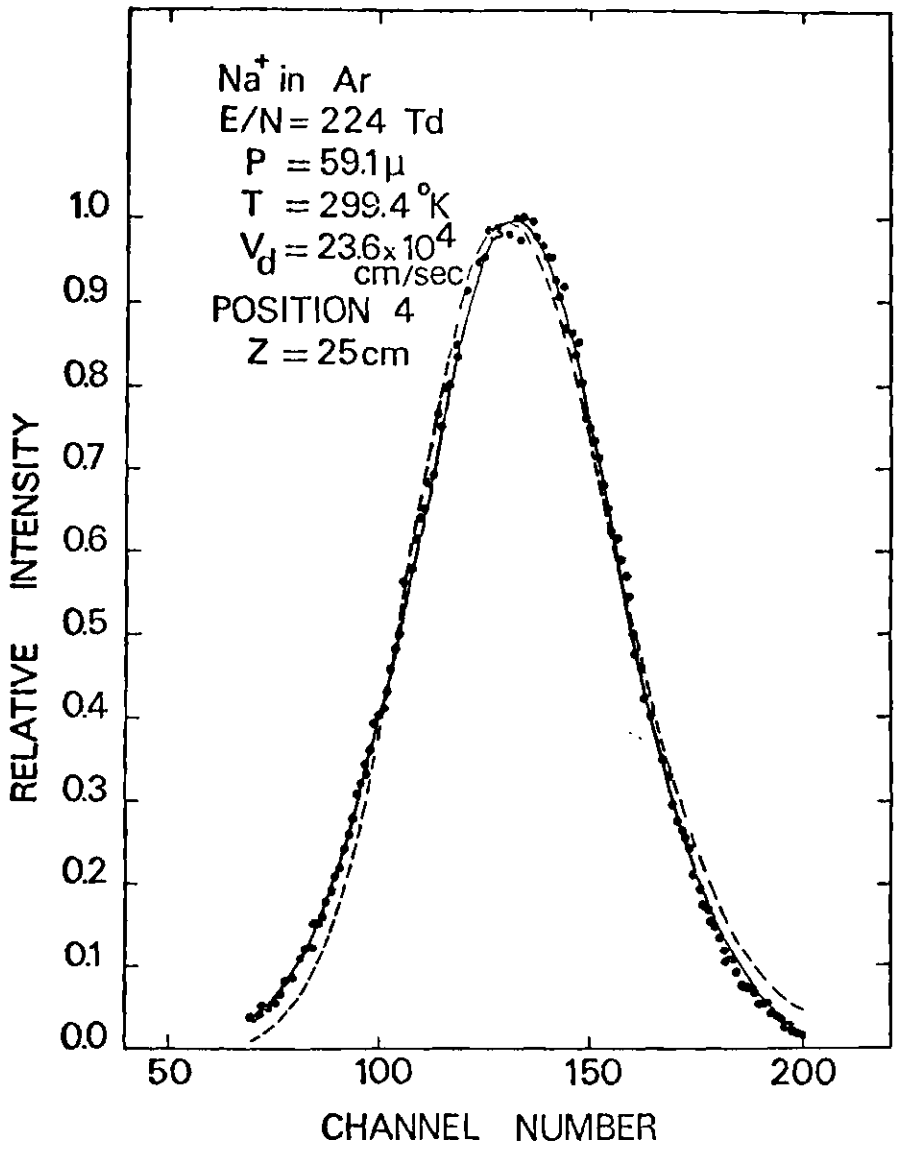

Fig. 17. Arrival Time Spectrum for Na^+ Ions in Argon Showing Both the Fickian and the Non-Fickian Theoretical Curves.

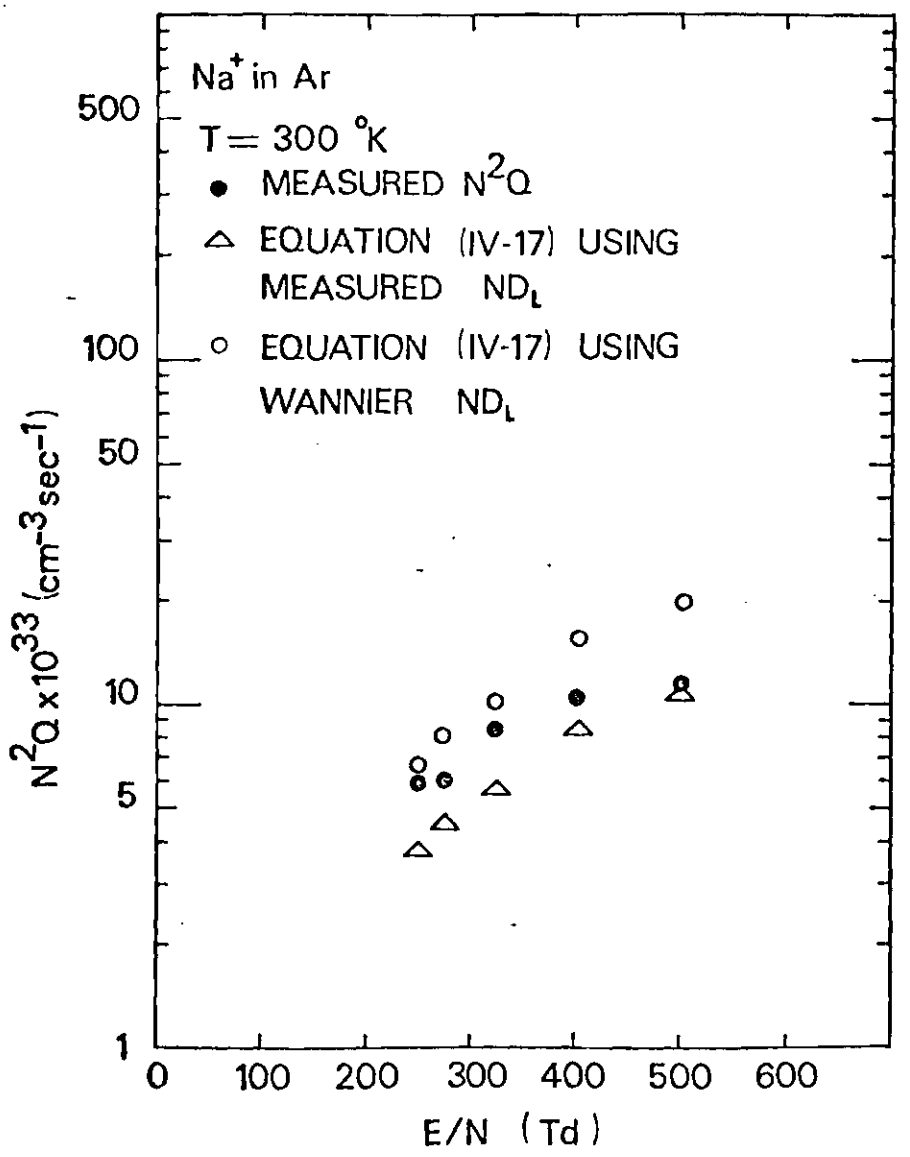

Fig. 18. Non-Fickian Coefficients for Na^+ Ions in Argon.

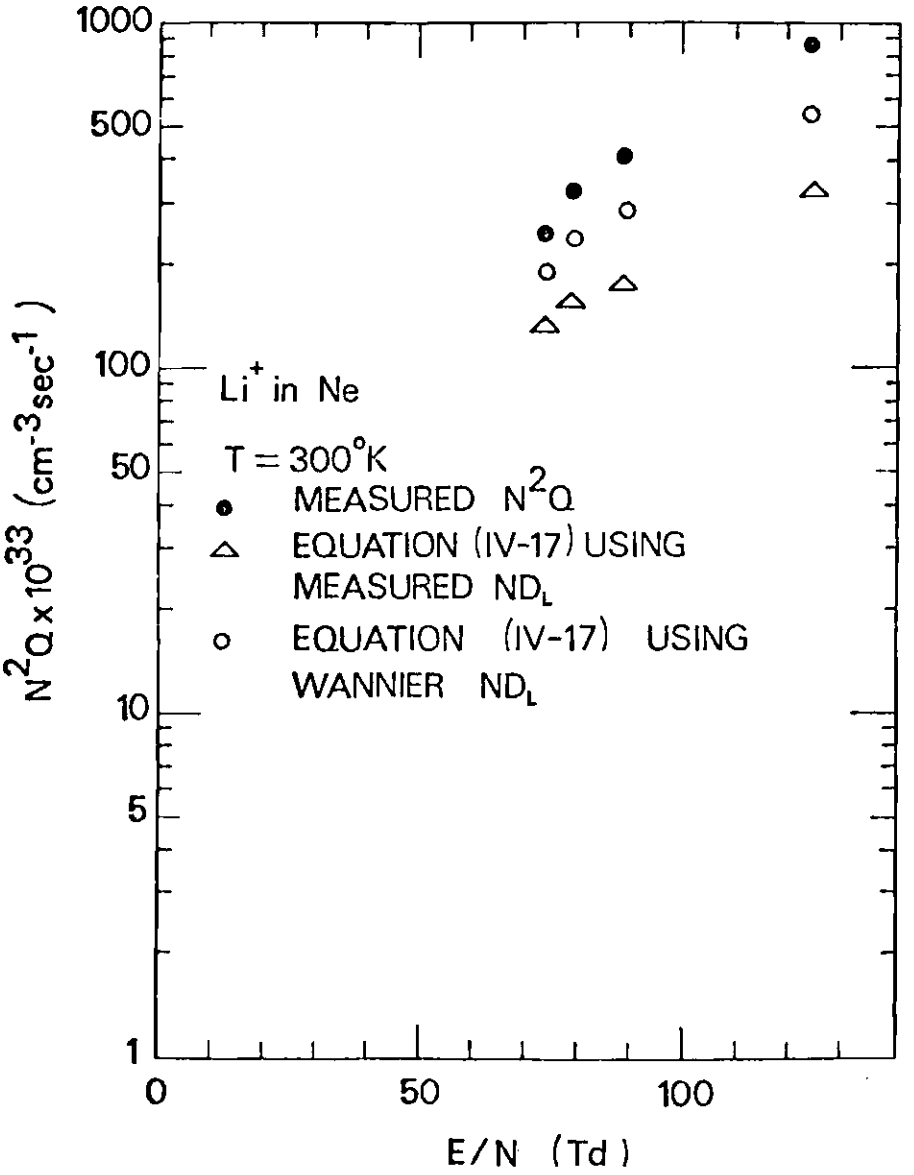

Fig. 19. Non-Fickian Coefficients for Li^+ Ions in Neon.

APPENDIX V

TABULATION OF TRANSPORT DATA

In this Appendix the transport data for Li^+ in He, Ne, and Ar, and for Na^+ in He, Ne, Ar, and CO_2 are tabulated. A separate table is included for each ion-gas combination. In each table, v_d, K_0, and ND_L are tabulated with the corresponding values of E/N, T, and P. E/N, the ratio of electric field strength E to the neutral gas number density N, is in Td, where 1 Td = 10^{-17} V-cm^2; T is the neutral gas temperature in ^oK; P is the neutral gas pressure in Torr; v_d is the drift velocity in units of 10^4 cm/sec; and ND_L, where D_L is the longitudinal diffusion coefficient, is in units of 10^{18} cm^{-1}sec^{-1}.

For the given value of E/N, pressure, and temperature, v_d was determined from equation (4-1). The reduced mobility K_0, was determined from this value of v_d by equations (1-1) and (1-2). The value of ND_L was determined by curve fitting the expression (5-1) to the arrival-time histogram to obtain a value for the longitudinal diffusion coefficient, D_L, and then multiplying by N. Using the ideal gas law gives

$$D_L = \left(0.1036 \frac{T}{P}\right) ND_L \ ,$$

where D_L is in cm^2/sec, T is in ^oK, P is in Torr, and ND_L is in units of 10^{18} cm^{-1}sec^{-1}.

Table 4. Transport Data for Li^+ Ions in Argon

E/N (Td)	P (Torr)	T (^oK)	v_d (10^4 cm/sec)	K_0 (cm^2/V-sec)	ND_L (10^{18}/cm-sec)
5.96	0.296	298.1	0.735	4.59	3.41
8.18	0.296	300.7	1.02	4.62	3.69
10.0	0.296	300.2	1.23	4.59	3.62
12.0	0.296	301.0	1.51	4.66	3.93
15.0	0.296	300.6	1.88	4.65	4.30
17.0	0.296	300.5	2.13	4.66	4.66
20.0	0.197	300.6	2.48	4.60	4.80
25.1	0.197	301.4	3.16	4.69	6.26
30.3	0.296	302.1	3.85	4.73	8.27
34.9	0.148	300.4	4.55	4.85	10.9
40.1	0.148	300.6	5.40	5.02	15.8
45.4	0.148	301.6	6.38	5.23	23.6
50.1	0.0985	300.8	7.39	5.48	32.4
55.1	0.0985	300.6	8.40	5.67	42.7
60.0	0.197	298.9	9.33	5.79	49.2
65.0	0.197	299.8	10.7	6.13	63.4
70.0	0.197	299.6	12.1	6.43	78.0
75.0	0.197	299.8	13.4	6.64	92.7
80.1	0.197	300.3	14.5	6.76	101
90.0	0.148	300.5	16.9	6.99	119
100	0.148	300.7	19.5	7.24	144
110	0.148	300.7	21.6	7.29	155
121	0.123	301.5	23.9	7.37	178
130	0.123	299.1	25.4	7.28	191
150	0.0985	298.3	29.1	7.25	229
160	0.0985	300.3	30.8	7.17	252
201	0.0788	301.4	37.0	6.84	322

Table 5. Transport Data for Li^+ Ions in Helium

E/N (Td)	P (Torr)	T (^oK)	v_d (10^4 cm/sec)	K_0 (cm^2/V-sec)	ND_L (10^{18}/cm sec)
2.02	0.493	301.0	1.25	23.1	17.0
2.53	0.394	300.5	1.57	23.1	17.3
3.01	0.394	300.6	1.86	23.0	17.2
3.51	0.296	299.9	2.17	23.1	17.6
4.00	0.394	300.5	2.48	23.0	17.5
4.50	0.493	299.5	2.79	23.0	18.3
5.01	0.296	299.8	3.11	23.2	18.2
5.48	0.493	300.3	3.44	23.4	19.7
6.00	0.394	300.1	3.80	23.5	20.3
7.00	0.296	299.9	4.46	23.7	21.4
8.19	0.296	301.1	5.26	23.9	23.2
8.99	0.296	299.6	5.84	24.1	25.7
10.1	0.296	301.2	6.59	24.2	28.4
12.0	0.296	300.7	7.92	-	35.0
15.1	0.296	300.7	10.5	25.9	52.2
17.0	0.296	299.2	12.3	27.0	68.3
20.0	0.296	299.7	14.9	27.7	92.3
25.1	0.296	300.8	20.5	30.4	162
29.9	0.296	300.2	25.2	31.3	-
35.1	0.296	300.2	30.6	32.5	251
40.0	0.296	299.0	35.1	32.7	286
45.0	0.296	300.1	39.4	32.7	335
50.1	0.296	300.0	44.0	32.7	349
55.1	0.296	300.3	47.9	32.4	420
60.2	0.296	300.9	52.0	32.2	434
70.2	0.246	301.6	59.8	31.7	505
75.2	0.197	300.6	63.7	31.5	528
90.5	0.197	301.0	74.0	30.4	646
99.7	0.177	299.2	79.5	29.7	720
150	0.128	299.5	109	27.2	1250
199	0.0887	297.9	133	25.0	1840

Table 6. Transport Data for Li^+ Ions in Neon

E/N (Td)	P (Torr)	T (^oK)	v_d (10^4 cm/sec)	K_0 (cm^2/V-sec)	ND_L (10^{18}/cm-sec)
2.99	0.394	300.0	0.851	10.6	7.50
3.50	0.394	300.5	1.01	10.7	7.81
4.00	0.394	300.6	1.16	10.7	8.12
4.99	0.394	300.0	1.43	10.7	8.12
5.99	0.394	299.9	1.72	10.7	8.67
7.91	0.394	299.8	2.28	10.7	9.70
9.01	0.394	300.6	2.62	10.8	10.9
9.97	0.394	299.6	3.01	10.9	12.8
12.2	0.394	299.6	3.66	11.2	15.2
15.0	0.296	299.8	4.80	11.9	21.5
17.1	0.394	301.6	5.60	12.2	27.5
19.9	0.296	299.0	6.82	12.7	38.0
26.8	0.197	300.7	10.0	14.0	64.1
29.9	0.296	298.4	11.5	14.3	80.2
33.4	0.197	300.6	13.4	14.9	92.9
36.8	0.296	300.9	15.0	15.2	-
43.4	0.296	300.2	17.7	15.3	129
45.1	0.296	300.8	18.5	15.3	-
50.2	0.246	300.6	20.3	15.3	150
65.3	0.197	301.5	26.4	15.0	201
70.1	0.197	300.5	27.9	14.9	215
74.3	0.197	298.0	29.0	14.7	223
80.0	0.148	298.9	31.4	14.6	250
89.7	0.148	299.4	34.0	14.2	272
125	0.0985	300.3	44.9	13.0	455

Table 7. Transport Data for Na^+ Ions in Helium

E/N (Td)	P (Torr)	T (^oK)	v_d (10^4 cm/sec)	K_0 (cm^2/V-sec)	ND_L (10^{18}/cm-sec)
1.00	0.493	299.4	0.605	22.6	17.6
2.01	0.296	300.5	1.23	22.6	18.4
2.50	0.296	300.1	1.52	22.7	18.2
3.00	0.296	300.4	1.83	22.7	18.2
3.33	0.296	299.4	2.04	22.7	18.7
3.49	0.296	299.7	2.12	22.6	18.5
4.00	0.296	300.2	2.46	22.6	19.0
4.50	0.296	300.2	2.76	-	18.8
5.05	0.296	299.8	3.11	22.8	19.3
6.08	0.296	300.0	3.73	22.7	20.0
7.09	0.296	300.4	4.39	22.9	22.3
8.10	0.296	300.3	5.03	23.1	22.5
9.00	0.197	299.8	5.67	-	24.7
9.81	0.197	299.1	6.22	23.4	26.0
12.0	0.197	300.0	7.68	23.8	28.5
14.5	0.296	299.7	9.42	24.1	36.4
17.1	0.296	300.0	11.3	24.6	46.8
19.3	0.197	298.5	13.0	25.1	54.3
24.2	0.296	300.6	16.7	25.7	77.7
30.2	0.197	299.8	21.2	26.1	93.0
35.0	0.197	299.8	24.4	25.9	110
39.9	0.148	298.9	27.5	25.6	115
45.1	0.197	300.3	30.7	25.4	140
49.9	0.197	300.0	33.3	24.9	153
74.8	0.148	299.2	45.8	22.8	197
99.7	0.0985	299.1	56.2	21.0	238
125	0.0985	299.2	65.9	19.6	313
149	0.0985	298.6	73.9	18.4	332
174	0.0985	298.7	82.4	17.6	413

Table 8. Transport Data for Na^+ Ions in Argon

E/N (Td)	P (Torr)	T (^oK)	v_d (10^4 cm/sec)	K_0 (cm^2/V-sec)	ND_L (10^{18}/cm-sec)
6.01	0.0985	300.6	0.495	3.08	2.26
8.04	0.0985	300.9	0.668	3.09	2.39
10.1	0.0985	300.5	0.834	3.07	2.37
12.6	0.0985	300.7	1.05	3.09	2.50
15.0	0.148	300.3	1.25	3.09	2.55
17.5	0.148	299.9	1.45	3.09	2.64
20.0	0.148	299.4	1.67	3.10	2.77
25.0	0.148	299.2	2.08	3.11	3.18
28.0	0.148	300.5	2.37	-	3.60
30.2	0.148	300.8	2.56	-	3.72
32.7	0.148	299.5	2.75	3.11	4.14
35.1	0.148	300.8	3.03	-	4.74
40.2	0.148	301.7	3.50	3.13	6.01
45.2	0.148	300.8	3.94	3.20	6.72
50.0	0.148	300.5	4.52	3.30	8.81
55.1	0.148	300.7	5.14	3.39	11.0
60.3	0.148	301.3	5.67	3.50	13.2
65.0	0.148	299.5	6.19	3.58	15.4
70.0	0.148	299.7	6.89	3.67	18.3
80.2	0.172	300.7	8.10	3.79	25.1
90.2	0.172	300.9	9.60	3.96	31.6
101	0.0985	301.9	10.9	4.03	32.5
110	0.0788	300.4	12.2	4.12	37.3
121	0.0985	301.7	13.6	4.18	43.2
130	0.0985	300.9	14.5	4.14	44.3
140	0.0985	300.0	15.6	4.14	48.0
160	0.0985	300.5	17.8	4.12	54.9
180	0.0739	300.5	19.7	4.08	60.5
200	0.0739	299.9	21.6	4.01	68.1
224	0.0591	299.4	23.6	3.91	74.0
249	0.0591	299.8	25.9	3.87	84.2
276	0.0591	300.5	28.1	3.80	95.1
326	0.0493	300.4	31.5	3.60	112
402	0.0394	300.7	37.7	3.41	152
502	0.0296	300.8	42.5	3.15	180

Table 9. Transport Data for Na^+ Ions in Neon

E/N (Td)	P (Torr)	T (^oK)	v_d (10^4 cm/sec)	K_0 (cm^2/V-sec)	ND_L (10^{18}/cm-sec)
3.99	0.148	299.2	0.887	8.28	6.52
5.96	0.148	299.0	1.32	8.25	6.96
7.03	0.296	300.9	1.55	8.21	6.70
8.12	0.197	298.4	1.81	8.30	7.25
10.0	0.197	298.0	2.25	8.30	7.71
12.4	0.197	298.0	2.81	8.32	8.73
14.9	0.197	298.1	3.41	8.50	10.3
17.3	0.197	298.9	4.10	8.82	13.0
19.9	0.197	298.6	4.77	8.92	16.0
24.8	0.296	297.8	6.14	9.23	21.9
30.0	0.296	300.6	7.58	9.42	28.7
35.3	0.296	299.4	9.12	9.62	34.6
40.2	0.296	300.2	10.5	9.70	40.8
45.0	0.246	299.4	11.7	9.70	45.0
50.7	0.197	300.3	13.1	9.61	45.4
55.1	0.246	300.1	14.2	9.59	54.1
60.2	0.246	300.6	15.2	9.43	56.0
69.8	0.197	299.8	17.3	9.25	59.7
80.0	0.0985	300.0	19.6	9.13	66.1
90.3	0.0985	300.9	21.7	8.92	75.5
99.9	0.0985	299.6	23.3	8.67	80.7
125	0.0985	299.6	27.5	8.19	98.6
150	0.0985	300.2	31.3	7.74	115
176	0.0985	302.2	34.5	7.28	129
199	0.0985	298.7	37.6	7.03	140

Table 10. Transport Data for Na^+ Ions in Carbon Dioxide

E/N (Td)	P (Torr)	T (^oK)	v_d (10^4cm/sec)	K_0 (cm^2/V-sec)	ND_L (10^{18}/cm-sec)
51.8	0.0739	299.9	2.27	1.63	1.58
60.7	0.0739	299.6	2.64	1.60	1.68
70.9	0.0739	299.5	3.04	1.60	1.83
77.2	0.0493	298.0	3.30	1.59	2.03
96.5	0.0493	298.6	4.06	-	2.32
101	0.0493	297.8	4.21	1.56	2.43
126	0.0493	297.9	5.14	1.52	2.93
151	0.0493	297.7	6.07	1.50	3.55
176	0.0739	298.9	6.96	1.47	4.51
201	0.0493	298.0	7.93	1.47	6.02
225	0.0739	298.3	8.91	1.47	8.08
252	0.0493	298.2	10.2	1.51	11.9
276	0.0739	298.5	11.4	1.53	17.6
303	0.0493	298.5	13.0	1.60	24.9
355	0.0246	300.2	16.8	1.76	46.7
402	0.0493	298.8	20.3	1.88	73.1
457	0.0246	300.2	25.0	2.04	98.8
497	0.0296	298.9	28.0	2.10	114
600	0.0296	299.1	36.1	2.23	136
659	0.0246	300.3	39.8	-	149
710	0.0296	300.7	43.7	2.29	164
762	0.0296	300.8	47.1	2.30	175

BIBLIOGRAPHY

1. A. M. Tyndall, The Mobility of Positive Ions in Gases (Cambridge University Press, Cambridge, 1938), p. 92.

2. G. E. Keller and R. A. Beyer, J. Geophys. Res. 76, 289 (1971).

3. Johnsen, Brown, and Biondi, Jour. Chem. Phys. 55, 186 (1971).

4. G. E. Keller, R. A. Beyer, and L. M. Colonna-Romano, Phys. Rev. A8, 1446 (1973).

5. P. Langevin, Ann. Chim. Phys. 5, 245 (1905). A complete translation appears in Appendix II of reference 34.

6. For a complete exposition of the Chapman-Enskog theory, see S. Chapman and T. G. Cowling, The Mathematical Theory of Non-Uniform Gases, Third Edition (Cambridge University Press, London, 1970).

7. G. H. Wannier, Bell System Technical Journal 32, 170 (1953).

8. T. Kihara, Rev. Mod. Phys. 25, 844 (1953).

9. J. H. Whealton and E. A. Mason, Ann. Phys. 84, 8 (1974).

10. L. A. Viehland and E. A. Mason, Ann. Phys. 91, 499 (1975).

11. D. L. Albritton, D. W. Martin, E. W. McDaniel, T. M. Miller, J. T. Moseley, Technical Report, Georgia Institute of Technology, Atlanta, Georgia (1967), Chapter II.

12. T. M. Miller, D. W. Martin, E. W. McDaniel, J. T. Moseley, R. M. Snuggs, Technical Report, Georgia Institute of Technology, Atlanta, Georgia (1968), Chapter II.

13. J. T. Moseley, D. W. Martin, E. W. McDaniel, R. M. Snuggs, T. M. Miller, Technical Report, Georgia Institute of Technology, Atlanta, Georgia (1968), Chapter II.

14. R. M. Snuggs, D. J. Voltz, J. H. Schummers, R. D. Laser, I. R. Gatland, D. W. Martin, and E. W. McDaniel, Technical Report, Georgia Institute of Technology, Atlanta, Georgia (1970), Chapter II.

15. J. H. Schummers, G. M. Thomson, D. R. James, E. Graham IV, I. R. Gatland, D. W. Martin, and E. W. McDaniel, Technical Report, Georgia Institute of Technology, Atlanta, Georgia (1972), Chapter II.

16. E. W. McDaniel and E. A. Mason, The Mobility and Diffusion of Ions in Gases (Wiley, New York, 1973).

17. D. L. Albritton, op. cit., Appendix IV.

18. H. R. Hasse', Phil. Mag. 1, 139 (1926).

19. G. H. Wannier, op. cit., pp. 176,7.

20. E. W. McDaniel and J. T. Moseley, Phys. Rev. A3, 1040 (1971).

21. R. E. Robson, Aust. J. Phys. 25, 685 (1972).

22. H. R. Skullerud, to be published

23. L. A. Viehland and E. A. Mason, J. Chem. Phys. 63, 2913 (1975).

24. I. R. Gatland, Case Studies in Atomic Physics 4, 369 (1974).

25. T. Kihara, op. cit., p. 847

26. L. A. Viehland and E. A. Mason, op. cit., Appendix.

27. L. A. Viehland and E. A. Mason, op. cit., equation (109).

28. J. T. Moseley, op. cit., Chapter IV.

29. J. T. Moseley, op. cit., Chapter V.

30. G. R. Akridge, H. W. Ellis, R. Y. Pai, and E. W. McDaniel, J. Chem. Phys. 62, 4578 (1975).

31. H. S. W. Massey, Electron and Ionic Impact Phenomena, Second Ed., Vol. 2 (Oxford Univ. Press, 1969), pp. 790-3.

32. D. R. James, E. Graham IV, G. R. Akridge, W. C. Keever, H. W. Ellis, I. R. Gatland, and E. W. McDaniel, Technical Report, Georgia Institute of Technology, Atlanta, Georgia (1975).

33. N. Takata, Phys. Rev. A10, 2336 (1974).

34. E. W. McDaniel, Collision Phenomena in Ionized Gases (Wiley, New York, 1964).

35. G. W. Catlow, M. R. C. McDowell, J. J. Kaufman, L. M. Sachs, and E. S. Chang, J. Phys. B3, 833 (1970).

36. W. F. Morrison, G. R. Akridge, H. W. Ellis, R. Y. Pai, E. W. McDaniel, L. A. Viehland, and E. A. Mason, J. Chem. Phys. 63, 2238 (1975).

37. J. T. Moseley, op. cit., pp. 86-91.

38. E. W. McDaniel and D. W. Martin, Rev. Sci. Inst. 42, 157 (1971).

39. E. Graham IV, D. R. James, W. C. Keever, I. R. Gatland, and E. W. McDaniel, Technical Report, Georgia Institute of Technology, Atlanta, Georgia (1974), p. 24.

40. C. F. Powell and L. Brata, Proc. Royal Soc. A138, 117 (1932).

41. R. Y. Pai, H. W. Ellis, G. R. Akridge, and E. W. McDaniel, 63, 2916 (1975).

42. J. H. Schumers, op. cit., p. 115.

43. M. Krauss, P. Maldonado, and A. C. Wahl, J. Chem. Phys. 54, 4944 (1971).

44. H. Inouye and S. Kita, J. Chem. Phys. 57, 1301 (1972).

45. L. Monchick, Phys. Fluids 2, 695 (1959).

46. J. O. Hirschfelder and M. A. Eliason, Ann. N. Y. Acad. Sci. 67, 451 (1957).

47. H. O'Hara and F. J. Smith, Comp. Phys. Comm. 2, 47 (1971).

48. E. W. McDaniel, op. cit., p. 443.

49. A. S. Dickinson, J. Phys. B 1, 395 (1968).

50. R. J. Munson and K. Hoselitz, Proc. R. Soc. A172, 43 (1939).

51. R. M. Snuggs, D. J. Voltz, J. H. Schummers, R. D. Laser, I. R. Gatland, D. W. Martin, and E. W. McDaniel, op. cit., p. 112. J. H. Schummers, G. M. Thomson, D. R. James, E. Graham IV, I. R. Gatland, D. W. Martin, and E. W. McDaniel, op. cit., p. 98. E. Graham IV, D. R. James, W. C. Keever, I. R. Gatland, and E. W. McDaniel, op. cit., p. 122. D. R. James, E. Graham IV, G. R. Akridge, W. C. Keever, H. W. Ellis, I. R. Gatland, and E. W. McDaniel, op. cit., p. 61.

52. I. S. Gradshteyn and I. M. Ryzhik, Table of Integrals Series and Products (Academic Press, New York, 1965), p. 341.

VITA

Garth Russell Akridge was born in ElDorado, Arkansas, on 17 June, 1940. He is the only child of Dr. Garth H. Akridge and Mrs. Ione R. Akridge. He was married to Marjorie Anita Stewart on 17 June 1962.

Mr. Akridge was graduated from Landon High School in Jacksonville, Florida in 1958. He entered the Georgia Institute of Technology that year. He received the degree of Bachelor of Science in Physics in June 1962, and the degree of Master of Science in Physics in June 1963. He served four years on active duty as an instructor in the Naval Officer's Nuclear Power School in Bainbridge, Maryland. While at Bainbridge, his son Floyd Russell Akridge was born. Also, while at Bainbridge, he attended the University of Delaware in Newark, Delaware. In June 1967 he was released from active duty, and entered the New Orleans Baptist Theological Seminary in New Orleans, Louisiana. In 1968 his daughter Sheryl Ellen Akridge was born. While at the New Orleans Baptist Theological Seminary, he was employed as a part-time physics teacher at Louisiana State University in New Orleans, Louisiana. He received the degree Master of Theology in 1970, and entered graduate school at the Georgia Institute of Technology the same year. While in graduate school, he was employed as a graduate teaching assistant in the Mathematics department, as a graduate teaching assistant in the Physics department, and as a research assistant in the Atomic Collisions Laboratory of the Physics department. In 1974 he accepted the position of physics teacher at Westminster High School, Atlanta, Georgia.